Thesis

The Chiral Anomaly of Quantum Chromodynamics at High Temperatures

Lattice Investigation of the Overlap Dirac Spectrum

Viktor Dick

April 2016

Dissertation
Fakultät für Physik
Universität Bielefeld

Contents

List of Figures

List of Tables

Introduction and Motivation

Symmetries of QCD

One of the most influential concepts for the development of our understanding of the physical world, in particular during the 20th and 21st centuries, has been, and still is, that of *symmetries*. For Newtonian physics and special relativity, for example, the requirement that the physical laws should be independent of the choice of inertial frame is a very important ingredient. Most of general relativity has been derived by elevating this principle even further, requiring all quantities about which a physical theory can make any statement to have a well-defined behavior under a general coordinate transformation. With the advent of quantum field theory, it was realized that electromagnetism can be understood as a local gauge theory, where the existence of photons as transmitters of the interaction as well as many of its properties follow from the assumption that the theory is symmetric under a local gauge group. The same principle was later found to be useful to describe the unified electroweak interaction and was also crucial in identifying Quantum Chromodynamics, QCD, as the local gauge theory that is able to explain the strong interaction.

QCD is a theory of quarks and gluons, but these are not directly observable in experiments in the same way an electron is. Instead, they form so-called *color-neutral* combinations, most of which can be classified into mesons and baryons. In the 1960s, Murray Gell-Mann developed the idea that mesons and baryons are in fact composite and not elementary, led by symmetry arguments to explain their observed properties and degeneracies in their masses [2]. He suggested the existence of three quark flavors which were subject to an approximate flavor symmetry, such that the physical laws are invariant if the three quark flavors are replaced by linear combinations of themselves—at least as far as the strong interaction is concerned. An additional gauge symmetry, which is exact and mixes an internal degree of freedom called *color*, explains why only specific combi-

nations are found in nature.

In contrast to quantum electrodynamics, the gauge group of QCD is non-Abelian, giving rise to self-interactions of the mediating gluons. At low energies, this induces *confinement*, which means that separating the quark constituents of a color-neutral combination requires an amount of energy that is sufficient to create new particles, binding to the constituents and again forming color-neutral states. At high energies, on the other hand, the interaction decreases and confinement breaks up, allowing free quarks; this phenomenon is called *asymptotic freedom*. Due to the large interaction at low energies and consequently also at low temperatures, the mass of a typical baryon is mostly determined by the binding energy and only a small fraction of it comes from the masses of the constituent quarks. In addition to the three quarks first proposed by Gell-Mann, three additional heavier quarks have been found, but the origin of the flavor symmetry lies in the fact that the three lightest quarks have masses that are much smaller than the hadronic energy scale of QCD provided by the baryon masses.

There are several ways in which the flavor symmetry—which is also called chiral symmetry—is restricted depending on external parameters like the temperature, giving rise to a rich phase structure of QCD. First, it is broken explicitly by the fact that the quark masses are not really vanishing, which for example is responsible for the masses of pions. Second, it is broken spontaneously at low enough temperatures such that the relevant states the system can occupy do not respect all of the symmetry even though the action does. Finally, a specific part of the symmetry is broken by the *axial anomaly*, which is linked to topological properties of the QCD medium. The spontaneously broken chiral symmetry as well as the axial anomaly are expected to be restored at high enough temperatures, the first because states with higher energies enter the thermal averages and the second because Debye screening suppresses the necessary color-electric fields.

The question whether the axial anomaly is already effectively restored at the chiral phase transition, where the spontaneously broken chiral symmetry becomes unbroken, is of great importance to understand this transition and the high temperature phase of QCD. Depending on the answer to this question, the relevant symmetries below and above the critical point and therefore the symmetry breaking pattern change. An understanding of

the symmetries that govern the phase transition of QCD is important to correctly interpret high energy collision experiments, which are relevant to understand, among other things, the state of the universe shortly after the Big Bang.

Numerical Calculations on the Lattice

Since QCD is characterized by a strong coupling constant and is confining at low temperatures, perturbative approaches where the theory is regarded as essentially describing free constituents and the interaction is included as a perturbation are inadequate except under special circumstances. While such methods are very successful for quantum electrodynamics, first principle calculations for QCD are more involved. One possibility that is not restricted to small couplings is *lattice QCD*, which was proposed by K. G. Wilson in 1974 [3]. By distributing the quantum fields of the theory on a discrete lattice, an ultraviolet cut-off is introduced. While the initial analytic computations done by Wilson were done in the limit where the coupling constant is infinite, it opened the door to numerical calculations at arbitrary coupling using computers. In numerical lattice QCD calculations, it is also straightforward to implement QCD at finite temperature, which is an active field of research and has produced many insights [4].

It is, however, not as easy to include quarks with the same chiral symmetry as in the continuum in lattice QCD calculations. Due to the *doubling problem*, a naive implementation of quarks results in too many particles, and the most direct way to circumvent this breaks chiral symmetry. Some compromises exist, which preserve chiral symmetry partly and also soften the doubling problem. The staggered fermion formulation is such a compromise and it has been successfully used to investigate the chiral transition. In the continuum limit, full chiral symmetry is restored, but at finite lattice spacings only a subgroup of the chiral symmetry group is fully present. In particular, the subgroup that is broken by the axial anomaly is not represented faithfully with staggered fermions. There is another lattice fermion formulation, so-called *overlap fermions*, that has no doublers and the same chiral symmetry as in the continuum, including the anomalous axial symmetry, which is broken by an analogous mechanism as in the continuum. The only problem with overlap fermions is that they are numerically very expensive, which makes simulations especially

at realistic parameters difficult.

In this work, a mixed approach has been used to investigate the role of the axial anomaly at the chiral transition temperature and beyond it. It is customary to split the computation of thermal observables into a step where gauge configurations are created that sample the thermal average according to the Boltzmann weight and a step where the observables in question are evaluated on these configurations. For this work, no new gauge configurations have been created but existing configurations using dynamical *highly improved staggered fermions* (HISQ) have been used. On these, the spectrum of the costly overlap Dirac operator has been computed, which encodes, among other things, the anomalous breaking of axial symmetry and possibly its restoration.

Many results of this work have been published in [5] and some of it has already been presented at the 31st *International Symposium on Lattice Field Theory* 2013 [6]. Preliminary results that are based on this work but are not included in this thesis were also presented at the 33rd *International Symposium on Lattice Field Theory* 2015 [7] and on the *Quark Matter* 2015 [8].

Outline of this Work

This work is structured as follows. The first chapter gives a general introduction to the theoretical framework and the necessary concepts that are relevant for this work. Then, a chapter is dedicated to lattice formulations that preserve chiral symmetry partly or fully. Staggered fermions are described relatively briefly, while overlap fermions are discussed in more detail. After that, a chapter about some details regarding the implementation and the more technical aspects follows. This also includes a discussion where different strategies to obtain the spectrum are compared. Finally, the results and their implications for the axial anomaly are presented. The conclusion summarizes the most important results and discusses further research opportunities regarding the topic of the axial anomaly in QCD.

1 Continuum and Lattice Quantum Chromodynamics

1.1 The Path Integral at Finite Temperature

A long-standing goal of the natural sciences in general and theoretical physics in particular has been to determine the lowest level of organization that the universe operates on, i.e., the fundamental entities of nature and the laws that govern them. One particular achievement in this regard has been the *standard model of particle physics*. It describes much of what we understand about nature through the unified framework of *quantum field theory* (QFT) and is, within its scope, the most fundamental theory available that has been firmly established by evidence. The goal of this section is to give an introduction to some aspects of QFT that are relevant for the work at hand but without yet going into Quantum Chromodynamics, which is the specific quantum field theory that describes strongly interacting matter. Most of it can also be found in various textbooks (cf. [9, 10, 11]), but some details like the effect of finite temperature or subtleties about gauge theories are often omitted.

In general, a quantum theory is given by a Hilbert space of possible states and a Hamilton operator that determines the time evolution of which state the system occupies. If, however, a thermodynamical ensemble of systems in equilibrium is examined, each of the systems is in an energy eigenstate whose time evolution is given by a trivial phase. For example, a microcanonical ensemble is characterized by assigning the same probability or weight within the ensemble to each state that gives the correct total energy, which is adequate to describe an isolated system. The canonical ensemble is obtained by taking a small subsystem of such an isolated system, in a manner where it is sensible to split the total energy into the energy of the subsystem and that of the rest. If only the subsystem is examined, the probability of a state with energy E is proportional to $\mathrm{e}^{-\beta E}$,

where $\beta = 1/T$ is the *inverse temperature* and depends on the energy of the total system as well as the distribution of degrees of freedom between the subsystem and the total system.

If a quantum system is in a specific quantum state $|\psi\rangle$ and some observable A is measured, the expectation value has to be obtained by an averaging over the eigenstates of A that contribute to $|\psi\rangle$,

$$\langle A\rangle_\psi = \langle\psi|A|\psi\rangle = \sum_a |\langle\psi|a\rangle|^2\, a.$$

If an ensemble is considered, the results have to be additionally averaged over which state the system might actually be in, giving in the case of the canonical ensemble

$$\langle A\rangle = \frac{1}{Z}\sum_n \mathrm{e}^{-\beta E_n}\,\langle n|A|n\rangle = \frac{1}{Z}\,\mathrm{tr}\left[\mathrm{e}^{-\beta H}A\right] \tag{1.1}$$

with the partition function $Z = \mathrm{tr}\left[\mathrm{e}^{-\beta H}\right]$ fixed by $\langle 1\rangle = 1$. Some operators that will turn out to be of interest are of the form

$$A = \prod_{i=1}^{n-1}(\mathrm{e}^{\tau_i H}A_i\mathrm{e}^{-\tau_i H}) \tag{1.2}$$

with $\beta = \tau_n > \tau_{n-1} > \cdots > \tau_0 = 0$ and the product defined in descending order, i.e.

$$\prod_{i=0}^{k+1} x_i = x_{k+1}\prod_{i=0}^{k} x_i.$$

These are equivalent to time ordered products of Heisenberg picture operators after a Wick rotation of the time variable onto the imaginary axis, but here they are defined without actually making use of the concept of time, which after all is not relevant in a system at thermal equilibrium. The trace becomes

$$\mathrm{tr}\left[\mathrm{e}^{-\beta H}A\right] = \mathrm{tr}\left[\mathrm{e}^{-(\beta-\tau_{n-1})H}A_n\mathrm{e}^{-(\tau_{n-1}-\tau_{n-2})H}A_{n-1}\ldots A_1\mathrm{e}^{-\tau_1 H}\right],$$

i.e., it consists of several *energy transporters* $\mathrm{e}^{-\tau H}$ which are interspersed by operators A_i and whose shifts sum up to β.

For example, taking two operators with $\tau_1 = 0$ and $\tau_2 = \tau$ results in

$$\begin{aligned}\langle A\rangle &= \frac{1}{Z}\operatorname{tr}\left[\mathrm{e}^{-(\beta-\tau)H}A_2\mathrm{e}^{-\tau H}A_1\right]\\ &= \frac{1}{Z}\sum_{m,n}\left\langle m\middle|\mathrm{e}^{-(\beta-\tau)H}A_2\middle|n\right\rangle\left\langle n\middle|\mathrm{e}^{-\tau H}A_1\middle|m\right\rangle\\ &= \frac{\sum_{m,n}\mathrm{e}^{-(\beta-\tau)E_m}\langle m|A_2|n\rangle\,\mathrm{e}^{-\tau E_n}\langle n|A_1|m\rangle}{\sum_m \mathrm{e}^{-\beta E_m}}\\ &= \frac{\sum_{m,n}\mathrm{e}^{-\beta(E_m-E_0)-\tau(E_n-E_m)}\langle m|A_2|n\rangle\langle n|A_1|m\rangle}{\sum_m \mathrm{e}^{-\beta(E_m-E_0)}}.\end{aligned}$$

Here, the trace is evaluated using the energy eigenstates $|n\rangle$ with energy E_n. Assuming that the ground state[1] is given by a single state with $E_0 < E_i\ \forall i \neq 0$, in the zero temperature limit ($\beta \to \infty$) the only relevant terms both in the nominator and in the denominator are those with $m = 0$, so

$$\lim_{\beta\to\infty}\langle A\rangle = \sum_n \mathrm{e}^{-\tau(E_n-E_0)}\langle 0|A_2|n\rangle\langle n|A_1|0\rangle\,.$$

For the choice $A_2 = A_1^\dagger$, the leading exponential decay for large τ is given by the lowest energy that has non-vanishing $\langle n|A_1|0\rangle$. If the spectrum of the considered theory contains particle excitations and $A_1|0\rangle$ is a superposition of several states with different particle numbers and momenta, the particle combination with the lowest mass will yield the lowest energy, which can be extracted in this way.

In order to compute the trace in (1.1), each transporter $\mathrm{e}^{-\Delta\tau H}$ is split into a large number of infinitesimal shifts of length ε with $\beta = N\varepsilon$ and it is assumed that each of these shifts—not only those at τ_i—is accompanied by operators A_k and B_k on both sides, most of which are simply $\mathbb{1}$. This gives

$$\mathrm{e}^{-\beta H}A = \prod_{k=0}^{N-1} T_k = \prod_{k=0}^{N-1}\left(A_k\mathrm{e}^{-\varepsilon H}B_k\right) \tag{1.3}$$

[1] The ground state is the state with the lowest energy, while the vacuum is the state with particle number 0, i.e., the state that is annihilated by all particle annihilation operators (see below). These are often conflated, but in an interacting theory they are not strictly equivalent.

The observable B_k could be combined with A_{k-1} of the next element, but this general form will allow for an easy split into coordinate- and momentum-dependent observables.

On each side of such an infinitesimal term, some sort of unit matrix in the form of an integral over all possible states of the system is inserted. In general, there will be bosonic as well as fermionic degrees of freedom, and the details of the integration differ between these.

1.1.1 Bosonic Path Integral

Starting with a Hamilton operator $H(Q, P)$ with n generalized coordinate operators Q^i and momentum operators P^i that obey the commutation relations $[Q^i, P^j] = i\delta_{ij}$ and $[Q^i, Q^j] = [P^i, P^j] = 0$, there are two obvious choices for a basis of the Hilbert space, consisting of either the product vectors $|q\rangle = |q^1 q^2 \dots\rangle$ or, similarly, $|p\rangle$. The notation here is such that upper indices denote different degrees of freedom, while lower indices will later be introduced to have different collections of these variables such that q_i is a vector consisting of n entries q_i^j. A unit matrix can be written as

$$\mathbb{1} = \int \mathrm{d}q \, |q\rangle \langle q| = \int \mathrm{d}p \, |p\rangle \langle p|$$

(with each q or p actually being a collection of n variables), a trace is given by

$$\mathrm{tr}\,[A] = \int \mathrm{d}q \, \langle q|A|q\rangle = \int \mathrm{d}p \, \langle p|A|p\rangle \,,$$

and the Fourier relation reads

$$\langle p|q\rangle = (2\pi)^{-n/2} \mathrm{e}^{ipq},$$

which gives another form of the unit matrix as

$$\begin{aligned} \mathbb{1} &= \int \mathrm{d}q \int \mathrm{d}p \, |q\rangle \langle q|p\rangle \langle p| = \int \mathrm{d}q \int \mathrm{d}p (2\pi)^{-n/2} \mathrm{e}^{-ipq} \, |q\rangle \langle p| \\ &\equiv \int \mathrm{d}[q,p] \mathrm{e}^{-ipq} \, |q\rangle \langle p| \end{aligned}$$

This gives

$$\begin{aligned}\operatorname{tr}\left[\mathrm{e}^{-\beta H}A\right] &= \int \mathrm{d}q_0 \left\langle q_0 \middle| \prod_{k=0}^{N-1} T_k \middle| q_0 \right\rangle \\ &= \int \mathrm{d}q_0 \left\langle q_0 \middle| \prod_{k=0}^{N-1} \left(\int \mathrm{d}[q_{k+1}, p_k] \mathrm{e}^{-ip_k q_{k+1}} \left|q_{k+1}\right\rangle \left\langle p_k\right| T_k \right) \middle| q_0 \right\rangle \\ &= \prod_{k=0}^{N-1} \left(\int \mathrm{d}[q_k, p_k] \mathrm{e}^{-ip_k q_{k+1}} \left\langle p_k | T_k | q_k \right\rangle \right) \Bigg|_{q_N = q_0} .\end{aligned}$$

For the remaining scalar product it will be assumed that the observable A_k in (1.3) is a function of P only and B_k of Q only. Also, the Hamilton operator H is a sum of terms that are sorted such that in each term all Ps are to the left of all Qs. Then,

$$\begin{aligned}\left\langle p_k | T_k | q_k \right\rangle &= a_k \left\langle p_k \middle| (1 - \varepsilon H(Q,P) + \mathcal{O}(\varepsilon^2)) \middle| q_k \right\rangle b_k \\ &= a_k b_k \mathrm{e}^{-\varepsilon H(q_k, p_k)} (2\pi)^{-n/2} \mathrm{e}^{ip_k q_k} + \mathcal{O}(\varepsilon^2),\end{aligned}$$

which, with

$$\int \mathcal{D}[q,p] \ldots = \prod_{k=0}^{N-1} \left(\int \frac{\mathrm{d}q_k \mathrm{d}p_k}{(2\pi)^n} \right) \ldots \Bigg|_{q_0 = q_N}$$

and $\dot{q}_k = \frac{q_k - q_{k-1}}{\varepsilon}$, gives the result

$$\begin{aligned}\operatorname{tr}\left[\mathrm{e}^{-\beta H}A\right] &= \int \mathcal{D}[q,p] \prod_k \left(a_k b_k \mathrm{e}^{-\varepsilon H(q_k,p_k) - ip_k(q_{k+1} - q_k)} \right) \\ &= \int \mathcal{D}[q,p] \prod_k (a_k b_k) \mathrm{e}^{-\varepsilon \sum_k (H(p_k,q_k) - ip_k \dot{q}_k)} \\ &= \int \mathcal{D}[q,p] A(p,q) \mathrm{e}^{-\int_0^\beta \mathrm{d}\tau (H(p,q) - ip\dot{q})}.\end{aligned} \tag{1.4}$$

In the last step, the observable

$$A(p,q) = \prod_i A_i(p(\tau_i), q(\tau_i))$$

has been reinserted and the sum over energy shifts has been written as an integral with p and q understood as functions of τ. This is the *Euclidean path integral* in phase space, where each "history" of the system (i.e., set of functions $p(\tau)$ and $q(\tau)$ defined on $[0, \beta]$ with $q(\tau)$ being periodic) makes a contribution to the trace.

In all cases that will be relevant, the Hamilton operator is quadratic in the momenta and, assuming that the observable does not depend on the momenta, these integrals can be evaluated to give a path integral in coordinate space. Starting with a quadratic function

$$G(p) = -A_{ij}p^i p^j + 2b_i p^i$$

with a real positive definite matrix A, it is possible to diagonalize $A = R^\dagger D R$ with an orthogonal matrix R and, using $\eta = Rb$, the integral becomes

$$\begin{aligned}
\int \mathrm{d}^n p \mathrm{e}^{G(p)} &= \int \mathrm{d}^n p \mathrm{e}^{-D_{ij}(Rp)^i(Rp)^j + 2\eta_i(Rp)^i} \\
&= \prod_i \left(\int \mathrm{d}x \mathrm{e}^{-D_{ii}x^2 + 2\eta_i x} \right) \\
&= \prod_i \left(\sqrt{\frac{\pi}{D_{ii}}} \mathrm{e}^{\eta_i^2 D_{ii}^{-1}} \right) \\
&= \pi^{n/2} |\det[A]|^{-1/2} \mathrm{e}^{(D^{-1})_{ij}\eta_i\eta_j} \\
&= \pi^{n/2} |\det[A]|^{-1/2} \mathrm{e}^{(A^{-1})_{ij}b_i b_j} \\
&= \pi^{n/2} |\det[A]|^{-1/2} \mathrm{e}^{G(A^{-1}b)}.
\end{aligned}$$

Except for the prefactor, this is exactly the result of evaluating the integrand $\mathrm{e}^{G(p)}$ at the point where $\frac{\mathrm{d}}{\mathrm{d}p}G(p) = 0$, which also holds if a constant is added to $G(p)$.

For $H = P^t \alpha P + \beta^t P + \gamma$, the momentum integral at one specific τ therefore becomes

$$\int \mathrm{d}^n p \mathrm{e}^{-\varepsilon(H(p,q) - i\dot{q}p)} = \pi^{n/2} \det[\varepsilon\alpha]^{-1/2} \mathrm{e}^{-\varepsilon(H(\bar{p},q) - i\dot{q}\bar{p})},$$

where $\bar{p}$ is defined by $i\dot{q} = \frac{\mathrm{d}}{\mathrm{d}p}H(p,q)|_{p=\bar{p}}$, i.e. $\bar{p} = 1/2\alpha(i\dot{q} - \beta)$. This, however, is just

$$\pi^{n/2} \det[\varepsilon\alpha]^{-1/2} \mathrm{e}^{-\varepsilon L_E(q,\dot{q})}$$

with the *Euclidean Lagrange function* $L_E(q,\dot{q}) = -L(q,i\dot{q})$.

In conclusion, the path integral in Lagrange form is

$$\begin{aligned}\mathrm{tr}\left[\mathrm{e}^{-\beta H}A\right] &= \prod_{k=0}^{N-1}\left(\int\frac{\mathrm{d}q_k}{(2\pi\varepsilon)^{n/2}}\right)\det[\alpha]^{-1/2}A(q)\mathrm{e}^{-\varepsilon\sum_k L_E(q,\dot{q})}\Big|_{q_N=q_0}\\ &\equiv \int\mathcal{D}qA(q)\mathrm{e}^{-\int_0^\beta \mathrm{d}\tau L_E(q,\dot{q})}\end{aligned} \tag{1.5}$$

There are a few complicating cases that will not be covered here in detail (but see [9]). For example, the matrix α that couples the time derivatives to each other could depend on the coordinates q. In this case the determinant can not be pulled out of the integral, inducing instead a change in the Lagrange function entering the path integral with respect to that of the classical theory by use of $\det[\alpha] = \mathrm{e}^{\mathrm{tr}[\ln\alpha]}$. Another possibility is that some of the fields only enter the Lagrange function directly and not also through their time derivatives. In this case, only a subset of the coordinates can be canonically quantized and the other ones provide constraints instead. Even though the path integral will not be performed over the other coordinates, it is sometimes possible to insert such an integral in addition to the others and thereby regain the original form of the Lagrange function. This is the case, for example, for a massive vector field.

A similar complication that is more interesting is that of a gauge field. Details of how the gauge field of quantum chromodynamics is defined will be given in the next chapter, but here it will be already mentioned that in the process of canonical quantization it has the difficulty that the time derivative of the time component does not enter the Lagrange function (as in the case of the massive vector field) and additionally that different gauge fields represent the same physical situation. Conceptually, one possible way to see the problem is that the time component of the gauge field lives, in a sense, between two adjacent points in time, which is problematic in the Hamilton formulation that is not build in terms of histories of the system but in terms of values at a specific time. On the level of the classical theory, this is articulated by the fact that it is not possible to get the gauge field at all times from its values and derivatives at one time. The solution can be found in [12] and is only sketched here. The gauge has to be partially fixed by demanding the gauge field in time direction to vanish. This restores determinism on the level of the gauge field, but

since there is still a spatial gauge freedom, the integrals over all states that are needed in the path integral derivation have to be performed only over physically different states. This can be done by inserting corresponding projections, which themselves can be written as integrals over an auxiliary field. This auxiliary field takes the place of the original time component of the gauge field, so the path integral is again over the original Lagrange function (with time derivatives as well as the time component of the gauge field multiplied by i) and with the integral performed over all gauge fields, even if some of them yield the same physical history. It is afterwards also possible to fix the gauge by separating the integral into one over different physical orbits and one over different gauge fields within one orbit, but it is not required except for perturbation theory.

1.1.2 Fermionic Path Integral

As in the case of bosons, exchanging two fermions of the same species does not yield a new state, but in this case the sign of the state changes. This results in creation and annihilation operators anticommuting with each other, which also carries over to the field operators. Taking again generalized coordinates Q^i and momenta P^i, this means $\{Q^i, P^j\} = i\delta_{ij}$ and $\{Q^i, Q^j\} = \{P^i, P^j\} = 0$. It is not possible to define eigenstates of these operators in the usual sense since they are nilpotent and the eigenvalues would also need to give zero when squared. While this is not possible for real numbers unless they are zero, the solution is to use *Grassmann numbers*, which are just elements of an algebra of numbers q^i, p^i which anticommute with each other as well as with the operators Q^i and P^i.

While in some theories P^i is related to the Hermitian conjugate of Q^i, sometimes they are independent and treating them as such will allow to cover both cases. The eigenstates are then defined as

$$|q\rangle = \exp\left(-i\sum_i P^i q^i\right)|0\rangle \qquad \langle p| = \langle 0|\exp\left(-i\sum_i p^i Q^i\right)$$

where $|0\rangle$ and $\langle 0|$ are states that fulfill $Q^a|0\rangle = 0$ and $\langle 0|P^a = 0$ for all a and are normalized by $\langle 0|0\rangle = 1$. All states of the system can be obtained by acting with some non-vanishing combination of P^is on $|0\rangle$ or Q^is on $\langle 0|$.

When checking that these are indeed eigenstates, it is necessary to split the exponential into the term containing P^i and the rest, using $\exp(\eta) = 1+\eta$ for η being a product of Grassmann variables and the fact that Q^i can be moved through the second term because it no longer contains P^i, which gives 0 because it then acts on $|0\rangle$:

$$\begin{aligned} Q^i |q\rangle &= Q^i(1 - iP^i q^i) \exp\left(-i \sum_{j\neq i} P^j q^j\right) |0\rangle \\ &= -i(i - P^i Q^i) q^i \exp\left(\sum_{j\neq i} P^j q^j\right) |0\rangle \\ &= q^i \exp\left(\sum_{j\neq i} P^j q^j\right) |0\rangle = q^i |q\rangle . \end{aligned}$$

In the last step, the missing term $1 - iP^i q^i$ was again inserted, which does not change the result because of $q^i q^i = 0$. In the same way it is possible to prove $\langle p| P^a = \langle p| p^a$. The scalar product of these states is given by

$$\begin{aligned} \langle p|q\rangle &= \left\langle 0 \middle| \prod_i (1 - ip^i Q^i) \prod_j (1 - iP^j q^j) \middle| 0 \right\rangle \\ &= \left\langle 0 \middle| \prod_{ij} \Big((1 - iP^j q^j)(1 - ip^i Q^i) + i\delta_{ij} q^j p^i \Big) \middle| 0 \right\rangle \\ &= \mathrm{e}^{-ipq} \end{aligned}$$

Integration over Grassmann variables is defined in such a way that it picks out coefficients of those terms that contain each variable over which the integration takes place exactly once. This can be achieved by requiring $\int \mathrm{d}\eta\eta = 1$ and $\int \mathrm{d}\eta = 0$ for any Grassmann variable. The relevant differences to the bosonic case lie in the completeness relation (i.e., the form of the unit operator) and the trace. For these, the particle states

$$|\alpha\rangle = \prod_{i\in\alpha} P^i |0\rangle \qquad\qquad \langle\alpha| = \langle 0| \widetilde{\prod_{i\in\alpha}} Q^i$$

are defined, where α is some subset of $\{1 \ldots n\}$ with n being the number of degrees of freedom, and the product with the tilde being understood in

the opposite order of that without it. The scalar product is given by

$$\langle\alpha|\alpha'\rangle = \delta_{\alpha\alpha'} \left\langle 0 \middle| \prod_{i\in\alpha} (Q^i P^i) \middle| 0 \right\rangle = \delta_{\alpha\alpha'} \left\langle 0 \middle| \prod_{i\in\alpha} (i - P^i Q^i) \middle| 0 \right\rangle = i^{|\alpha|} \delta_{\alpha\alpha'},$$

giving the completeness relation

$$\mathbb{1} = \sum_\alpha i^{-|\alpha|} \left|\alpha\right\rangle \left\langle\alpha\right| .$$

Using the Grassmann integration measure $\int \mathcal{D}[q,p] = \int \prod_i (\mathrm{d}q^i \mathrm{d}p^i)$, the completeness relation in terms of the eigenstates $|q\rangle$ and $\langle p|$ is then given by

$$\begin{aligned}
\mathbb{1} &= \sum_\alpha i^{-|\alpha|} \left|\alpha\right\rangle \left\langle\alpha\right| \\
&= \int \mathcal{D}[q,p] \prod_i (p^i q^i) \sum_\alpha i^{-|\alpha|} \prod_{j\in\alpha} P^j \left|0\right\rangle \left\langle 0\right| \widetilde{\prod_{k\in\alpha}} Q^k \\
&= i^{-n} \int \mathcal{D}[q,p] \sum_\alpha \prod_{i\notin\alpha} (ip^i q^i) \prod_{j\in\alpha} (-iP^j q^j) \left|0\right\rangle \left\langle 0\right| \prod_{k\in\alpha} (-ip^k Q^k) \\
&= i^{-n} \int \mathcal{D}[q,p] \prod_i (1 + ip^i q^i) \prod_j (1 - iP^j q^j) \left|0\right\rangle \left\langle 0\right| \prod_k (1 - ip^k Q^k) \\
&= i^{-n} \int \mathcal{D}[q,p] \mathrm{e}^{ipq} \left|q\right\rangle \left\langle p\right|
\end{aligned}$$

The equivalence of the third and fourth line of this derivation is due to the fact that any term that survives the integration has to contain exactly one of each p^i and q^i, so when the products in the fourth line are multiplied, for each i either the linear term of the first product has to be paired with the constant terms of the other products or the other way round.

Similarly, the trace of a bosonic operator can be written as

$$\begin{aligned}
\mathrm{tr}\,[A] &= \sum_\alpha i^{-|\alpha|} \left\langle\alpha|A|\alpha\right\rangle \\
&= i^{-n} \int \mathcal{D}[q,p] \prod_{i\notin\alpha} (ip^i q^i) \sum_\alpha \left\langle 0 \middle| \prod_{j\in\alpha} (ip^j Q^j) A \prod_{k\in\alpha} (-iP^k q^k) \middle| 0 \right\rangle \\
&= i^{-n} \int \mathcal{D}[q,p] \mathrm{e}^{ipq} \left\langle -p|A|q\right\rangle .
\end{aligned}$$

The rest of the derivation proceeds similarly to the bosonic case, with

$$\begin{aligned}\operatorname{tr}\left[\mathrm{e}^{-\beta H}A\right] &= \int \mathcal{D}[q_0,p_0]\mathrm{e}^{ip_0q_0}\left\langle -p_0\middle|\prod_{k=0}^{N-1}T_k\middle|q_0\right\rangle \\ &= \int\prod_{k=0}^{N-1}\left(\mathcal{D}[q_k,p_k]\mathrm{e}^{ip_kq_k}\right)\left\langle -p_0\middle|\prod_{k=1}^{N-1}\left(T_k\left|q_k\right\rangle\left\langle p_k\right|\right)T_0\middle|q_0\right\rangle .\end{aligned}$$

The factors i^n are irrelevant and omitted because they cancel with corresponding factors in $1/Z$. Assuming that the Hamilton is sorted such that any P is to the left of any Q, this gives elements like

$$\begin{aligned}\mathrm{e}^{ip_kq_k}\left\langle p_k\middle|\mathrm{e}^{-\varepsilon H(P,Q)}\middle|q_{k-1}\right\rangle &= \mathrm{e}^{ip_k(q_k-q_{k-1})-\varepsilon H(p_k,q_{k-1})} \\ &= \mathrm{e}^{-\varepsilon(H(p_k,q_{k-1})-ip_k\dot{q}_{k-1})}\end{aligned}$$

with possible extra terms from the observable. The leftmost element requires special care,

$$\begin{aligned}\mathrm{e}^{ip_0q_0}\left\langle -p_0\middle|\mathrm{e}^{-\varepsilon H(P,Q)}\middle|q_{N-1}\right\rangle &= \mathrm{e}^{ip_0q_0-\varepsilon H(-p_0,q_{N-1})+ip_0q_{N-1}} \\ &= \mathrm{e}^{-\varepsilon(H(p_N,q_{N-1})-ip_N\dot{q}_{N-1})}\Big|_{\substack{q_N=-q_0\\p_N=-p_0}}\end{aligned}$$

and the result is

$$\begin{aligned}\operatorname{tr}\left[\mathrm{e}^{-\beta H}A\right] &= \int\mathcal{D}[q,p]A(p,q)\mathrm{e}^{-S_E[p,q]} \\ S_E[p,q] &= \varepsilon\sum_{k=0}^{N-1}\left(H(p_{k+1},q_k)-ip_{k+1}\dot{q}_k\right)\Big|_{\substack{q_N=-q_0\\p_N=-p_0}}\end{aligned} \tag{1.6}$$

In contrast to the bosonic case, the momentum integrals are not solved in order to arrive at the Lagrange form of the path integral. Instead, in the cases of interest the Lagrange function is given by

$$L(q,\bar{q},\dot{q}) = \bar{q}A\dot{q} - \bar{q}Bq, \tag{1.7}$$

where q is a complex vector and $\bar{q}$ is proportional to the complex conjugate of q. The degrees of freedom are given by the real and imaginary parts of the entries in $q = x + iy$, but by analytic continuation to complex x and y

it is possible to make a change of variables from x, y to $q, \bar{q}$, which are then again restricted to real values. Therefore, q and $\bar{q}$ have to be regarded as independent variables in such a construction. The advantage is that in (1.7), of the $2n$ coordinates only an n-dimensional submanifold enters the Lagrange function in the form of a time derivative and by this procedure there is a clear separation into those coordinates with time derivative (q) and those without ($\bar{q}$).

In order to obtain the Hamilton function, a Legendre transformation with respect to $\dot{q}$ has to be performed, giving

$$H(q,\bar{q},p) = \sup_{\dot{q}} \left(p\dot{q} - L(q,\bar{q},\dot{q})\right) = \sup_{\dot{q}} \left((p-\bar{q}A)\dot{q} + \bar{q}Bq\right).$$

this is only finite if $p = \bar{q}A$, so it is only defined in this point and has the value $H = \bar{q}Bq$ there.[2] Variation of p in the classical theory and the proper anticommutation relations in the canonically quantized theory can be obtained indirectly through $\bar{q}$, so the correct quantization prescription would be to require $\{q^i, (\bar{q}A)^j\} = i\delta_{ij}$. As long as A is constant, the fermionic integrals over q and p can as well be performed over q and $\bar{q}$, giving

$$\begin{aligned} S_E &= \int_0^\beta \mathrm{d}\tau L_E(q,\bar{q},\dot{q}) \\ L_E(q,\bar{q},\dot{q}) &= H(q,\bar{q},p) - ip\dot{q}|_{p=\bar{q}A} = \bar{q}Bq - i\bar{q}A\dot{q} = -L(q,\bar{q},i\dot{q}), \end{aligned}$$

exactly as in the bosonic case.

1.2 Quantum Chromodynamics

The standard model of particle physics consists of the underlying framework of quantum field theory on the one hand and a specific particle con-

[2] The definition of the Legendre transformation given here is more general than the prescription often found in lectures on classical mechanics which involves taking the derivative of the function with respect to the variable in question. In particular, applying the Legendre transformation to the Hamilton function should again return the Lagrange function, but it is not possible to take a derivative with respect to a variable if the function is only defined at one value of this variable. However,

$$\sup_{p\in\{\bar{q}A\}} \left(p\dot{q} - H(q,\bar{q},p)\right) = \bar{q}A\dot{q} - H(q,\bar{q},\bar{q}A) = L(q,\bar{q},\dot{q}).$$

tent on the other hand. The content of the theory is highly restricted by the requirement of Poincaré symmetry, which requires the degrees of freedom to transform according to some representation of the Poincaré group. By forming special combinations of the translation and boost generators of this symmetry group (or, rather, of its subgroup that is simply connected to the identity transformation), it is possible to specify each representation by a pair of numbers (A, B) which are multiples of $1/2$. Space inversion, which is not part of this simply connected subgroup, takes a particle of the representation (A, B) and transforms it into a particle of the representation (B, A). In order to describe a theory that is invariant under space inversions, the particles therefore either have to be in a representation of the form (A, A) or in the direct sum $(A, B) \oplus (B, A)$.

The theory of interest for this work is Quantum Chromodynamics (or QCD), which is a quantum field theory that very successfully describes the strong nuclear interaction. As far as it is currently known, the strong interaction respects space inversion symmetry, and QCD is usually constructed to reflect this. Its constituents are quarks of the type $(1/2, 0) \oplus (0, 1/2)$ (i.e., Dirac fermions) and gluons of the type $(1/2, 1/2)$. Requiring the theory to respect causality results in a formulation in terms of quantum fields that are specific combinations of particle creation and annihilation operators. In the case of quarks these are denoted by $\psi(x)$ and its conjugate $\bar{\psi}(x)$, which like all Dirac fermions have 4 internal degrees of freedom owing to the dimensionality of the Dirac representation. In the case of QCD, the number of degrees of freedom is additionally multiplied by 3 because they come in three *colors*, which are just three distinct particle species that are equal in all respects except this additional quantum number.

The starting point for deriving the QCD Lagrange density is that of free Dirac particles,

$$\mathcal{L}_E(x) = \bar{\psi}(x)\gamma_\mu \partial_\mu \psi(x) + m\bar{\psi}(x)\psi(x)$$

which is here given directly in the Euclidean formulation with the Euclidean gamma matrices that fulfill $\{\gamma_\mu, \gamma_\nu\} = 2\delta_{\mu\nu}$. The theory is symmetric under the global transformation

$$\psi'(x) = \Omega\psi(x) \qquad \bar{\psi}'(x) = \bar{\psi}\Omega^\dagger \qquad \Omega \in \mathrm{SU}(3)$$

that mixes the different color components using a unitary transformation with determinant 1. The full gauge theory can be derived more or less

completely by the requirement that this symmetry also holds for any *local gauge transformation*, where Ω can be different on each point in spacetime. For bilinears like $\bar{\psi}(x)\psi(x)$, this is trivially the case. The derivative term, however, becomes

$$\begin{aligned}\bar{\psi}'\gamma_\mu\partial_\mu\psi' &= \bar{\psi}\gamma_\mu\Omega^\dagger\partial_\mu(\Omega\psi)\\ &= \bar{\psi}\gamma_\mu\partial_\mu\psi + \bar{\psi}\gamma_\mu(\Omega^\dagger\partial_\mu\Omega)\psi. \end{aligned} \tag{1.8}$$

The problem is that $\partial_\mu\psi(x)$ is a difference between fermion fields at infinitesimally different spacetime points and before they can be subtracted and contracted with $\bar{\psi}(x)$ they have to be *gauge transported* onto the same point. This situation is similar to that in general relativity, where in a curved spacetime a vector that is parallel transported around a closed path generally changes its direction. A fermion field $\psi(x)$ and its gauge transported version at y along a specific path $\mathcal{C}$ are related by an SU(3) matrix $U_\mathcal{C}$. It is additive, in the sense that the gauge transporter along the path $\mathcal{C}_1 + \mathcal{C}_2$ where $\mathcal{C}_2$ is appended to $\mathcal{C}_1$ is given by

$$U_{\mathcal{C}_1+\mathcal{C}_2} = U_{\mathcal{C}_2}U_{\mathcal{C}_1}.$$

Additionally, it has to commute with a local gauge transformation, i.e., it should not make a difference if a field at x is first transported to y and then transformed with $\Omega(y)$ or first transformed with $\Omega(x)$ and then transported. This requires the gauge transporter itself to transform according to

$$U'_\mathcal{C} = \Omega(y)U_\mathcal{C}\Omega^\dagger(x) \qquad\qquad \mathcal{C} : x \to y.$$

Writing an infinitesimal transporter that transports from $x + \varepsilon\hat{\mu}$ to x, where $\hat{\mu}$ is the unit vector in direction μ, as $U_{\varepsilon\mu} = \exp(i\varepsilon A_\mu(x))$, the *covariant derivative*—which is like the derivative, but includes a gauge transport before subtracting fields at different points—is given by

$$\begin{aligned}D_\mu(x)\psi(x) &= \lim_{\varepsilon\to 0}\frac{1}{\varepsilon}\left(\mathrm{e}^{i\varepsilon A_\mu(x)}\psi(x+\varepsilon\hat{\mu}) - \psi(x)\right)\\ &= (\partial_\mu + iA_\mu(x))\psi(x)\end{aligned}$$

The field $A_\mu(x)$ is called *gauge field* and the particles described by it are called *gluons*. In order for $\exp(i\varepsilon A_\mu(x))$ to be an element of SU(3), A_μ

has to be an element of the Lie algebra su(3), i.e., it has to be a traceless and Hermitian 3×3 matrix. The transformation property under gauge transformations can be derived from that of $U_{\varepsilon\mu}$, giving

$$\begin{aligned} 1 + i\varepsilon A'_\mu &= \Omega(x)(1 + i\varepsilon A_\mu)\Omega^\dagger(x + \varepsilon\hat{\mu}) \\ &= 1 + i\varepsilon\Omega A_\mu\Omega^\dagger + \varepsilon\Omega\partial_\mu\Omega^\dagger - \underbrace{\varepsilon\partial_\mu(\Omega\Omega^\dagger)}_{=0} \\ \Rightarrow \quad A'_\mu &= \Omega A_\mu\Omega^\dagger + i\partial_\mu\Omega\Omega^\dagger. \end{aligned} \tag{1.9}$$

The covariant derivative transforms according to

$$\begin{aligned} D'_\mu \ldots &= \partial_\mu(\Omega\Omega^\dagger \ldots) + i\Omega A_\mu\Omega^\dagger \cdots - \partial_\mu\Omega\Omega^\dagger \ldots \\ &= \Omega\partial_\mu(\Omega^\dagger \ldots) + i\Omega A_\mu\Omega^\dagger \ldots \\ &= \Omega D_\mu(\Omega^\dagger \ldots), \end{aligned}$$

giving

$$(D_\mu\psi)' = \Omega D_\mu\psi$$

and therefore

$$\mathcal{L}'_E = \mathcal{L}_E \qquad \text{with} \quad \mathcal{L}_E = \bar{\psi}(\gamma_\mu D_\mu + m)\psi.$$

The contraction $\gamma_\mu D_\mu$ is often denoted by $\not{D}$ in continuum formulations where there is only this one form, but for consistency with the lattice formulation given later this *Dirac operator* is just written as D.

In analogy to the curvature tensor in general relativity, which encapsulates information about parallel transportation along an infinitesimal closed path, a field strength tensor can be defined by

$$F_{\mu\nu} = -i[D_\mu, D_\nu] = \partial_\mu A_\nu - \partial_\nu A_\mu + i[A_\mu, A_\nu],$$

Since it inherits the transformation property from D_μ, a gauge invariant object can be constructed by

$$\operatorname{tr}\left[F_{\mu\nu}F_{\mu\nu}\right].$$

A term proportional to this is compatible with the required (i.e., Poincaré and gauge) symmetries and because it is also renormalizable[3], it generally has to be included. It contains the kinetic term of the gauge field as well as self-interactions, which are automatically included into the theory. The Lagrange density of continuum QCD for a single quark species now compactly reads

$$\mathcal{L} = \bar{\psi}(D + m)\psi + \frac{1}{2g^2} \operatorname{tr}\left[F_{\mu\nu}F_{\mu\nu}\right],$$

where g is the coupling constant. It is called like this because it is possible to rescale the gauge fields such that the kinetic term is independent of g, which then instead appears in front of the interaction term $i\bar{\psi}\gamma_\mu A_\mu \psi$.

Even if quarks are ignored and only the gauge part of the action is investigated, it is the source for a variety of phenomena because of the self-interaction encoded in the non-commutativity of the SU(3) gauge group. This theory is usually called by the name of *Yang-Mills theory* or just *pure gauge theory*.

1.3 Chiral Symmetry and the Axial Anomaly

In nature, until now six quark flavors have been found, which are usually categorized into three families by their weak interaction quantum numbers. They come with widely different masses, which are listed in table 1.1. However, quarks never have been observed as free particles but only in color-neutral combinations, so it is problematic to unambiguously define (or, for that matter, measure) their masses. The way they enter the QCD action is as bare parameters, which can only be assigned some physical value within some renormalization scheme. Possibilities to build color-neutral combinations include mesons and baryons, which are states that are approximately built out of either a quark-antiquark pair or three quarks. The lightest mesons are the pions with masses of around 140 MeV and the lightest baryons are the proton and the neutron, both with masses of about 1 GeV. There is a hierarchical separation with the up and down

[3] This is a requirement that eliminates terms with too high powers of the contained fields, because these would require coupling constants of negative mass dimension, which for example results in diverging cross-sections at high energies [13].

flavor	mass	
up (u)	2.3(7)	MeV
down (d)	4.8(5)	MeV
strange (s)	95(5)	MeV
charm (c)	1.275(25)	GeV
beauty (b)	4.18(3)	GeV
truth (t)	160(5)	GeV

Table 1.1: Approximate masses of the different known quark flavors in $\overline{MS}$ renormalization at $\mu \approx 2\,\mathrm{GeV}$ [1].

quarks being almost massless in comparison with the hadronic scale and the strange quark being heavier but still comparable to hadrons, while the charm and heavier quarks are so heavy that they can be neglected in many applications since they will not be produced by thermal fluctuations except at very high temperatures.

In the limit of one or multiple quark flavors with vanishing mass, the QCD Lagrange density has additional internal symmetries consisting of rotations among these flavors. They are usually combined under the name of *chiral symmetry* and the limit where the masses of some of the quarks are sent towards zero is called the *chiral limit*. The simplest form of this symmetry is already present in the most general case; the quark field ψ of each flavor can be multiplied by a phase, while $\bar{\psi}$ is multiplied with the opposite phase, which therefore cancel. This *vector rotation* is actually the starting point of U(1) gauge theory, i.e. electrodynamics.

If N quark flavors have the same (not necessarily vanishing) mass, it is possible to extend these vector rotations to also mix different flavors. If the different flavors are combined into a vector with components ψ_f, the vector rotation reads

$$\bar{\psi}' = \bar{\psi}\mathrm{e}^{-iT} \qquad\qquad \psi' = \mathrm{e}^{iT}\psi \tag{1.10}$$

with $(T\psi)_f = T_{ff'}\psi_{f'}$ and T being an element of the Lie algebra of U(N), i.e. a combination of the unit matrix and a Hermitian traceless part. The rotation group can accordingly be split into $\mathrm{U}(N) \cong \mathrm{U}(1) \times \mathrm{SU}(N)$. It can easily be checked that this generalized vector rotation is indeed a symmetry of the QCD Lagrangian since $D + m$ is trivial (i.e., diagonal)

with regard to the flavor index and therefore commutes with T, so the factor e^{iT} can be pulled past it and cancels with e^{-iT}.

While the presence of this vector symmetry has been crucial for identifying quarks as the constituents out of which all the mesons and baryons are built, it can be argued that for current research the more interesting case is that of *axial symmetry*, where not only the flavors but also the Dirac components are mixed. Taking the general ansatz

$$\bar{\psi}' = \bar{\psi}\mathrm{e}^{i\bar{T}} \qquad\qquad \psi' = \mathrm{e}^{iT}\psi$$

with *a priori* independent T and $\bar{T}$, the invariance of $\bar{\psi}D\psi$ is provided by

$$\bar{T}D = -DT \qquad\qquad \Rightarrow \mathrm{e}^{i\bar{T}}D = D\mathrm{e}^{-iT},$$

while the invariance of $\bar{\psi}m\psi$ requires $\bar{T} = -T$, which gives the vector rotations discussed above. However, if the mass is zero this term vanishes and there is an additional solution with $T = \bar{T}$ for some T that anticommutes with D. Requiring T to only act on internal degrees of freedom, it has to anticommute with each γ_μ separately, which is satisfied if $T \propto \gamma_5 = \prod_\mu \gamma_\mu$. Separating out γ_5 from T, the axial rotation is given by

$$\bar{\psi}' = \bar{\psi}\mathrm{e}^{i\gamma_5 T} \qquad\qquad \psi' = \mathrm{e}^{iT\gamma_5}\psi \tag{1.11}$$

with T now again only acting in flavor space. Again, T is a linear combination of the unit matrix and a traceless Hermitian part, so the axial rotation group can also be split as $\mathrm{U}(N) \cong \mathrm{U}(1) \times \mathrm{SU}(N)$. The name *chiral symmetry* often only refers to the special case of axial symmetry.

Even if the action of a theory is invariant under some symmetry transformation, it turns out that the path integral measure $\int\mathcal{D}[\psi,\bar{\psi}]$ can also change, which results in expectation values not being invariant under the symmetry in question. This is the case for the singlet axial symmetry $\mathrm{U}_A(1)$, i.e. $\psi' = \mathrm{e}^{i\alpha\gamma_5}\psi, \bar{\psi}' = \bar{\psi}\mathrm{e}^{i\gamma_5\alpha}$ with $\alpha \in \mathbb{R}$. This results in the nonconservation of the axial current, which is known as the *axial anomaly*. In order to derive this, it is necessary to regularize the path integral, i.e. somehow make the integral over infinitely many integration variables finite with some parameter that can be sent towards some limit at the end of the calculation such that the regulator is removed. In section 2.2, a derivation that uses the lattice as a regulator will be given. Another derivation with a different regulator can be found in [14].

There is also another case where a symmetry of the action does not translate to expectation values respecting this symmetry. This is provided by the important concept of spontaneous symmetry breaking, where there is a family of states of the system that yield the same minimal energy, i.e. multiple degenerate vacua. Naively, the thermal expectation value $\mathrm{tr}\left[\mathrm{e}^{-\beta H} A\right]$ would still respect the symmetry because it is given by a sum over all states and each vacuum state enters with the same weight. However, even a small disturbance will set one particular vacuum apart, changing the expectation values drastically. In the case of chiral symmetry, it has been observed that for $N = 2$, even the remaining $\mathrm{SU}_A(2)$ that is not affected by the anomaly is broken spontaneously, which can for example be demonstrated by the fact that protons and neutrons have masses of about 940 MeV [1] while their parity partner N^* has a mass of about 1535 MeV—if chiral symmetry were respected by the ground state, these masses would be degenerate [15]. While the masses of the lightest quarks of about 5 MeV can not explain such a large breaking of chiral symmetry directly, they can provide the small perturbation that picks a specific vacuum for the spontaneously broken symmetry. For large temperatures, any spontaneously broken symmetry will be restored because states with higher energy (and therefore also the other vacua) enter the trace. For chiral symmetry, this is the case beyond the transition temperature of 154(9) MeV [16].

The order of this chiral phase transition and the exact symmetry breaking pattern are of great interest for the understanding of the phase diagram of strongly interacting matter and its properties at different extreme conditions. In this context it is important to know how large the effects of the axial anomaly at the chiral transition temperature are, since this affects the effective symmetries that a strongly interacting system below and above T_c has. If the symmetry breaking pattern is known, further details like the order of the transition and critical exponents can be obtained by analyzing different systems with the same symmetries, which are therefore in the same universality class [17, 18, 19, 20].

With respect to chiral symmetry, Dirac fermions do not furnish an irreducible representation. Instead, they can be decomposed into chiral (i.e.,

left- and righthanded) parts by

$$\psi_\pm = P_\pm \psi = \frac{1 \pm \gamma_5}{2}\psi \qquad\qquad \bar{\psi}_\pm = \bar{\psi} P_\mp .$$

Since $\{\gamma_5, D\} = 0$ and therefore $P_\pm D = D P_\mp$, the Lagrange density can be written in terms of these fields as

$$\begin{aligned}\bar{\psi}(D+m)\psi &= \sum_\pm \bar{\psi} P_\mp^2 (D+m)\psi = \sum_\pm \bar{\psi}_\pm P_\mp (D+m)\psi \\ &= \sum_\pm \bar{\psi}_\pm (D P_\pm + m P_\mp)\psi \\ &= \sum_\pm \bar{\psi}_\pm D \psi_\pm + m \sum_\pm \bar{\psi}_\pm \psi_\mp .\end{aligned}$$

Therefore, for vanishing quark mass the right- and lefthanded fields enter the Lagrange density independently and the action is invariant under independent axial (or vector) rotations of these chiral fields. A parity transformation still transforms them into each other.

In order to decide whether chiral symmetry is spontaneously broken or restored at a given temperature, an order parameter has to be measured that is sensitive to this. One candidate is the *chiral condensate*

$$\Sigma = \frac{1}{N_f}\frac{T}{V}\left\langle \bar{\psi}\psi \right\rangle = \frac{1}{N_f}\frac{T}{V}\sum_\pm \left\langle \bar{\psi}_\pm \psi_\mp \right\rangle ,$$

where N_f is the number of flavors that are included in the spinors $\bar{\psi}$ and ψ—usually 2 because the chiral symmetry of two light flavors is considered—and the combination $\bar{\psi}\psi$ is understood to be summed over all degrees of freedom, including an integral over spacetime. The prefactor T/V with T being the temperature of the system and V the three-dimensional volume normalizes Σ by the four-dimensional volume, making it an intensive quantity.[4] If the action is invariant under the axial $\mathrm{SU}_A(2)$ rotation (for example, (1.11) with $T = \alpha\,\mathrm{diag}(1,-1)$ acting in flavor space), $\left\langle \bar{\psi}'\psi' \right\rangle$ must be equal to $\left\langle \bar{\psi}\psi \right\rangle$ because one can be obtained

[4] In the literature, this distinction is often obfuscated by the notation, such that $\left\langle \bar{\psi}\psi \right\rangle$ is written when the intensive quantity is meant.

from the other by a change of integration variables. On the other hand,

$$\begin{aligned}\left\langle \bar{\psi}'\psi' \right\rangle &= \left\langle \bar{\psi} \mathrm{e}^{2i\gamma_5 T} \psi \right\rangle \\ &= \left\langle \cos(2\alpha)\bar{\psi}\psi + i\sin(2\alpha)(\bar{u}\gamma_5 u - \bar{d}\gamma_5 d) \right\rangle \\ &= \cos(2\alpha) \left\langle \bar{\psi}\psi \right\rangle .\end{aligned}$$

Therefore, if chiral symmetry is restored, the chiral condensate must vanish. If, on the other hand, chiral symmetry is spontaneously broken, even a small mass will give significantly more weight to those configurations where the chiral condensate takes a specific value because they are coupled in the Lagrange density as $\mathrm{e}^{-m\bar{\psi}\psi}$. Even after averaging over all gauge configurations, the chiral condensate will therefore take a nonvanishing value.

In contrast to the non-anomalous chiral symmetry, which is a genuine symmetry of the action for vanishing quark masses that is spontaneously broken at low temperatures, it is not so easy to find an order parameter for the anomalous axial symmetry $U_A(1)$. Since $U_A(1)$ is a symmetry of the action, it induces a Noether current that would be conserved if the measure were also invariant, namely the anomalous current

$$J^5_\mu = \bar{\psi}\gamma_\mu\gamma_5\psi.$$

It can be shown that $\partial_\mu J^5_\mu$ is proportional to the topological charge density, which suggests that at high temperatures the axial anomaly has to be suppressed because topological objects like instantons need non-vanishing color-electric fields, which can not fluctuate at high temperatures due to Debye screening [17]. The magnitude of $\partial_\mu J^5_\mu$ could be used as a measure for the restoration of $U_A(1)$, but it is not easy to translate this to a lattice observable. Instead, it is possible to take two observables where one can be obtained from the other by a $U_A(1)$ rotation and compute their difference. While the vanishing of the difference can give an indication of $U_A(1)$ restoration, the possibility that some other pair of observables still gives a finite difference remains.

For example, the difference between the *susceptibilities* of the *pion* and *delta meson* can be used. Both are mesons that are built from *up* and

down quarks and they are described by the (local) operators

$$\delta^i(x) = \frac{1}{\sqrt{2}}\bar{\psi}(x)\tau^i\psi(x)$$
$$\pi^i(x) = \frac{i}{\sqrt{2}}\bar{\psi}(x)\tau^i\gamma_5\psi(x),$$

where τ^i is a Pauli matrix acting on the *up* and *down* flavor components of ψ. For example, $\delta^3(x) = \left(\bar{u}(x)u(x) - \bar{d}(x)d(x)\right)/\sqrt{2}$. The pion is obtained from the delta meson by a $U_A(1)$ rotation with $\alpha = \pi/4$:

$$\begin{aligned}\delta^i(x) = \frac{1}{\sqrt{2}}\bar{\psi}(x)\tau^i\psi(x) &\to \frac{1}{\sqrt{2}}\bar{\psi}(x)\mathrm{e}^{i\alpha\gamma_5}\tau^i\mathrm{e}^{i\alpha\gamma_5}\psi(x)\\ &= \frac{1}{2\sqrt{2}}\bar{\psi}(x)(1+i\gamma_5)\tau^i(1+i\gamma_5)\psi(x)\\ &= \frac{i}{\sqrt{2}}\bar{\psi}(x)\tau^i\gamma_5\psi(x) = \pi^i(x).\end{aligned}$$

The susceptibilities are defined by integration of the correlators, i.e.

$$\begin{aligned}\chi_\delta &= \int \mathrm{d}^4x \left\langle \delta^i(x)\delta^i(0)\right\rangle = \frac{T}{V}\int \mathrm{d}^4x \int \mathrm{d}^4y \left\langle \delta^i(x)\delta^i(y)\right\rangle\\ &= \frac{1}{2}\frac{T}{V}\left\langle \bar{\psi}\tau^i\psi\bar{\psi}\tau^i\psi\right\rangle \end{aligned} \tag{1.12}$$

and similarly for χ_π. Here, no sum over i is intended and it can easily be checked that any choice of i gives the same result. In the last term, $\bar{\psi}\tau^i\psi$ is as always to be understood as scalar product that sums over all degrees of freedom including two flavors and an integral over spacetime. If more flavors are included that are not part of the chiral symmetry under consideration, they do not contribute since τ^i is zero if acting on any other flavor. If more than two flavors are to be considered as degenerate, an analogous chiral symmetry will connect meson susceptibilities that can be expressed by replacing the Pauli matrices with the appropriate generators of SU(n).

With these definitions in place, a measure for $U_A(1)$ breaking is given by

$$\omega = \chi_\pi - \chi_\delta.$$

1.4 QCD Topology

Any gauge configuration that gives a non-vanishing contribution to the path integral must have a finite action, which requires that the Lagrange density for large distances $|x|$ to the origin falls faster than $|x|^{-4}$. Usually, this would require the gauge field A_μ to vanish faster than $|x|^{-1}$, but there are special solutions where it only vanishes as fast as $|x|^{-1}$, as long as the only term of that order is a *pure gauge field*, i.e., gauge-equivalent to $A_\mu = 0$. Using the transformation property (1.9), this simply means

$$0 = \Omega A_\mu \Omega^\dagger + i\partial_\mu \Omega \Omega^\dagger \qquad \Rightarrow A_\mu = -i\Omega^\dagger \partial_\mu \Omega$$

with some element of the gauge group Ω at each point in spacetime.

By only looking at the asymptotic behavior for large distances, Ω can be assumed to only depend on the direction and not on the distance. The solutions can therefore be classified by some mapping from the unit sphere to the gauge group. Actually, there is some freedom in changing Ω by a fixed group element that leads to the same A_μ, which implies that the set of relevant mappings can be reduced to only include those that map a specific point of the unit sphere onto the unit group element. Now it turns out that there are pairs of such mappings that can not be continuously deformed into each other, similar to closed paths on a circle where a path that effectively winds n times around the circle can not be continuously deformed into a path that effectively winds $n' \neq n$ times around it. In the language of topology, the *homotopy group* $\pi_3(\mathrm{SU}(3))$ is not trivial but isomorphic to $\mathbb{Z}$ [14].

This means that there are topologically different gauge configurations that can not be continuously deformed into each other without crossing regions that have infinite action, so the set of all gauge configurations is split into respective equivalence classes. They can be classified by the *topological charge*

$$Q = \frac{1}{16\pi^2} \int \mathrm{d}^4x \, \mathrm{tr}\left[F_{\mu\nu}\tilde{F}_{\mu\nu}\right] = \frac{1}{32\pi^2} \varepsilon_{\mu\nu\rho\sigma} \int \mathrm{d}^4x \, \mathrm{tr}\left[F_{\mu\nu}F_{\rho\sigma}\right], \tag{1.13}$$

which takes an integer value [21] for any gauge field. In order to find a local minimum of the action within a topological sector, it is helpful to

use the inequality

$$\begin{aligned} 0 &\leq \mathrm{tr}\left[\int \mathrm{d}^4x \left(F_{\mu\nu} \pm \tilde{F}_{\mu\nu}\right)^2\right] \\ &= \mathrm{tr}\left[\int \mathrm{d}^4x \left(2F_{\mu\nu}F_{\mu\nu} \pm 2F_{\mu\nu}\tilde{F}_{\mu\nu}\right)\right] \\ \Rightarrow \quad S[F] &\geq \frac{1}{2g^2}\left|\int \mathrm{d}^4x\, \mathrm{tr}\left[F_{\mu\nu}\tilde{F}_{\mu\nu}\right]\right|, \end{aligned}$$

where $\tilde{F}_{\mu\nu}\tilde{F}_{\mu\nu} = F_{\mu\nu}F_{\mu\nu}$ has been used. In order to reach the lower bound of the action, the gauge field has to be *self-dual* or *anti-self-dual*, which just means that the field strength tensor F is equal in magnitude and equal or opposite in sign to its dual $\tilde{F}$, such that the bracket in the first inequality vanishes.

For $Q = 1$, such a solution has been found in [22], having the form

$$A_\mu(x) = -i\left(\frac{|x|^2}{|x|^2+\rho^2}\right)\Omega^\dagger\partial_\mu\Omega, \qquad \Omega = \frac{x_\mu\alpha_\mu}{|x|}$$

with $\alpha_4 = \mathbb{1}$ and $\alpha_j = i\sigma_j \otimes \mathbb{1}$ for $j = 1, 2, 3$. Here, the Pauli matrices σ_j are acting on the first two color components (i.e., on an SU(2) subgroup of SU(3)) while $\mathbb{1}$ is acting on the third.

This solution is self-dual and localized at $x = 0$ with a size of ρ. Other solutions can be obtained by translations or changes of ρ and they are collectively called *instantons*. Gauge configurations that contain multiple instantons can be constructed by superimposing instanton solutions that are far enough apart that they do not interfere. These solutions have a topological charge of n, where $n \in \mathbb{N}$ is the number of instantons. An anti-instanton can be created by replacing Ω with $\Omega^\dagger$, which changes the sign of A_μ and gives a topological charge of -1. Instantons can also be found in Euclidean formulations of other quantum mechanical systems like a simple double-well potential [23], where it can be seen to be related to a tunneling process that connects one minimum to another. Similarly, in axially fixed gauge ($A_4 = 0$) it is possible to compute a topological index for a three dimensional gauge configuration, which classifies different vacua of the system. A configuration that contains n instantons is then a path that connects vacua with indices that differ by n [24, 25, 14].

In QCD, which is a system that consists of fermions and gauge fields, there is an intricate interaction between these. Since Grassmann variables are rather unintuitive and it is not easy to imagine—or, for that matter, numerically represent—a fermionic path, the phenomenological picture usually introduces a separation. The gauge field is then regarded as a background on which *fermionic modes* live. These are defined as the eigenvectors of the (massive) Dirac operator, because this ensures that the action splits into a sum of terms that each includes a single fermionic mode. Given a fixed background, the fermionic modes do not interact and each mode gives an independent contribution to specific observables, usually as a function of its eigenvalue. Infrared modes, where the eigenvalues are near zero, often contribute the most to these observables. However, the background is not fixed since the presence of fermions influences the weight of each gauge configuration as it enters the path integral. The interaction between different fermion modes is therefore mediated by the gauge field. In particular, it will be shown later that the effect of the fermion modes on the gauge fields is given by the so-called *fermion determinant*, i.e., the product of the eigenvalues of the massive Dirac operator. Therefore, even though infrared modes have a large contribution to observables within a configuration, their presence suppresses the configurations that produce them. The computation of their effect therefore requires great care.

If the fermionic modes on the gauge configuration that is given by the instanton solution above are calculated, it is found that there is a mode that is localized around the instanton with an eigenvalue of the massless Dirac operator of zero [23]. Their form is given by

$$\psi(x) = \frac{\sqrt{2}\rho}{\pi}\left(x^2+\rho^2\right)^{-3/2}\gamma_\mu\hat{x}_\mu\phi_+ \tag{1.14}$$

with ϕ_+ being a constant righthanded spinor which because of $\{\gamma_\mu,\gamma_5\}=0$ makes ψ lefthanded and $\hat{x}_\mu$ being the unit vector pointing from the origin to the space-time point x. At finite quark mass, the eigenvalue is shifted by this mass such that the fermion determinant does not actually vanish. In the chiral limit, however, these zero modes suppress the occurrence of instantons and unless an observable diverges in the chiral limit on a fixed background, configurations with non-trivial topological charge will not contribute to it. However, it is possible to construct gauge fields that contain instantons and anti-instantons at the same time which are not too

far apart, such that the actual fermion modes are superpositions of the would-be zero mode solutions. The interaction can shift the eigenvalues away from zero such that these configurations are not suppressed and, depending on the intricate interplay between gauge fields and fermions, their contribution to certain observables might survive the chiral limit.

1.5 Lattice Discretization of Gauge Invariance

In this section, the lattice regularized version of the purely gluonic path integral is to be given. This introduction is kept very brief, since most of it has already been prepared in section 1.2 and no crucial point hinges on any details that can not be obtained at least equally well from any introductory text book on lattice field theory, like [15, 26, 27].

In order to give a mathematically well-defined meaning to the path integral of any quantum field theory, some sort of regularization has to be introduced. The problem is that there is usually a finite number of integrals to be performed for a single point in spacetime, but since there are infinitely many spacetime points and some of them are infinitely close together, such integrals are ill-defined. The most straightforward regularization is a lattice, which has already been hinted at in the derivation of the path integral where the imaginary time interval has been split into many infinitesimal steps and the step count has been sent to infinity at the end.

Introducing a similar discretization for the space points and postponing the continuum limit, a lattice field theory is defined on a four-dimensional lattice with lattice points $n = (n_1, n_2, n_3, n_4)$ with $n_\mu \in \mathbb{N}$ that correspond to physical points $x = an$. a is the lattice spacing and the continuum limit is performed by sending a to zero. For a Euclidean path integral representation of an expectation value in a canonical ensemble at inverse temperature β, the points in time direction (n_4) are restricted to the values $0, \ldots, N_\tau - 1$ with $aN_\tau = \beta$. At least for numerical calculations it is also necessary to restrict the spatial coordinates to only take values within some box of volume $V = L^3 = (aN_\sigma)^3$, i.e. $n_i \in \{0, \ldots, N_\sigma - 1\}$. The number of integration variables for the path integral thereby becomes finite and the action of a specific configuration becomes a sum over lattice points of a lattice Lagrange density instead of a spacetime integral.

The introduction of local gauge invariance on the lattice works exactly as in the continuum, except that it stops with the gauge transporters U_μ instead of going to their infinitesimal version A_μ because there are no fields that need to be transported any distance that is not the difference between two lattice points. Specifically, fermionic fields that transform according to the fundamental representation of SU(3) have three color components which are rotated by a local gauge transformation $\Omega(n)$ to give

$$\psi'(n) = \Omega(n)\psi(n) \qquad\qquad \bar{\psi}'(n) = \bar{\psi}(n)\Omega^\dagger(n).$$

Whenever fields at different points are to be coupled, they have to be gauge transported to the same point, which makes the introduction of a field of matrices $U_\mu(n)$ necessary. These live on the link between the lattice points n and $n+\hat{\mu}$[5] and they are elements of the group SU(3), in contrast to the algebra-valued A_μ. If $\psi(n+\hat{\mu})$ is defined on the lattice site $n+\hat{\mu}$, $U_\mu(n)\psi(n+\hat{\mu})$ is its gauge transported version at n. In order to gauge transport a field from n to $n+\hat{\mu}$, the inverse link variable has to be used:

$$U_{-\mu}(n+\hat{\mu})\psi(n) \equiv U_\mu(n)^\dagger\psi(n)$$

In this way, gauge symmetry is incorporated exactly in the lattice description, in contrast to Lorentz symmetry, which is approximated by a discrete subgroup and only restored when taking the continuum limit.

As a convenient shorthand for using matrix and vector notation for all (i.e., internal and spacetime) degrees of freedom, the operator U_μ is defined by

$$(U_\mu\psi)(n) = U_\mu(n)\psi(n+\hat{\mu}).$$

The non-interacting case is given by $U_\mu(n) = \mathbb{1}$, such that U_μ is given by a simple shift. Gauge invariant fermion bilinears can therefore be build in the form of

$$\bar{\psi}\Gamma U_\mu\psi,$$

[5] Since it is defined as connecting the points n and $n+\hat{\mu}$, $U_\mu(n+\hat{\mu}/2)$ would probably be a clearer notation, but this is usually not used in the literature.

with Γ acting on the Dirac degrees of freedom. Here,

$$\bar{\psi}A\psi = a^4 \sum_{n,n'} \bar{\psi}(n)A(n|n')\psi(n').$$

It is also possible to couple more distant fields with each other by inserting an appropriate product of such one-link gauge transporters between them.

As was already seen in the description of the continuum gauge fields, gauge transporters transform under gauge transformations as

$$U'_\mu(n) = \Omega(n)U_\mu(n)\Omega(n+\hat{\mu})^\dagger.$$

Similarly, for any product of link variables along some path the transformation is given by the gauge rotations at the endpoints. Therefore, in order to construct a gauge invariant quantity that only involves the gauge field, it is necessary to multiply link variables along a closed path and take the trace of the result. The simplest closed path is the *plaquette*

$$U_{\mu\nu}(n) = U_\mu(n)U_\nu(n+\hat{\mu})U_\mu(n+\hat{\nu})^\dagger U_\nu(n)^\dagger,$$

which can be used to create the simplest form of the gauge action that gives the correct naive continuum limit ($a \to 0$), namely the *Wilson gauge action*

$$S_G[U] = \frac{2}{g^2} \sum_n \sum_{\mu<\nu} \mathrm{Re}\,\mathrm{tr}\left[1 - U_{\mu\nu}(n)\right]. \tag{1.15}$$

It is possible to improve the discretization errors by adding further terms, but the details will be omitted here.

For the full definition of the lattice path integral for gauge fields, the only thing missing is the measure $\int \mathcal{D}[U]$. Here it will only be mentioned that the *Haar measure* that is used is constructed such that the measure is also invariant under gauge transformations.

1.6 Discretizing Fermions

The task of introducing fermions in a lattice formulation is significantly more problematic. The obvious problem of the necessity of Grassmann variables only affects numerical computations and can be solved relatively

straightforwardly. More subtle and more challenging is the so-called *doubling problem*, which has its origin in the fact that the Dirac Lagrange function only contains a first derivative of the quark fields and no second derivatives.

1.6.1 Numerical Computation of the Fermionic Path Integral

Any lattice discretization of the fermionic part of the QCD action takes the form

$$S_F = \bar{\psi} D_m \psi$$

with some (massive) Dirac operator D_m that somehow discretizes the continuum Dirac operator $\gamma_\mu D_\mu + m$ and respects gauge invariance in the sense discussed in the last section.

Since Grassmann numbers can not be represented in any simple way on a computer, the fermionic part of the path integral has to be transformed analytically. This is possible because the fermionic part is a bilinear, which can be solved similarly to a Gaussian integral, giving

$$\begin{aligned} Z &= \int \mathcal{D}[\psi, \bar{\psi}, U] \exp\left(-\bar{\psi} D_m[U] \psi - S_G[U]\right) \\ &= \int \mathcal{D}[U] \det(D_m[U]) \exp(-S_G[U]). \end{aligned}$$

This formula can be easily obtained by diagonalizing D_m and writing the exponential as a power sum which terminates after a finite number of terms because the square of a Grassmann number is zero. If some fermionic observables are inserted in the path integral, the integration transforms them into specific components of D_m^{-1}, which can be looked up in detail in, for example, [15]. More interestingly, the fermion determinant $\det[D_m]$ can be written as a path integral over bosonic variables ϕ and $\bar{\phi}$, so-called *pseudofermions*, by use of

$$\det[D_m] \propto \int \mathcal{D}[\phi, \bar{\phi}] \exp(-\bar{\phi} D_m^{-1} \phi).$$

Any path integral can therefore be written purely in terms of bosonic variables, which can be represented in a computer by simple numbers. Numerically, it is quite demanding to compute the pseudofermion action

because it contains the application of the inverse Dirac operator. For many applications it is therefore assumed that the fermion determinant is essentially constant and can be omitted from the calculation, giving the *quenched approximation*. However, for investigations of the chiral limit and topological properties this approximation should be avoided because, for example, the effect of infrared fermionic modes suppressing certain gauge configurations is mediated through the fermion determinant and is lost if the determinant is ignored.

1.6.2 The Doubling Problem

There are two obvious possibilities to discretize a derivative, namely the one-sided difference

$$f'(x) = \frac{f(x+\varepsilon) - f(x)}{\varepsilon} + \mathcal{O}(\varepsilon)$$

and the symmetric difference

$$f'(x) = \frac{f(x+\varepsilon) - f(x-\varepsilon)}{2\varepsilon} + \mathcal{O}(\varepsilon^2).$$

The gauge version of the symmetric difference is given by

$$\nabla_\mu = \frac{1}{2a}(U_\mu - U_{-\mu}),$$

which results in the naive Dirac operator

$$D_m^{\text{naive}} = \sum_\mu \gamma_\mu \nabla_\mu + m. \tag{1.16}$$

Taking instead the one-sided difference has several problems, namely that the resulting Dirac operator does not have any useful hermiticity properties and, more severely, that it creates non-covariant contributions to the fermion self-energy and vertex function [28]. The massless part of the given Dirac operator is antihermitian because $U_\mu^\dagger = U_{-\mu}$. But, more importantly, the full naive Dirac operator is γ_5-Hermitian, which means

$$\gamma_5 D \gamma_5 = D^\dagger.$$

This ensures that the Dirac operator is normal, which is required for the fermion modes to form an orthogonal basis. It also helps in the numerical calculation since it ensures that the fermion determinant is real[6],

$$\det[D]^* = \det[D^\dagger] = \det[\gamma_5 D \gamma_5] = \det[D].$$

Using the abbreviations $\gamma_{-\mu} = -\gamma_\mu$ and

$$\sum_{\pm\mu} = \sum_{\mu=1}^{4} + \sum_{\mu=-4}^{-1},$$

the naive Dirac operator can also be written as

$$D_m^{\text{naive}} = \frac{1}{2a} \sum_{\pm\mu} \gamma_\mu U_\mu + m.$$

In the non-interacting case, its eigenmodes can easily be obtained by the ansatz $\psi(n) = \psi_0 \mathrm{e}^{iapn}$. In the spatial dimensions, in order to have translational symmetry the eigenmodes are usually required to be periodic, $\psi(n + N_\sigma \hat{\mu}) = \psi(n)$ for $\mu \in \{1, 2, 3\}$. In the temporal direction, according to section 1.1.2 the integration variables have to be antiperiodic, i.e. $\psi(n + N_\tau \hat{4}) = -\psi(n)$. This restricts p_μ to values

$$p_i = \frac{2\pi}{L} k_i \qquad\qquad p_4 = 2\pi T \left(k_4 + \frac{1}{2}\right)$$

with integer-valued k_μ. Since adding a multiple of N_μ to k_μ gives the same function, the values of k_μ can be restricted to, for example, $\{0, \ldots, N_\mu - 1\}$. Using

$$\sum_{n'} \delta_{n', n+\hat{\mu}} \mathrm{e}^{iapn'} = \mathrm{e}^{iap_\mu} \mathrm{e}^{iapn},$$

iD_m^{naive} becomes when acting on this spinor

$$\begin{aligned} \lambda &= \frac{i}{2a} \sum_\mu \gamma_\mu \left(\mathrm{e}^{iap_\mu} - \mathrm{e}^{-iap_\mu}\right) + im \\ &= im - a^{-1} \sum_\mu \gamma_\mu \sin(ap_\mu). \end{aligned} \tag{1.17}$$

[6] If a chemical potential is included, this is usually no longer the case, which presents a great challenge and is an active field of research, see for example [29].

However, the symmetric difference has its own problem, which becomes especially visible in the chiral limit at fixed background gauge. If the lattice is split into even and odd points such that all nearest neighbors of an even point are odd and vice versa, the fermion and antifermion fields ψ and $\bar{\psi}$ can be split into fields defined on these sublattices, giving $\psi_{e/o}$ and $\bar{\psi}_{e/o}$. Now ψ_e is only coupled with $\bar{\psi}_o$ and vice versa, splitting the degrees of freedom into two subsets that do not influence each other. Another way to phrase the problem is that the lattice is discretized with a lattice spacing a while the discretization of the derivative involves the distance $2a$. This results in additional fermion modes, so-called *doublers*. For each fermion species that was to be described by the naive action, there are 15 additional copies, which in the non-interacting case described above correspond to values where $\sin(ap_\mu)$ becomes small even though ap_μ is not near 0 but instead near π. To make things worse, these copies do not possess a continuum limit, i.e., they give contributions to observables that oscillate and do not converge when the continuum limit is performed. This can be seen most directly by computing the fermion propagator D_0^{-1} in the non-interacting case and with infinitesimal temperature, which for the doublers gives solutions that change sign from one lattice point to the next [26]. There is no smooth continuum limit of such an oscillating function. It only becomes well-defined if every second lattice point is discarded, which again shows that the even and odd sublattices have independent solutions. The naive action can therefore not even be used to describe 16 degenerate fermion species.

One relatively simple solution is to somehow include terms of the form $\frac{1}{a}(1-\cos(ap_\mu))$ to the eigenvalue (1.17), which becomes 0 for the proper pole at $p_\mu \approx 0$, but gives a non-vanishing contribution that diverges in the continuum limit for $ap_\mu \approx \pi$. Thus the doublers become heavy and do not contribute as relevant degrees of freedom. Such an addition is achieved by the so-called *Wilson Dirac operator*

$$\begin{aligned} D_m^W &= m + \sum_\mu \gamma_\mu \nabla_\mu - \frac{a}{2}\sum_\mu \Delta_\mu \\ &= \left(m + \frac{4}{a}\right) - \frac{1}{2a}\sum_{\pm\mu}(1-\gamma_\mu)U_\mu \end{aligned} \tag{1.18}$$

with

$$\Delta_\mu = \frac{1}{a^2}(U_{-\mu} - 2 + U_\mu)$$

discretizing the second derivative $f''(x)$. Like the naive Dirac operator, the Wilson Dirac operator is also γ_5-Hermitian such that the determinant becomes real. For large enough mass m, it will also be positive.

Even though Wilson fermions have been very successful in lattice QCD calculations, they are unable to adequately capture consequences of chiral symmetry. The reason is that even in the massless case the essential relation

$$\{\gamma_5, D\} = 0$$

is broken by the Wilson term and only restored in the continuum limit. At finite lattice spacing, there is no symmetry of the lattice action that corresponds to the axial symmetry in the continuum.

There is a famous *no-go theorem* by Nielsen and Ninomiya [30] that prohibits any simple doubler-free and chirally symmetric fermion lattice discretization. In the next chapter, another solution that keeps chiral symmetry at least partially is presented, followed by a discussion of overlap fermions, which implement exact chiral symmetry at the cost of a certain locality property.

2 Chiral Fermions on the Lattice

2.1 The Staggered Fermion Action

A solution to the doubling problem that preserves at least some subgroup of chiral symmetry even at finite lattice spacing is given by staggered or Kogut-Susskind fermions [31]. It attacks the problem of doublers from a different angle, namely by changing the effective lattice spacing for the fermion fields to $b = 2a$ so it is possible to use a symmetric difference approximation of the first derivative that also uses the same distance. This couples even and odd lattice sites of the finer lattice with lattice spacing a in such a way that no solutions of the fermion propagator involves factors that flip sign from one lattice site to the next [26], ensuring a sensible continuum limit of all degrees of freedom.

This is achieved by defining a fermionic theory on a coarse lattice Λ' with lattice spacing $b = 2a$ that is doubler-free and has a remainder of chiral symmetry, and distributing the degrees of freedom of each point n' on Λ' over the hyper cube of the finer lattice Λ that consists of the points $n = 2n' + \xi$ with $\xi_\mu \in \{0, 1\}$ and is therefore attached to n'. Since there are $16 = 2^4$ points in such a hyper cube and $4 \times 3 \times N_f$ degrees of freedom for one lattice site corresponding to Dirac, color and flavor components, this redistribution does not affect the color but it is necessary to have at least $N_f = 4$. Staggered fermions therefore by default describe 4 flavors with degenerate masses, which in this context are called *tastes*.

Denoting the coarse fermion fields by $\bar{q}^t_\alpha$ and q^t_α with taste t and Dirac component α, the Dirac operator has the form

$$D^{\mathrm{st},c}_m = m + \sum_\mu \gamma_\mu \nabla_{2\mu} - \frac{b}{2} \sum_\mu T_\mu \Delta_{2\mu} \tag{2.1}$$

such that the action becomes

$$S = b^4 \sum_{n',m' \in \Lambda'} \bar{q}(n') D^{\mathrm{st},c}_m(n'|m') q(m').$$

This is similar to the Wilson operator except for the operator T_μ which acts on Dirac and taste components and will determine how much of chiral symmetry is still intact. The operators $\nabla_{2\mu}$ and $\Delta_{2\mu}$ are versions of the discretized derivative operators on Λ', so they involve the difference b instead of a.

The derivation of the staggered formulation usually starts with a naive Dirac operator and takes linear combinations of the Dirac components within a hyper cube such that the Dirac operator becomes diagonal in Dirac space. Then, all but one of the Dirac components are omitted, giving the staggered operator

$$D_m^{\mathrm{st}}(n|l) = m\delta_{nl} + \sum_\mu \eta_\mu(n)\nabla_\mu(n|l) \tag{2.2}$$

with

$$\eta_\mu(n) = \prod_{\nu<\mu} (-1)^{n_\nu}$$

taking the role of γ_μ. Recombining these components to four tastes with four Dirac components that live on the coarse lattice then gives (2.1), with

$$T_\mu = \gamma_5\tau_5\tau_\mu.$$

Here, τ_μ and τ_5 are the complex conjugates of γ_μ and γ_5, but acting on the tastes instead of the Dirac components. The details of this derivation are omitted here because it becomes quite technical and can be found in any of the introductory text books that were cited in earlier chapters.

A continuum theory with four tastes or flavors would be invariant under $\mathrm{SU}_V(4)\times\mathrm{SU}_A(4)$ rotations with the exception of the anomaly, but the taste mixing term breaks most of the vector as well as axial symmetries. There remains one vector symmetry generated by $\mathbb{1}$ and one axial symmetry generated by $\gamma_5\tau_5$ because of $\{T_\mu, \gamma_5\tau_5\} = 0$, so the staggered action is invariant under $\mathrm{U}_V(1)\times\mathrm{U}_A(1)$. This axial symmetry is not to be confused with the anomalous $\mathrm{U}_A(1)$, which is generated by γ_5. The staggered action does not have an anomalous symmetry but instead a genuinely unbroken remaining axial symmetry that allows some of the features of QCD in the chiral limit to be studied with staggered fermions. In the continuum limit, the taste breaking term vanishes and full chiral symmetry is restored.

If the non-interacting staggered action is written in momentum space by Fourier transforming the fermion fields, the result becomes [26]

$$D_m^{\mathrm{st}}(p) = i \sum_\mu \gamma_\mu \sin\left({}^{bp_\mu}/_2\right) + m,$$

which demonstrates that the staggered formulation has no doublers because for $bp_\mu \in [-\pi, \pi]$ there is only one value where $\sin({}^{bp_\mu}/_2)$ vanishes—in contrast to naive fermions, where this factor is instead $\sin(ap_\mu)$ and has an additional zero at $ap_\mu = \pi$. In this form, the action is in fact invariant under the full vector and axial symmetries, but the derivation requires a change of variables that is local in momentum space but in coordinate space mixes fields that are far apart. It is therefore possible to write the staggered action in a form where full chiral symmetry is preserved, but the action is then no longer ultra-local (only involving a finite number of points in the neighborhood of each point) and not even local ($|D(n|m)|$ falling exponentially with $|n - m|$).

Although the staggered formulation only allows the simulation of fermions that come in degenerate groups of four tastes, it is possible to circumvent this restriction with a trick that is not unquestionable. It builds on the observation that it is easy to replace a specific particle that is described by a Lagrange density by a multiplet of n independent clones. For this it is only necessary to add an additional index that distinguishes these clones and take the sum over the original contributions to the action as new action. In the case of fermions, this has the effect of raising the fermion determinant to the power n. The idea is now to take the staggered fermion determinant to the power ${}^1/_4$ (or, in order to describe two degenerate quark flavors, ${}^1/_2$). Since the determinant is not calculated explicitly but translated into a path integral for pseudofermions, this has the effect of changing the pseudofermion action by taking advantage of $\det[D_m]^x = \det[D_m^x]$. If the four tastes were completely independent, this would have the effect of reducing this degeneracy and only describing one quark species. Since at non-vanishing lattice spacing the tastes are mixed by the Wilson-like term in (2.1), it is not clear if this *rooting* has the desired effect. However, in practice it has been very successful.

2.2 Exact Chiral Symmetry on the Lattice from Blocked Continuum Fields

In order to implement exact chiral symmetry in a lattice formulation of QCD even relatively far from the continuum limit, a systematic way is provided by the blocking procedure. It was first used in statistical mechanics systems and extended by K. G. Wilson [32] to systematically derive effective lattice actions for gauge field theories from their continuum counterparts. In 1982 [33], P. H. Ginsparg and K. G. Wilson used this approach to derive the form that chiral symmetry should take on a lattice, which resulted in the famous Ginsparg-Wilson (GW) equation. It is possible to use the same approach with any internal symmetry of a quantum field theory [15]. This presentation follows that of Gattringer and Lang with some additional remarks.

Starting from continuum QCD with fermionic fields $\phi(x)$ and $\bar{\phi}(x)$ and generator-valued gauge fields $A_\mu(x)$, the goal of the blocking procedure is to replace these by lattice degrees of freedom with an effective action that gives the same partition function. As an intermediate step, blocked variables $\phi^B(n)$, $\bar{\phi}^B(n)$ and $U_\mu^B(n)$ are defined as appropriate combinations of the continuum fields. For each given configuration they provide an appropriate averaging of the continuum degrees of freedom around a lattice point. They are, however, not used directly for the effective action, which instead takes the form

$$\mathrm{e}^{-S_{\mathrm{eff}}[U,\psi,\bar{\psi}]} = \int \mathcal{D}[A,\phi,\bar{\phi}] K[U,\psi,\bar{\psi};U^B,\phi^B,\bar{\phi}^B] \mathrm{e}^{-S[A,\phi,\bar{\phi}]}. \tag{2.3}$$

Here, $S[A,\phi,\bar{\phi}]$ is the continuum action and $K[\dots]$ is a kernel coupling the lattice degrees of freedom to the blocked fields. The action can also include terms that couple observables to source fields such that expectation values can be obtained in the usual way, namely by derivatives of the logarithm of the partition function with respect to the source fields. In order for the partition function to describe the same system, the kernel has to become constant when integrated over the lattice fields. For a simple identification of the lattice and blocked variables, it takes the form of a delta function. However, it is easier for the calculation if this relation is smoothed and the variables are allowed to fluctuate around their blocked counterparts. In the case of gauge links, this also opens some freedom in the construction of

the blocked variables because they do not need to be restricted to elements of the gauge group. The coupling can then be chosen in such a way that the lattice fields fluctuate smoothly around some projection of the blocked fields onto the group manifold.

Specifically, a blocked link variable connecting the points n and $n+\hat{\mu}$—where $\hat{\mu}$ is the unit vector in direction μ and the lattice spacing is set to 1—that maintains gauge invariance can be obtained by a linear combination of gauge transporters connecting n and $n+\hat{\mu}$ along every possible path,

$$U_\mu^B(n) = \int_{\mathcal{C}_{n,n+\hat{\mu}}} \mathrm{d}p\mathcal{P} \exp\left(i \int_p \mathrm{d}x A\right).$$

Here, $\mathcal{C}_{n,n+\hat{\mu}}$ is the set of all continuous paths connecting the endpoints and the measure $\mathrm{d}p$ gives different weights for each path – a sensible choice should assign the same weight for different paths that are related to each other by symmetry transformations and will give most weight to the paths in a vicinity around the most direct one. As a sum of gauge transporters, the blocked gauge field transforms under local gauge transformations $\Omega(x)$ as

$$U_\mu^B(n) \to \Omega(n) U_\mu^B(n) \Omega(n+\hat{\mu})^\dagger,$$

which is the desired transformation of a lattice link connecting these sites. However, since a linear combination of special unitary matrices in general does not retain this property, the gauge part of the kernel becomes more involved. This is, however, not important for this discussion since the goal is to describe a fermionic symmetry and the gauge field—continuum or lattice—can be regarded as a fixed background for this.

For the fermion fields, a similar approach with a possibly different path measure $\mathrm{d}'p$ gives the general form

$$\phi^B(n) = \int \mathrm{d}x \omega_{nx} \phi(x) = \int \mathrm{d}x \int_{p\in\mathcal{C}(x,n)} \mathrm{d}'p\mathcal{P} \exp\left(i \int_p \mathrm{d}y A\right) \phi(x)$$
$$\bar{\phi}^B(n) = \int \mathrm{d}x \bar{\phi}(x) \omega_{xn}^\dagger$$

The fermionic part of the coupling kernel is simply given by

$$K_F = \mathrm{e}^{-\xi\left(\bar{\psi}-\bar{\phi}^B\right)\left(\psi-\phi^B\right)},$$

resulting in

$$\mathrm{e}^{-\bar{\psi}D\psi} = \int \mathcal{D}[\phi,\bar{\phi}]\mathrm{e}^{-\xi\left(\bar{\psi}-\bar{\phi}^B\right)\left(\psi-\phi^B\right)-S_F[\phi,\bar{\phi}]}, \tag{2.4}$$

which defines the lattice Dirac operator D. In general, instead of the prefactor ξ it is also possible to insert a nontrivial matrix inside the scalar product in the exponent, but in this case it is sufficient to only consider the case where this matrix is proportional to $\mathbb{1}$. The magnitude of ξ controls how far the lattice fields are allowed to deviate from the blocked fields.

The next step is to regard an internal global symmetry of the fermionic fields that takes the form

$$\phi' = \mathrm{e}^{i\varepsilon T}\phi \qquad\qquad \bar{\phi}' = \bar{\phi}\mathrm{e}^{i\varepsilon\bar{T}} \tag{2.5}$$

in the continuum and

$$\psi' = \mathrm{e}^{i\varepsilon M}\psi \qquad\qquad \bar{\psi}' = \bar{\psi}\mathrm{e}^{i\varepsilon\bar{M}} \tag{2.6}$$

on the lattice. The generators T and $\bar{T}$ are independent and given and the goal is to derive the corresponding lattice generators M and $\bar{M}$. In order to achieve this, the generating function on the lattice,

$$W[J,\bar{J}] = \int \mathcal{D}[\psi,\bar{\psi}]\mathrm{e}^{\bar{\psi}J+\bar{J}\psi-\bar{\psi}D\psi} = \det[D]\,\mathrm{e}^{\bar{J}D^{-1}J} \tag{2.7}$$

is defined and its path integral is evaluated by a change of variables to use ψ' and $\bar{\psi}'$ instead of ψ and $\bar{\psi}$:

$$\begin{aligned} W[J,\bar{J}] &= \int \mathcal{D}[\psi',\bar{\psi}']\mathrm{e}^{-\bar{\psi}'D\psi'+\bar{\psi}'J+\bar{J}\psi'} \\ &= \int \mathcal{D}[\psi,\bar{\psi}]\det\left[\mathrm{e}^{i\varepsilon M}\right]\det\left[\mathrm{e}^{i\varepsilon\bar{M}}\right]\mathrm{e}^{-\bar{\psi}D\psi+\bar{\psi}\mathrm{e}^{i\varepsilon\bar{M}}J+\bar{J}\mathrm{e}^{i\varepsilon M}\psi} \\ &= \left(1+i\varepsilon\,\mathrm{tr}\left[\bar{M}+M\right]+\mathcal{O}(\varepsilon^2)\right)W\left[\mathrm{e}^{i\varepsilon\bar{M}}J,\bar{J}\mathrm{e}^{i\varepsilon M}\right] \end{aligned} \tag{2.8}$$

Here, it was used that the lattice action $\bar{\psi}D\psi$ is invariant under the symmetry (2.6) and the Jacobi determinants were expanded to first order in ε.

The same calculation can be performed with a change of variables using the continuum symmetry (2.5), but first the generating function has to

be expressed by a continuum path integral. This is done by inserting (2.4) into (2.7) and performing the integral over ψ and $\bar{\psi}$. Using the abbreviations $\eta = \xi^{-1}J + \phi^B$ and $\bar{\eta} = \xi^{-1}\bar{J} + \bar{\phi}^B$, the result is

$$\begin{aligned} W[J,\bar{J}] &= \int \mathcal{D}[\phi,\bar{\phi}] \mathrm{e}^{-S_F[\phi,\bar{\phi}] - \xi\bar{\phi}^B\phi^B} \int \mathcal{D}[\psi,\bar{\psi}] \mathrm{e}^{-\xi\left(\bar{\psi}\psi - \bar{\eta}\psi - \bar{\psi}\eta\right)} \\ &= \int \mathcal{D}[\phi,\bar{\phi}] \mathrm{e}^{-S_F[\phi,\bar{\phi}] - \xi\bar{\phi}^B\phi^B} \int \mathcal{D}[\psi,\bar{\psi}] \mathrm{e}^{-\xi\left(\bar{\psi} - \bar{\eta}\right)(\psi - \eta) + \xi\bar{\eta}\eta} \\ &= C\mathrm{e}^{\xi^{-1}\bar{J}J} \int \mathcal{D}[\phi,\bar{\phi}] \mathrm{e}^{-S_F[\phi,\bar{\phi}] + \bar{J}\phi^B + \bar{\phi}^B J}, \end{aligned}$$

where $C = \int \mathcal{D}[\psi,\bar{\psi}] \mathrm{e}^{-\xi\bar{\psi}\psi}$ is an irrelevant constant. Since the blocked fields $\bar{\phi}^B$ and ϕ^B are linear combinations of the continuum fields, their transformation is the same, giving

$$\begin{aligned} W[J,\bar{J}] &= C\mathrm{e}^{\xi^{-1}\bar{J}J} \int \mathcal{D}[\phi',\bar{\phi}'] \mathrm{e}^{-S_F + \bar{J}\phi'^B + \bar{\phi}'^B J} \\ &= \left(1 + i\varepsilon\mathcal{A} + \mathcal{O}(\varepsilon^2)\right) \mathrm{e}^{\xi^{-1}\left(\bar{J}J - \bar{J}\mathrm{e}^{i\varepsilon T}\mathrm{e}^{i\varepsilon\bar{T}}J\right)} W\left[\mathrm{e}^{i\varepsilon\bar{T}}J, \bar{J}\mathrm{e}^{i\varepsilon T}\right]. \end{aligned} \tag{2.9}$$

The possible anomaly from the change of integration measure has been written as $\mathcal{A}$.

Equating (2.8) and (2.9) and using the explicit form of (2.7) for the remaining occurrences of W, the result is

$$\begin{aligned} &\left(1 + i\varepsilon \operatorname{tr}\left[\bar{M} + M\right] + \mathcal{O}(\varepsilon^2)\right) \mathrm{e}^{\bar{J}\mathrm{e}^{i\varepsilon M} D^{-1} \mathrm{e}^{i\varepsilon\bar{M}} J} \\ &\qquad = \left(1 + i\varepsilon\mathcal{A} + \mathcal{O}(\varepsilon^2)\right) \mathrm{e}^{\xi^{-1}\left(\bar{J}J - \bar{J}\mathrm{e}^{i\varepsilon T}\mathrm{e}^{i\varepsilon\bar{T}}J\right) + \bar{J}\mathrm{e}^{i\varepsilon T} D^{-1} \mathrm{e}^{i\varepsilon\bar{T}} J}. \end{aligned}$$

For $J = \bar{J} = 0$, this implies

$$\mathcal{A} = \operatorname{tr}\left[\bar{M} + M\right].$$

Expanding the exponentials in ε, on the other hand, gives to first order

$$MD^{-1} + D^{-1}\bar{M} = -\xi^{-1}(T + \bar{T}) + TD^{-1} + D^{-1}\bar{T}. \tag{2.10}$$

Multiplying this equation with D from the left as well as from the right now yields the generalized *Ginsparg-Wilson equation*:

$$DT + \bar{T}D = \xi^{-1}D(T + \bar{T})D \tag{2.11}$$

Here the relation $DM + \bar{M}D = 0$ has been used, which follows from

$$\bar{\psi}' D\psi' = \bar{\psi} \mathrm{e}^{i\varepsilon \bar{M}} D \mathrm{e}^{i\varepsilon M} \psi \overset{!}{=} \bar{\psi} D \psi$$

by expansion to first order in ε.

The magnitude of the anomaly can also be obtained directly from (2.10), namely by multiplying with D and taking the trace:

$$\mathcal{A} = \mathrm{tr}\left[(T + \bar{T})(1 - \xi^{-1} D)\right].$$

There are different solutions to (2.10) used in the literature, all having the form

$$M = T - \xi^{-1} G D \qquad\qquad \bar{M} = \bar{T} - \xi^{-1} D \bar{G}$$

with $G + \bar{G} = T + \bar{T}$, but with different choices of G and $\bar{G}$.

In the specific case of chiral symmetry, the axial rotation is given by $T = \bar{T} = \gamma_5 F$ with $F \in \mathrm{u}(N_f)$ mixing the different flavors, which (with $\xi = 2r$ and restricting to the case where D is diagonal in flavor space) results in the *Ginsparg-Wilson* relation

$$\{D, \gamma_5\} = \frac{1}{r} D \gamma_5 D. \tag{2.12}$$

The anomaly is given by $\mathcal{A} = -\frac{1}{r}\,\mathrm{tr}[\gamma_5 D]$ for $F = \mathbb{1}$, while it vanishes if F is a generator of $\mathrm{SU}(N_f)$ because then $\mathrm{tr}\,[F] = 0$. Therefore, only the singlet axial symmetry $U_A(1)$ is anomalously broken. The axial rotation on the lattice is of the form

$$\psi' = \mathrm{e}^{i\varepsilon\gamma_5(1 - \zeta/rD)F}\psi \qquad\qquad \bar{\psi}' = \bar{\psi}\mathrm{e}^{i\varepsilon F(1-(1-\zeta)/rD)\gamma_5} \tag{2.13}$$

with ζ usually chosen to be $0, 1/2$ or 1. In order to restore $\bar{\psi}' = \bar{\psi}$ and $\psi' = \psi$ at $\varepsilon = 2\pi$, the operators in the exponent should give $\mathbb{1}$ when squared because then

$$\mathrm{e}^{i\varepsilon A} = \cos(\varepsilon) + i \sin(\varepsilon) A.$$

Assuming $F^2 = \mathbb{1}$, this is the case for $\zeta = 0$ and $\zeta = 1$ because then

$$\left[\gamma_5 \left(1 - \frac{\zeta}{r} D\right)\right]^2 = \mathbb{1} - \frac{\zeta}{r}\gamma_5\{D, \gamma_5\} + \frac{\zeta^2}{r^2}\gamma_5 D \gamma_5 D = \mathbb{1},$$

and similarly $[(1 - \zeta/rD)\gamma_5]^2 = \mathbb{1}$.

2.3 The Ginsparg-Wilson Equation and its Consequences

The purpose of this section is to give an overview over the consequences of the exact implementation of chiral symmetry on the lattice provided by a fermion action that implements the Ginsparg-Wilson (GW) equation

$$\{D, \gamma_5\} = \frac{1}{r} D\gamma_5 D.$$

Most of the results can also be found in textbooks, p.e. [15, 27], but sometimes the derivations are omitted there.

The parameter r fixes the scale of the Dirac operator, i.e., if a solution to the GW equation is multiplied by a factor α, the new Dirac operator obeys a GW equation where r is replaced by αr. One possible choice is to match the naive continuum limit of non-interacting fermions to the corresponding continuum Dirac operator, which will be done later for the overlap solution.

2.3.1 Spectrum of the Ginsparg-Wilson Dirac Operator

In addition to the GW equation, Dirac operators are usually constructed such that they are γ_5-Hermitian, i.e. $D^\dagger = \gamma_5 D \gamma_5$. This property is shared by continuum fermions as well as Wilson and staggered fermions and the later discussed overlap solution to the GW equation inherits it from the Wilson Dirac operator. Multiplying the GW equation by γ_5 from either side then implies

$$D + D^\dagger = \frac{1}{r} D^\dagger D = \frac{1}{r} D D^\dagger. \tag{2.14}$$

It follows that a γ_5-Hermitian Dirac operator obeying the GW equation is *normal*, i.e. $[D, D^\dagger] = 0$, which implies that it has an orthonormal set of eigenvectors that form a basis for the vector space. Also, eigenvectors of D with eigenvalue $x + iy$ can be diagonalized in such a way that they are also eigenvectors of $D^\dagger$, with eigenvalue $x - iy$. Plugging this into (2.14), this implies

$$\begin{aligned} & 2rx = x^2 + y^2 \\ \Leftrightarrow \qquad & (x - r)^2 + y^2 = r^2, \end{aligned}$$

i.e., the eigenvalues lie on a circle in the complex plane with radius r and center $r + 0i$. They can therefore be parametrized as $\lambda = r\left(1 - \mathrm{e}^{-i\phi}\right)$ with $\phi \in (-\pi, \pi]$. The real valued $r\phi$ is often used instead of the complex valued λ. The mapping between these representations is bijective and eigenvalues near zero are mapped onto values of $r\phi$ near zero, with $\lambda \approx ir\phi$. The histograms and other visualizations will use this mapping, although the eigenvalue is usually still denoted by λ. There should not be any confusion about which representation is used in any given context—if an axis is labeled by λ and the values on it are real, these are actually the values of $r\phi$, since the actual eigenvalues do not take real values except at 0 and $2r$.

The spectrum can be further classified by introducing the operator $H = \gamma_5 D$. It is Hermitian because of

$$H^\dagger = D^\dagger \gamma_5 = \gamma_5 D \gamma_5 \gamma_5 = H$$

and the GW equation is equivalent to

$$\{\gamma_5, H\} = \frac{1}{r} H^2. \tag{2.15}$$

Starting with an eigenvector $\mathbf{x}$ of H with eigenvalue ε, $\mathbf{x}$ and $\gamma_5\mathbf{x}$ span a subspace U that is one-dimensional if $\mathbf{x}$ is also an eigenvector of γ_5 and two-dimensional otherwise. In the second case, it has to contain two orthogonal eigenvectors of H since U is invariant under the application of H:

$$\begin{aligned} H\mathbf{x} &= \varepsilon\mathbf{x} \in U \\ H\gamma_5\mathbf{x} &= \left(\frac{1}{r}H^2 - \gamma_5 H\right)\mathbf{x} \\ &= -\varepsilon\mathbf{x} + \frac{\varepsilon^2}{r}\gamma_5\mathbf{x} \in U \end{aligned}$$

A vector orthogonal to $\mathbf{x}$ is constructed by the Gram-Schmidt procedure as

$$\tilde{\mathbf{y}} = (1 - \mathbf{x}\mathbf{x}^\dagger)\gamma_5\mathbf{x} = \gamma_5\mathbf{x} - (\mathbf{x}^\dagger\gamma_5\mathbf{x})\mathbf{x}$$

which results in

$$\begin{aligned} H\tilde{\mathbf{y}} &= \left(\frac{1}{r}H^2 - \gamma_5 H\right)\mathbf{x} - \varepsilon \mathbf{x}\mathbf{x}^\dagger\gamma_5\mathbf{x} \\ &= \varepsilon\left(\frac{\varepsilon}{r}\mathbf{x} - \gamma_5\mathbf{x} - \mathbf{x}\mathbf{x}^\dagger\gamma_5\mathbf{x}\right) \\ &= -\varepsilon\tilde{\mathbf{y}} + \varepsilon\left(\frac{\varepsilon}{r} - 2\mathbf{x}^\dagger\gamma_5\mathbf{x}\right)\mathbf{x} \end{aligned}$$

Since $\tilde{\mathbf{y}}$ has to be an eigenvector of H, this implies

$$\chi \equiv \mathbf{x}^\dagger\gamma_5\mathbf{x} = \frac{\varepsilon}{2r},$$

which yields the normalized eigenvector

$$\mathbf{y} = \frac{\tilde{\mathbf{y}}}{|\tilde{\mathbf{y}}|} = \frac{\gamma_5\mathbf{x} - \chi\mathbf{x}}{\sqrt{1-\chi^2}}$$

with eigenvalue $-\varepsilon$. The action of γ_5 on these vectors can now be written as

$$\begin{aligned} \gamma_5\mathbf{x} &= \tilde{\mathbf{y}} + \chi\mathbf{x} \\ \gamma_5\tilde{\mathbf{y}} &= \mathbf{x} - \chi\left(\tilde{\mathbf{y}} + \chi\mathbf{x}\right) = \left(1-\chi^2\right)\mathbf{x} - \chi\tilde{\mathbf{y}}. \end{aligned}$$

Since the eigenvalues of H in U are given by ε and $-\varepsilon$, H^2 is constant on U and commutes with γ_5. Since they commute on all such two-dimensional subspaces and also on the one-dimensional ones where γ_5 and H have the same eigenvectors, they commute on the whole vector space.

Being invariant under both γ_5 and H, U also has to be invariant under $D = \gamma_5 H$. U must therefore contain two eigenvectors of D and taking the ansatz $\psi = \alpha\mathbf{x} + \beta\gamma_5\mathbf{x}$ gives

$$\begin{aligned} D\psi &= \alpha\varepsilon\gamma_5\mathbf{x} + \beta\gamma_5\left(\frac{1}{r}H^2 - \gamma_5 H\right)\mathbf{x} \\ &= \varepsilon\left[\left(\alpha + 2\chi\beta\right)\gamma_5\mathbf{x} - \beta\mathbf{x}\right] \\ &\stackrel{!}{=} \lambda\left(\alpha\mathbf{x} + \beta\gamma_5\mathbf{x}\right) \end{aligned}$$

Comparison of the coefficients in front of $\mathbf{x}$ and $\gamma_5\mathbf{x}$ separately yields

$$(\alpha + 2\chi\beta)\,\varepsilon = \lambda\beta \qquad\qquad -\beta\varepsilon = \lambda\alpha$$

and, by elimination of λ,

$$\begin{aligned} & 0 = \alpha^2 + 2\chi\alpha\beta + \beta^2 \\ \Rightarrow \qquad & \alpha = \beta\left(-\chi \pm i\sqrt{1-\chi^2}\right). \end{aligned}$$

From this, the eigenvalues

$$\lambda_\pm = \varepsilon\chi \pm i\varepsilon\sqrt{1-\chi^2}$$

and eigenvectors

$$\begin{aligned} \psi_\pm &= \beta\left(\left(-\chi \pm i\sqrt{1-\chi^2}\right)\mathbf{x} + \gamma_5\mathbf{x}\right) \\ &= \beta\sqrt{1-\chi^2}\,(\pm i\mathbf{x} + \mathbf{y}) \\ &= \frac{1}{\sqrt{2}}(\mathbf{y} \pm i\mathbf{x}) \end{aligned} \tag{2.16}$$

are obtained by appropriate choice of β.

One eigenvector of D in the subspace U can be obtained from the other one by a simple application of γ_5, although the phases are then different than in (2.16). This can either be derived from (2.16) or directly from the GW equation:

$$\begin{aligned} D\gamma_5\psi_\pm &= \left(\frac{1}{r}D\gamma_5 D - \gamma_5 D\right)\psi_\pm \\ &= \frac{\lambda_\pm}{r}D\gamma_5\psi_\pm - \lambda_\pm\gamma_5\psi_\pm \\ \Rightarrow \qquad D\gamma_5\psi_\pm &= \frac{r\lambda_\pm}{\lambda_\pm - r}\gamma_5\psi_\pm = \frac{\varepsilon\lambda_\pm}{2\chi\lambda_\pm - \varepsilon}\gamma_5\psi_\pm \end{aligned}$$

Therefore, $\gamma_5\psi_\pm$ is an eigenvector of D with eigenvalue $\frac{\lambda_\pm}{2\chi\lambda_\pm - \varepsilon}$. Since the subspace U is invariant under the application of γ_5, this vector has to be

the same as $\psi_\mp$ up to a phase and the eigenvalue has to be identical to $\lambda_\mp$. The latter can be checked easily:

$$\begin{aligned} & \frac{\varepsilon\lambda_\pm}{2\chi\lambda_\pm - \varepsilon} \stackrel{!}{=} \lambda_\mp \\ \Leftrightarrow \quad & \varepsilon(\lambda_\pm + \lambda_\mp) = 2\chi\lambda_\mp\lambda_\pm \\ \Leftrightarrow \quad & 2\chi\varepsilon^2 = 2\chi\varepsilon^2\left(\chi^2 + 1 - \chi^2\right) \qquad \checkmark \end{aligned}$$

It also follows that the eigenvectors of D that come in such pairs have zero chirality:

$$\psi_\pm^\dagger\gamma_5\psi_\pm \propto \psi_\pm^\dagger\psi_\mp = 0$$

If, on the other hand, the invariant subspace U is one-dimensional, the corresponding eigenvector of H is also an eigenvector of γ_5 and, therefore, also of D. The eigenvalue of γ_5 for this eigenvector is ± 1, so

$$0 = \left(\{\gamma_5, D\} - \frac{1}{r}D\gamma_5 D\right)\psi = \pm\lambda\left(2 - \frac{\lambda}{r}\right)\psi.$$

This is only possible if $\lambda = 0$ or $\lambda = 2r$, i.e., for the real values of the eigenvalue circle. Since $\mathrm{tr}[\gamma_5] = 0$, the number of righthanded ($\psi^\dagger\gamma_5\psi = 1$) and lefthanded ($-1$) eigenmodes of D has to be equal, but *a priori* they can be distributed arbitrarily between zero modes and $\lambda = 2r$ modes. It turns out that no configuration with left- as well as righthanded zero modes should be or has been observed, so if a configuration has n zero modes, they all have the same chirality, which must be compensated by the $\lambda = 2r$ modes.

The reasoning is as follows. If a configuration had n_+ righthanded and n_- lefthanded modes with $n_+ \geq n_-$, it would not necessarily be distinguishable from a situation with $n_+ - n_-$ righthanded and no lefthanded modes, and n_- pairs of accidental zero modes, i.e., pairs of modes characterized by a two-dimensional invariant subspace U that just happens to correspond to the eigenvalue $\varepsilon = 0$. Specifically, a pair of chiral modes ψ_+ and ψ_- that have eigenvalue 0 can be replaced by the pair consisting of $\frac{1}{\sqrt{2}}(\psi_+ + \psi_-)$ and $\frac{1}{\sqrt{2}}(\psi_+ - \psi_-)$, which have H-eigenvalues $\pm\varepsilon$ with $\varepsilon = 0$, chirality 0 and can be obtained from each other by application of γ_5. However, such accidental zero modes can be continuously deformed

into modes that have small but non-zero eigenvalues. Since a pair of near-zero modes can take a continuum of values when disturbing the gauge background infinitesimally, the probability of getting exactly zero is zero.

The same argument can not be made for the remaining zero modes when there are no zero modes with opposite chirality left, since a shift to a non-zero value would require a mode from $\lambda = 2r$ to discontinuously jump to a value near zero.

According to section 2.2, the chiral anomaly can be computed as

$$\begin{aligned}\mathcal{A} &= \operatorname{tr}\left[2\gamma_5(1 - {}^{D}\!/_{2r})\right] \\ &= -\frac{1}{r}\operatorname{tr}\left[\gamma_5 D\right].\end{aligned}$$

The zero modes do not contribute to the trace and the contributions from the modes in a non-zero pair cancel each other. The only contribution comes from the $\lambda = 2r$ modes and for n'_+ righthanded and n'_- lefthanded modes it is given by

$$\mathcal{A} = 2(n'_- - n'_+)$$

Since the total trace of γ_5 is 0, the difference $n'_- - n'_+$ is equal to the difference $n_+ - n_-$ of right- and lefthanded zero modes, so the anomaly can also be written as $\mathcal{A} = 2(n_+ - n_-)$. The *topological charge* of a configuration is given by

$$Q = \frac{1}{2r}\operatorname{tr}\left[\gamma_5 D\right] = n_- - n_+$$

and the fact that it takes an integral value is another expression of the fact that continuous deformations of the gauge fields can not change its topological charge, i.e., they can not move a non-paired zero mode away from zero. An exception is provided when the Dirac operator itself is non-analytic, which is the case in special circumstances for the overlap solution discussed in the next subsection.

To summarize, the eigenvalues of an operator that obeys the GW equation are given by

$$\lambda = \frac{1}{2r}\left(\varepsilon^2 + i\varepsilon\sqrt{4r^2 - \varepsilon^2}\right), \tag{2.17}$$

where ε is the eigenvalue of $H = \gamma_5 D$. The zero modes can also be included in this representation by $\varepsilon = 0$ and the ultraviolet modes at

$\lambda = 2r$ correspond to $\varepsilon = \pm 2r$, with the sign depending on their chirality. Applying γ_5 to a mode with nonzero imaginary part changes the sign of ε, which turns λ into its complex conjugate.

2.3.2 Chiral Projections

As in the continuum, it is possible to split the fermion fields into left- and righthanded fields that decouple in the massless limit. However, the choice of projectors has to be adjusted and, specifically, it is necessary to use different projections for fermion and antifermion fields.

In general, the split is done using pairs of projectors $P_\pm$ and $\bar{P}_\pm$ with $P_+ + P_- = \bar{P}_+ + \bar{P}_- = 1$, such that

$$\psi_\pm = P_\pm \psi \qquad\qquad \bar{\psi}_\pm = \bar{\psi}\bar{P}_\pm$$

The requirement that the massless action splits into independent parts for each chirality becomes

$$\bar{\psi} D \psi = \bar{\psi}_+ D \psi_+ + \bar{\psi}_- D \psi_-,$$

i.e., any mixing term $\bar{\psi}_\pm D \psi_\mp$ has to be zero, which is equivalent to

$$\bar{P}_\pm D = D P_\pm. \tag{2.18}$$

Introducing $\Gamma = 2P_+ - 1$ and $\bar{\Gamma} = 2\bar{P}_+ - 1$, the projectors can be written in the form $P_\pm = \frac{1}{2}(1 \pm \Gamma)$ and $\bar{P}_\pm = \frac{1}{2}(1 \pm \bar{\Gamma})$ with

$$\Gamma^2 = \bar{\Gamma}^2 = 1. \tag{2.19}$$

(2.18) then becomes

$$\begin{aligned} & (1 \pm \bar{\Gamma}) D = D (1 \pm \Gamma) \\ \Leftrightarrow \quad & D\Gamma - \bar{\Gamma} D = 0. \end{aligned}$$

Comparing with the Ginsparg-Wilson equation in the form

$$D\gamma_5 + \gamma_5 D - \frac{1}{r} D \gamma_5 D = 0,$$

a set of solutions is given by

$$\Gamma = \gamma_5 \left(1 - \frac{\eta}{r} D\right) \qquad \bar{\Gamma} = \left(\frac{1-\eta}{r} D - 1\right) \gamma_5$$

Plugging these solutions into (2.19) in order to ensure that $P_\pm$ and $\bar{P}_\pm$ really are projectors, the result is

$$\begin{aligned} 1 = \Gamma^2 &= \gamma_5^2 - \frac{\eta}{r}\gamma_5\{\gamma_5, D\} + \frac{\eta^2}{r^2}\gamma_5 D \gamma_5 D \\ &= 1 - \frac{\eta(1-\eta)}{r^2}\gamma_5 D \gamma_5 D \end{aligned}$$

and similarly for $1 = \bar{\Gamma}^2$, allowing only $\eta \in \{0, 1\}$. Using, for example, $\eta = 0$, the splitting into left- and righthanded fermions on the lattice is therefore given by

$$\psi_\pm = \frac{1}{2}(1 \pm \gamma_5)\psi \qquad \bar{\psi}_\pm = \frac{1}{2}\bar{\psi}(1 \mp (1 - {}^{D}\!/_{r})\gamma_5) \tag{2.20}$$

2.3.3 Massive Ginsparg-Wilson Fermions

If chiral symmetry is to be incorporated on a fundamental level even at nonvanishing lattice spacing, these left- and righthanded (i.e., chiral) fermion fields are more fundamental than the Dirac fields. A symmetry breaking mass term should therefore not be introduced as $m\bar{\psi}\psi$ but rather as mixing of left- and righthanded fields, i.e.

$$\begin{aligned} m \sum_\pm \bar{\psi}_\pm \psi_\mp &= m\bar{\psi} \sum_\pm \bar{P}_\pm P_\mp \psi \\ &= \frac{m}{4}\bar{\psi}\left((1+\bar{\Gamma})(1-\Gamma) + (1-\bar{\Gamma})(1+\Gamma)\right)\psi \\ &= \frac{m}{2}\bar{\psi}\left(1 - \bar{\Gamma}\Gamma\right)\psi \\ &= m\bar{\psi}\left(1 - {}^{D}\!/_{2r}\right)\psi. \end{aligned}$$

The massive Dirac operator for one quark flavor with mass m is therefore given by

$$D_m = D + m\left(1 - {}^{D}\!/_{2r}\right) = \left(1 - \frac{m}{2r}\right) D + m. \tag{2.21}$$

This has consequences for fermionic observables since the massive Dirac operator enters the partition function

$$Z = \int \mathcal{D}[U,\psi,\bar{\psi}] \mathrm{e}^{-S_G[U]-\sum_f \bar{\psi}_f D_{m_f} \psi_f} = \int \mathcal{D}[U] \mathrm{e}^{-S_G[U]} \prod_f \det[D_{m_f}]. \tag{2.22}$$

It has therefore a more involved mass dependence than in the continuum or with Wilson or staggered actions. For example, since the chiral condensate is used as a measure for chiral symmetry breaking, it should be defined by the operator that couples to the mass, which after all is the term that explicitly breaks chiral symmetry. Therefore,

$$\Sigma = \frac{1}{N_f} \frac{T}{V} \left\langle \sum_{\pm} \bar{\psi}_{\pm} \psi_{\mp} \right\rangle = \frac{1}{N_f} \frac{T}{V} \frac{\mathrm{d}}{\mathrm{d}m} \ln Z.$$

Since

$$\frac{\mathrm{d}}{\mathrm{d}m} \det[A] = \det[A] \operatorname{tr}\left[A^{-1} \frac{\mathrm{d}}{\mathrm{d}m} A \right]$$

for any invertible matrix A, such observables involve the *shifted propagator*

$$\begin{aligned} \tilde{D}^{-1} &= D_m^{-1} \frac{\mathrm{d}}{\mathrm{d}m} D_m \\ &= D_m^{-1} (1 - D/2r) = D_m^{-1} \left(1 - \frac{D_m - m}{2r - m} \right) \\ &= \frac{2r}{2r-m} \left(D_m^{-1} - \frac{1}{2r} \right). \end{aligned} \tag{2.23}$$

Sometimes, the form

$$\tilde{D}^{-1} = \frac{2r - D}{2r D_m} = \frac{2r - D}{(2r-m)D + 2rm}$$

is more convenient. Interestingly, if acting on a zero mode of D, this gives $1/m$ as in the continuum, and if acting on a real mode at the other end of the spectrum, i.e. $\lambda = 2r$, it vanishes. The second property would not hold for $(D+m)^{-1}$ or D_m^{-1}. The inverse of the shifted propagator,

$$\tilde{D} = \frac{2rD - mD + 2rm}{2r - D} = \frac{2rD}{2r - D} + m =: f(D) + m,$$

has a simple m-dependence, which simplifies the calculation of some traces.

Written in terms of the eigenvalues λ of D, where $|\lambda|^2 = \varepsilon^2$ and $\mathrm{Re}(\lambda) = {}^{\varepsilon^2}/_{2r}$ (cf. (2.17)), and which are either real with $\lambda \in \{0, 2r\}$ or come in complex conjugate pairs, the following relations hold:

$$\begin{aligned} f(0) &= 0 \\ f(2r) &= \infty \\ \mathrm{Re} f(\lambda) &= \mathrm{Re}\frac{2r\lambda(2r-\bar{\lambda})}{|2r-\lambda|^2} \propto 2r\,\mathrm{Re}\lambda - |\lambda|^2 = 0 \\ |f(\lambda)|^2 &= \frac{4r^2|\lambda|^2}{4r^2 - 4r\,\mathrm{Re}\lambda + |\lambda|^2} = \frac{4r^2\varepsilon^2}{4r^2-\varepsilon^2}. \end{aligned}$$

For the chiral condensate, this results in

$$\begin{aligned} \mathrm{tr}\left[\tilde{D}^{-1}\right] &= \sum_\lambda \frac{1}{f(\lambda)+m} \\ &= \frac{|Q|}{m} + \sum_{\mathrm{Im}\lambda>0} \frac{f(\bar{\lambda})+m+f(\lambda)+m}{|f(\lambda)+m|^2} \\ &= \frac{|Q|}{m} + \sum_{\mathrm{Im}\lambda>0} \frac{2m}{|f(\lambda)+m|^2} \\ &= \sum_\lambda \frac{m}{|f(\lambda)+m|^2} \\ &= \sum_\varepsilon \frac{m}{\frac{4r^2}{4r^2-\varepsilon^2}\varepsilon^2 + m^2} \end{aligned}$$

and therefore

$$\Sigma = \frac{T}{V}\left\langle \sum_\varepsilon \frac{m}{m^2 + \frac{4r^2}{4r^2-\varepsilon^2}\varepsilon^2} \right\rangle. \tag{2.24}$$

The continuum limit can be obtained by $r \to \infty$, which restores the anti-commutation relation $\{\gamma_5, D\} = 0$ from the Ginsparg-Wilson relation and the familiar form

$$\Sigma_{\mathrm{cont.}} = \int \mathrm{d}\lambda \frac{m\rho(\lambda, m)}{m^2+\lambda^2} \qquad \text{for} \qquad \rho(\lambda, m) = \frac{T}{V}\left\langle \sum_\varepsilon \delta(\lambda - \varepsilon) \right\rangle.$$

The mass dependence of $\rho(\lambda, m)$ is hidden in the fermion determinant that is used to evaluate $\langle \cdots \rangle$. In the chiral limit, $\frac{m}{m^2+\lambda^2} \to \pi\delta(\lambda)$, which under the assumption that the limit can be taken separately gives the famous *Banks-Casher relation*

$$\lim_{m\to 0} \Sigma_{\text{cont.}} = \pi\rho(0,0). \tag{2.25}$$

There is a complication in translating meson operators like $\delta^i(x) = \bar{\psi}(x)\tau^i\psi(x)$ to a lattice with finite lattice spacing and exact chiral symmetry because they are given by a scalar product but the spacetime position is not summed over. Since the chiral projection for either $\bar{\psi}$ or ψ is no longer diagonal in the spacetime coordinates, $\delta^i(x)$ will, for example, involve $\bar{\psi}$ at all lattice points but ψ only at x. $\delta^i(x)$ thus becomes dependent on the choices that are made for the parameters in the chiral rotation and the projections to left- and righthanded fields (namely, if the relation for ψ or that of $\bar{\psi}$ is modified from its continuum form). This becomes even worse if $\pi^i(x)$ is constructed such that it results from an axial rotation of $\delta^i(x)$.

However, these complications vanish if the susceptibilities are considered, which can be written in terms of complete scalar products including an integral over x (cf. (1.12)). The delta meson susceptibility is then modified similarly to the chiral condensate, giving

$$\begin{aligned}
\chi_\delta &= \frac{1}{2}\frac{T}{V}\left\langle \bar{\psi}\tau^i(1 - {}^{D}\!/_{2r})\psi\bar{\psi}\tau^i(1 - {}^{D}\!/_{2r})\psi \right\rangle \\
&= \frac{1}{2}\frac{T}{V}\left\langle \left(\operatorname{tr}\left[\tau^i\tilde{D}^{-1}\right]\right)^2 - \operatorname{tr}\left[\left(\tau^i\tilde{D}^{-1}\right)^2\right] \right\rangle \\
&= -\frac{T}{V}\left\langle \operatorname{tr}\left[\tilde{D}^{-2}\right] \right\rangle .
\end{aligned}$$

Here, τ^i is again a generator of $\mathrm{SU}(N_f)$ where N_f is the number of flavors that are considered to be approximately massless and can therefore be mixed by an axial transformation. The spinor ψ can contain more flavors, but τ^i acting on these gives zero. $\tau^i D$ is to be understood as direct product between the flavor operator τ^i and the one-flavor Dirac operator D.

In terms of the eigenvalues,

$$\operatorname{tr}\left[\tilde{D}^{-2}\right] = \sum_\lambda \frac{1}{(f(\lambda)+m)^2} = -\frac{\mathrm{d}}{\mathrm{d}m}\operatorname{tr}\left[\tilde{D}^{-1}\right].$$

This could be written as a relation between χ_δ and Σ, but then some care has to be taken that the derivative only affects the trace and not the fermion determinant, which is also present in $\langle \dots \rangle$.

Applying a chiral singlet rotation ((2.13) with $\xi = 1$ for simplicity) by $\pi/4$ to $\bar{\psi}(1 - D/2r)\psi$ results in

$$\begin{aligned}
\bar{\psi}'(1 - D/2r)\psi' &= \frac{1}{2}\bar{\psi}\left(1 + i\gamma_5\right)\left(1 - D/2r\right)\left(1 + i\gamma_5\left(1 - D/r\right)\right)\psi \\
&= \frac{1}{2}\bar{\psi}(1 + i\gamma_5)(1 + i\gamma_5 - D/2r - i\gamma_5 D/2r)\psi \\
&= \frac{1}{2}\bar{\psi}(1 + i\gamma_5)(1 + i\gamma_5)(1 - D/2r)\psi \\
&= i\bar{\psi}\gamma_5(1 - D/2r)\psi.
\end{aligned}$$

The same result is obtained for the other possible choice, $\xi = 0$. The pion susceptibility can therefore be written as

$$\begin{aligned}
\chi_\pi &= -\frac{1}{2}\frac{T}{V}\left\langle \bar{\psi}\tau^i\gamma_5(1 - D/2r)\psi\bar{\psi}\tau^i\gamma_5(1 - D/2r)\psi \right\rangle \\
&= -\frac{1}{2}\frac{T}{V}\left\langle \left(\mathrm{tr}\left[\tau^i\gamma_5\tilde{D}^{-1}\right]\right)^2 - \mathrm{tr}\left[\left(\tau^i\gamma_5\tilde{D}^{-1}\right)^2\right] \right\rangle \\
&= \frac{T}{V}\left\langle \mathrm{tr}\left[\left(\gamma_5\tilde{D}^{-1}\right)^2\right] \right\rangle = \frac{T}{V}\left\langle \mathrm{tr}\left[\left(\tilde{D}^{-1}\right)^\dagger \tilde{D}^{-1}\right] \right\rangle.
\end{aligned}$$

In the last step, it was used that the γ_5-hermiticity of D propagates to the shifted propagator $\tilde{D}^{-1}$. In terms of the eigenvalues,

$$\mathrm{tr}\left[\left(\tilde{D}^{-1}\right)^\dagger \tilde{D}^{-1}\right] = \sum_\lambda \frac{1}{|f(\lambda) + m|^2} = \frac{1}{m}\,\mathrm{tr}\left[\tilde{D}^{-1}\right],$$

implying

$$\chi_\pi = \frac{1}{m}\Sigma.$$

The measure for $U_A(1)$ restoration, $\omega = \chi_\pi - \chi_\delta$, can therefore be written as

$$\begin{aligned}
\omega &= \left\langle \left(\frac{1}{m} - \frac{\mathrm{d}}{\mathrm{d}m}\right)\mathrm{tr}\left[\tilde{D}^{-1}\right] \right\rangle = -m\left\langle \frac{\mathrm{d}}{\mathrm{d}m}\left(\frac{1}{m}\,\mathrm{tr}\left[\tilde{D}^{-1}\right]\right) \right\rangle \\
&= \frac{T}{V}\left\langle \sum_\varepsilon \frac{2m^2}{\left(m^2 + \frac{4r^2}{4r^2 - \varepsilon^2}\varepsilon^2\right)^2} \right\rangle.
\end{aligned} \tag{2.26}$$

In the continuum, this corresponds to

$$\omega_{\text{cont.}} = \int \mathrm{d}\lambda \frac{2m^2 \rho_m(\lambda)}{\left(m^2 + \lambda^2\right)^2}.$$

2.3.4 The Overlap Solution

Since a normal operator whose eigenvalues lie on a unit circle in the complex plane has to be unitary, a Dirac operator obeying the Ginsparg-Wilson equation can be written in the form

$$D = r(1 + V) \qquad \text{with} \qquad V^\dagger V = \mathbb{1}.$$

The unitary operator V, on the other hand, can be written as the sign function of some normal kernel W, i.e.

$$V = \operatorname{sgn}(W) = \frac{W}{\sqrt{W^\dagger W}}.$$

Since such a construction is numerically very demanding (cf. section 3.1), it is important to ensure that a GW Dirac operator actually is an improvement over simpler schemes.

One property that is easy to obtain is γ_5-hermiticity. In order to obtain a γ_5-Hermitian Dirac operator, it is sufficient to choose W to be γ_5-Hermitian, which implies that $K = \gamma_5 W$ is Hermitian and the Dirac operator can be written as

$$D = r(1 + \gamma_5 \sigma) = r\left(1 + \gamma_5 \frac{K}{\sqrt{K^2}}\right).$$

Since $\sigma^2 = 1$ as well as $\gamma_5^2 = 1$, this also ensures the Ginsparg-Wilson equation:

$$\{\gamma_5, D\} - \frac{1}{r} D\gamma_5 D = r\left(2\gamma_5 + \sigma + \gamma_5\sigma\gamma_5 - (1 + \gamma_5\sigma)\gamma_5(1 + \gamma_5\sigma)\right) = 0$$

D should also be local in the sense that $|D(n|m)|$ falls exponentially with $|n - m|$, which ensures a fixed interaction length in lattice units and an infinitesimal interaction length in physical units when the continuum limit is performed. Because of the square root in the denominator, it will

not be *ultra-local*, i.e., only involving a few lattice points in the immediate neighborhood. But since the sign function is defined by its polynomial expansion, a good way to start would be to demand ultra-locality from W. The overlap solution to the GW equation consists of choosing $W = D^W_{-M}$, i.e., the Wilson Dirac operator with negative mass (cf. section 1.6), and its locality has been analyzed in detail in [34].

Additionally, the Dirac operator should be free of doublers and reproduce continuum physics in the continuum limit, which at least in the non-interacting case can be easily demonstrated for the overlap solution. In momentum space, the free Wilson Dirac operator is given by

$$W \propto \sum_\mu (1 - c_\mu + i\gamma_\mu s_\mu) - aM$$

with $c_\mu = \cos(ap_\mu)$ and $s_\mu = \sin(ap_\mu)$. If the momentum is in the vicinity of one of the poles of the naive Dirac propagator, i.e. $ap_\mu = \pi n_\mu + \varepsilon_\mu$ with $n_\mu \in \{0, 1\}$ and $n = \sum_\mu n_\mu$, an expansion in ε_μ gives

$$\begin{aligned} c_\mu &= 1 - 2\delta_{1n_\mu} + \mathcal{O}(\varepsilon^2) \\ s_\mu &= (1 - 2\delta_{1n_\mu})\varepsilon_\mu + \mathcal{O}(\varepsilon^3) \end{aligned}$$

For the check that there are no doublers, only the constant terms are of interest. In this case the overlap operator becomes

$$D = r\left(1 + \frac{2n - aM}{|2n - aM|}\right) = \begin{cases} 0 & 2n < aM \\ 2r & 2n > aM \end{cases}$$

In order for the Dirac operator to vanish at the proper pole ($n = 0$) but not at the doublers ($n \geq 1$), the value of aM has to be between 0 and 2. Additionally, r should be of order $1/a$ in order for the doublers to decouple in the continuum limit.

For the comparison with the continuum Dirac operator, the linear terms have to be kept but it is possible to restrict the calculation to the proper pole. Omitting the summation sign, this gives

$$W \propto -M + i\gamma_\mu p_\mu + \mathcal{O}(p^2)$$

and, therefore,

$$\begin{aligned} D &= r\left(1 + \frac{-M + i\gamma_\mu p_\mu}{\sqrt{M^2}}\right) + \mathcal{O}(p^2) \\ &= \frac{r}{M} i\gamma_\mu p_\mu + \mathcal{O}(p^2). \end{aligned}$$

The correct continuum limit $i\gamma_\mu p_\mu$ is therefore obtained with $r = M$. Since the mass of the doublers is given by $2r$, the best result is obtained by choosing aM close to 2, but since interactions can disturb the exact border where the doublers become massless again, it must not be too close. Usually, $aM = 1.8$ was used.

As discussed before, a continuous deformation of the gauge field can not change the topological charge unless the Dirac operator is non-analytic. This will be the case if M is chosen in such a way that K^2 has zero modes, in which case the sign function becomes ill-defined. Specifically, if M is changed continuously and the lowest eigenvalue of K^2 touches zero and rises again to some non-zero value, the topological charge will in general have changed. Numerically, an eigenvalue of K^2 that is close to zero makes the approximation of the sign function difficult and results in a badly satisfied Ginsparg-Wilson equation unless the eigenmodes of K^2 are computed to a very high precision. As will be discussed in section 3.1, the lowest eigenvalues of K^2 were computed before the spectrum of the overlap operator, so if the lowest eigenvalue turned out to be exceptionally small, aM was changed to a value of, for example, 1.7, and the Wilson spectrum was recomputed.

3 Algorithmical and Numerical Details

3.1 Setup

The gauge configurations used in this work were created with dynamical staggered fermions with two light quark flavors and one heavier strange quark flavor, using an improved action called *Highly Improved Staggered Quarks* (HISQ) [35]. This action is constructed such that the effects of the taste mixing term in the standard staggered action are suppressed, which eliminates many $\mathcal{O}(a^2)$ lattice artifacts. The gauge action has also been improved by further closed gauge loops in addition to the simple plaquettes in (1.15) in order to reduce discretization errors. While the HISQ discretization scheme has been very successful for finite temperature studies and even allows relatively small quark masses, at finite lattice spacing there is no clear connection between its infrared modes and its topological structure and unless the continuum limit is already taken, the chiral symmetry is not the same as in the continuum and the chiral limit can not be readily taken. That is why the topological content was instead probed using the overlap operator, which has a clear index theorem and a well-defined chiral symmetry corresponding to the continuum even at finite lattice spacing.

An overview over the used gauge ensembles is given in table 3.1. Most of the gauge configurations were created by the HotQCD collaboration [16]. They have lattice sizes of $32^3 \cdot 8$ or $24^3 \cdot 6$ with temperatures close to T_c, at $1.2\,T_c$ and at $1.5\,T_c$, where T_c is the pseudo-critical temperature as determined in [16]. The strange quark masses in these configurations are tuned to their physical values, while the light quark masses are at $m_s/20$, which is slightly larger than the average of the physical up and down quark masses of about $m_s/27$. This results in a pion mass of 160 MeV instead of the physical value of about 135 MeV. In addition, one set of configurations

#	$N_\sigma^3 \cdot N_\tau$	β	m_l/m_s	T[MeV]	N_{conf}	N_λ
1	$24^3 \cdot 6$	6.150	$1/20$	170	120	100
2	$32^3 \cdot 6$	6.150	$1/40$	162	90	200
3	$32^3 \cdot 8$	6.445	$1/20$	170	120	100
4	$24^3 \cdot 6$	6.341	$1/20$	205	110	50
5	$32^3 \cdot 8$	6.608	$1/20$	200	120	50
6	$32^3 \cdot 8$	6.800	$1/20$	240	160	50

Table 3.1: Lattice size, inverse coupling β, quark mass ratio, temperature, number of configurations and number of computed non-zero eigenmode pairs per configuration for each ensemble.

near T_c with a smaller light quark mass of $m_s/40$ was used that has been produced by the Bielefeld-BNL collaboration [36]. It has a larger volume than the other configurations because the smaller light quark masses imply a smaller pion mass of about 110 MeV and therefore a larger pion wavelength, so the volume has to be larger in order for the ratio of spatial extent to pion wavelength to remain large enough. The configurations of this ensemble turned out to be very rough, slowing convergence to the point that the computation of the spectrum was not feasible. To remedy this, the configurations were subjected to two steps of HYP smearing in order to remove ultraviolet fluctuations. This improved convergence speed greatly but hopefully did not change any infrared behavior since only two steps were used.

The computation of the infrared spectrum of the overlap operator was done using the Kalkreuter-Simma Ritz algorithm, which will be discussed in section 3.2. There are different possibilities to obtain the overlap spectrum (cf. section 3.3). For each configuration, the 50 lowest eigenvectors of $D^\dagger D$ have been computed, followed by a computation of N_λ eigenvectors of the chirally projected operator $P_\pm D P_\pm$ on a chirality that does not have zero modes, with each eigenmode of $P_\pm D P_\pm$ corresponding to an eigenmode pair of D. N_λ was chosen differently for the different ensembles, depending on the size of the eigenvalues. The code was based on a C++ framework that has been developed by the Bielefeld lattice QCD group over the last few years, called ParallelLatticeCode [37]. In section 3.4,

some details about how this code was extended to facilitate the necessary computations will be explained.

As discussed in section 2.3.4, the overlap operator is given by

$$D = r(1 + \gamma_5 \sigma)$$

with $\sigma = {}^{K}/\sqrt{K^2}$, $K = \gamma_5 W$ and $W = D^W_{-M}$ being the Wilson Dirac operator ((1.18)) with negative mass $-M$. In order to match the normalization of the continuum Dirac operator, r and M have to be equal, but for the computation of the eigenvectors the choice of r is irrelevant and the eigenvalues as computed by different choices of r are trivially related. The numerical implementation therefore simply used $r = 1$. The overlap operator and its Hermitian conjugate can be written as $D = 1 + WI(K^2)$ and $D^\dagger = 1 + I(K^2)W^\dagger$, with $I(K^2) = {}^{1}/\sqrt{K^2}$. In order to evaluate $I(K^2)$, the lowest $n = 20$ eigenvectors of K^2 are treated explicitly and the rest is approximated by a rational function. Denoting the eigenvectors and eigenvalues of K^2 as k_i and κ_i and using a rational function of order $[m-1, m]$, this results in

$$I(K^2) \approx \sum_{i=1}^{n} \frac{1}{\sqrt{\kappa_i}} k_i k_i^\dagger + Q(K^2) \left(1 - \sum_{i=1}^{n} k_i k_i^\dagger\right)$$

$$\text{with} \qquad Q(t) = \frac{\sum_{i=1}^{m-1} a_i t^i}{\sum_{i=1}^{m} b_i t^i} = \sum_{i=1}^{m} \frac{c_i}{d_i + t}.$$

$Q(t)$ is a Zolotarev rational function [38, 39], which means that the coefficients are chosen such that the maximal deviation from ${}^{1}/\sqrt{t}$ on some positive interval is minimized. The interval is chosen such that all eigenvalues of K^2 can be found inside of it, with the exception of the lowest n, which are treated explicitly and do not need to be included. The order m of the Zolotarev function is chosen such that the maximal deviation over the given interval is below the threshold of, for example, 10^{-9}. This order is not found analytically, but in a loop between some minimal and some maximal value of m the corresponding Zolotarev coefficients and from those the maximal deviation are computed, stopping once the deviation is small enough.

The application of $Q(K^2)$ on a spinor x involves the solution of the set of linear equations

$$(K^2 + d_i) y_i = x,$$

such that $Q(K^2)x = \sum_{i=1}^{m} c_i y_i$. These equations require multiple inversions, each with the same operator but different shifts. Since the operator is Hermitian, a conjugate gradient (CG) solver can be used, and since the Krylov space for the different shifted operators is the same, they can in fact be solved simultaneously by a multi-shift CG [40]. The number of times the operator has to be applied to a spinor is then equal to the case if only the smallest of the shifts d_i had to be solved and the other solutions can be obtained by additionally performing some linear algebra. Since this multi-shift inversion is the most time-consuming part of the calculation, a highly optimized routine from the QUDA library [41] has been used, which performs it on an Nvidia graphics card. A CPU implementation has also been implemented as a cross-check, but even though the results are essentially the same the CPU solution is far too slow to be used for the actual calculation.

The explicitly treated lowest eigenvectors of K^2 are also computed using the Kalkreuter-Simma algorithm. While this requires some additional computing time, it greatly improves the convergence speed of the remaining inversion. The reason is that the convergence speed is determined by the conditioning number, i.e., the ratio of largest and smallest eigenvalue of the operator that is inverted, where eigenvectors that are orthogonal to the right hand side can be ignored. Since the lowest eigenvalues of K^2 often show a rapid increase, such that the 10th or 15th eigenvalue is several orders of magnitude larger than the 1st, subtracting those contributions gives a large improvement. The interval where the Zolotarev function has to match $1/\sqrt{t}$ is also further away from zero, considerably increasing the lowest shift and often also decreasing the number of terms needed for the approximation. Since the overlap operator has to be applied many hundreds of times for any given configuration, the overhead of first computing some Wilson eigenvectors is well invested.

For a random normalized spinor x, the numbers

$$x^\dagger(\gamma_5 D + D^\dagger\gamma_5 - D^\dagger\gamma_5 D)x \qquad \text{and} \qquad 1 - \|\sigma x\|^2$$

give the deviation from the Ginsparg-Wilson relation and how well the sign function is approximated. At the beginning of the overlap spectrum calculation, these are computed in order to see if the approximation is good enough. Values of the order $\mathcal{O}(10^{-8})$ or smaller turned out to give good

results, with a spectrum that is consistent with the analytical expectations (cf. section 3.3). If the values were considerably larger, the reason was usually that the Wilson eigenvectors had not been determined well enough or that the smallest Wilson eigenvalue was close to zero. The convergence criteria of the multi-shift CG were also adjusted such that these deviations were sufficiently small.

3.2 Kalkreuter-Simma Algorithm

For this work, the spectrum of multiple operators had to be computed. The algorithm that was used for this was the *Kalkreuter-Simma Ritz Conjugate Gradient algorithm*, or shortly KS algorithm. It was first described by Kalkreuter and Simma in [42]. This section will only give an overview of the main idea; some detailed derivations that were sometimes also omitted from the original paper can be found in [43].

The KS algorithm is a modification of a nonlinear conjugate gradient (CG) algorithm. The original linear CG is used to solve the equation $Ax = b$ with some Hermitian operator A and some vector b in a large vector space, or, equivalently, to find the vector x that minimizes the quadratic function $x^\dagger Ax - x^\dagger b - b^\dagger x$. It is described in great detail in [44]. Here, the function that is to be minimized is instead given by

$$\mu(x) = \frac{x^\dagger Ax}{x^\dagger x}, \tag{3.1}$$

which is called the *Ritz function*. If x is decomposed into contributions from the different eigenvectors of A, the Ritz function can easily be shown to be equal to a weighted sum over the eigenvalues, with weights determined by the coefficients. This weighted sum is minimized if the lowest eigenvalue gives the only nonvanishing contribution, i.e., if x is the eigenvector of A with the lowest eigenvalue. Minimizing $\mu(x)$ is therefore equivalent to finding the eigenvector of A that has the smallest eigenvalue.

The nonlinear CG is an iterative algorithm that at each step produces a candidate vector x_i and a search direction p_i. The next candidate x_{i+1} is constructed as the linear combination of x_i and p_i which minimizes (3.1). The next search direction p_{i+1} is constructed from p_i, x_{i+1} and the

gradient $\mu'(x_{i+1})$, with

$$\mu'(x) = \frac{\partial}{\partial x^\dagger}\mu(x) = \frac{Ax - \mu(x)x}{x^\dagger x}. \tag{3.2}$$

Since the Ritz function is invariant under rescaling of x, x is usually normalized after each step, which simplifies some formulae. The exact choice of the coefficients in the construction of p_{i+1} is somewhat involved. It is partly taken from the linear CG, where that particular choice ensures that the search directions that are encountered during the algorithm are all A-orthogonal to each other, i.e., $p_i^\dagger A p_j = 0$. This has the effect that the candidate vector at each step minimizes the quadratic function within the corresponding *Krylov space*, which grows larger with each step. In the nonlinear case, the search directions instead need to be orthogonal with respect to the Hesse matrix

$$\mu''(x) = \frac{1}{x^\dagger x}(A - \mu - \mu' x^\dagger - x\mu'^\dagger),$$

which is not constant, so the orthogonality can only be exact if i and j are not too far apart. The term proportional to x_{i+1} can be added without breaking this property, since $\mu''(x_{i+1})x_{i+1} = 0$ by construction. It can, however, be used to ensure that the search directions and the candidates in each step are orthogonal to each other in the ordinary sense, which also simplifies the calculation.

If the lowest eigenvector of A has already been found, the next one can be obtained by a similar procedure with the addition that the search space is restricted to the space orthogonal to the lowest eigenvector. By making the initial candidate as well as each computed gradient orthogonal to all already found eigenvectors, it is similarly possible to compute the next eigenvector. In practice, it is not necessary to do these orthogonalizations in each step. The original random candidate and its gradient should be made orthogonal to the lower modes, but afterwards it is only necessary to refresh the orthogonalization in regular intervals of a few dozen steps. In that case, all occurring vectors should be orthogonalized instead of just the gradient.

The improvement of Kalkreuter and Simma to this Ritz CG algorithm is to break the computation into several steps, such that a lower eigenvector does not need to be computed to very high precision before higher

eigenvectors are considered. For each vector, the algorithm spends some time minimizing the Ritz function on the subspace orthogonal to lower vectors until either a maximal number of steps is reached or the norm of the gradient has fallen by a fixed ratio. Then the algorithm proceeds with the next vector, until the desired number of vectors has been processed. At the end of this KS step, linear combinations of the found vectors are constructed such that they span the same vector space and such that the matrix $M_{ij} = x_i^\dagger A x_j$ becomes diagonal. This ensures that contributions belonging to lower eigenvectors which have not been picked up by the corresponding candidates but have later been picked up by candidates for higher eigenvectors are accordingly redistributed. These intermediate diagonalizations are done using the Jacobi algorithm, which creates the matrix M_{ij} with the original vectors and iteratively replaces it by

$$M \to G_n M G_n^\dagger$$

with G_n being a simple unitary matrix chosen such that the largest non-diagonal element of M becomes zero, increasing the contribution of the diagonal of M to its Frobenius-norm. The total unitary matrix that is required to transform M from its original form to an essentially diagonal form then can be used to rotate the vectors such that M is diagonal if computed with the new vectors.

After these intermediate diagonalizations, the next KS step again starts with the lowest vector and continues as before. From the change of an eigenvalue estimate during one KS step and the drop of the gradient norm, Kalkreuter and Simma were also able to determine a realistic error estimate for each eigenvalue at the end of the step.

Since higher eigenvector estimates can pick up contributions that belong to lower eigenvectors, which are then redistributed during the intermediate diagonalizations, it is usually more efficient to compute a few more eigenvectors than are actually needed. These *dummies* are included in the algorithm like all the other vectors, but their error estimates are not included in the convergence criteria and at the end of the algorithm an additional diagonalization without the dummies is performed and only the original spinors are stored as results. Essentially, this means that $n + m$ Krylov spaces are searched in order to find the n lowest eigenvectors.

3.3 Representations of the Spectrum

As was shown in section 2.3, the spectrum of the massless overlap Dirac operator can be split into three subsets. There are $n_+ + n_-$ modes with Dirac eigenvalue zero and chiralities $+1$ and -1. A configuration with righthanded as well as lefthanded zero modes occurs with probability zero, so either n_+ or n_- is zero. Further, there are non-zero modes with eigenvalues that lie on the circle with $|\lambda - r| = r$. These come in pairs such that for each eigenvector ψ with eigenvalue λ the vector $\gamma_5\psi$ is also an eigenvector, with the complex conjugate eigenvalue $\bar{\lambda}$. These modes have chirality zero. Finally, there are further real modes with $\lambda = 2r$. These can again be diagonalized to have chiralities ± 1, and like with the zero modes any pair of modes with opposite chiralities can be combined to look like a pair of non-zero modes, which will be shifted away from the real axis by any small perturbation. The number of remaining exact $\lambda = 2r$ modes that can not be disturbed away from the real axis is the same as the number of exact zero modes and their chiralities are opposite to theirs, such that the total trace of γ_5 is zero.

Since the conjugate gradient algorithm as well as its improved version by Kalkreuter and Simma is only able to compute eigenvectors of Hermitian operators, it is unable to work directly with $D = D_{\text{ov}}$. The simplest extension would be to use the Hermitian operator $\gamma_5 D$, but its smallest eigenvalues are not related to the infrared modes of D but to modes near $\lambda = 2r$. In fact, the different eigenmodes of D can be mapped to eigenmodes of $\gamma_5 D$: a zero mode with $D\psi = 0$ will trivially also yield $\gamma_5 D\psi = 0$, a non-zero mode pair $(\psi, \gamma_5\psi)$ with $D\psi = \lambda\psi$ and $D\gamma_5\psi = \bar{\lambda}\gamma_5\psi$ can be rotated to give two eigenmodes of $\gamma_5 D$ with eigenvalues $\pm|\lambda|$ and on the subspace with $D\psi = 2r\psi$ diagonalization of γ_5 yields modes with $\gamma_5 D\psi = \pm 2r\psi$. Since the KS algorithm computes the eigenvectors with the smallest eigenvalues, if applied to $\gamma_5 D$ it would give modes with $\gamma_5 D\psi \approx -2r\psi$.

There are still multiple possibilities to create a Hermitian operator A from the overlap operator such that its infrared modes can be derived from the lowest modes of A. This section will discuss several possibilities with their advantages and disadvantages.

3.3.1 Direct Computation with the Squared Operator

The most direct possibility is to choose $A = D^\dagger D$. Since the overlap operator is normal, there is a complete set of eigenvectors of D that are also eigenvectors of $D^\dagger$. If $D\psi = \lambda\psi$ for such an eigenvector, the complex conjugate of

$$\psi^\dagger D\psi = \lambda$$

implies $D^\dagger\psi = \bar{\lambda}\psi$. Applying A to this vector therefore gives the eigenvalue $|\lambda|^2$, which with the representation (2.17) gives

$$|\lambda|^2 = \left|\frac{1}{2r}\left(\varepsilon^2 + i\varepsilon\sqrt{4r^2-\varepsilon^2}\right)\right|^2 = \frac{1}{4r^2}\left(\varepsilon^4 + \varepsilon^2(4r^2-\varepsilon^2)\right) = \varepsilon^2.$$

Zero modes of D are therefore mapped onto zero modes of A, which are the smallest modes of this operator. A pair of non-zero modes ψ, $\gamma_5\psi$ with complex conjugate eigenvalues λ and $\bar{\lambda}$ is mapped onto a pair of modes that have the same eigenvalue $|\lambda|^2$. In fact, because of this degeneracy any linear combination is also an eigenvector of A and the KS algorithm can not be expected to give exactly the eigenvectors of D. Instead, it will in general compute a pair

$$x = c\psi + zs\gamma_5\psi \qquad\qquad y = z'(c\gamma_5\psi - \bar{z}s\psi)$$

with some real non-negative coefficients c and s that obey $c^2 + s^2 = 1$ and some phases z, z' with $|z| = |z'| = 1$. There is no phase in front of $c\psi$ because it can be absorbed into ψ, which only needs to be determined up to a phase. x and y are also eigenvectors of A with eigenvalues ε^2.

While ψ and $\gamma_5\psi$ have chirality zero, this no longer holds for x and y. Instead,

$$\chi_x \equiv x^\dagger\gamma_5 x = 2sc\,\mathrm{Re}z \qquad\qquad \chi_y = -2sc\,\mathrm{Re}z.$$

Therefore, the chiralities will be some arbitrary numbers between -1 and 1 with equal magnitude and opposite sign. This expectation can be used in addition to the error estimates of the eigenvalues from the KS algorithm to decide if the algorithm has converged. In particular, it allows to clearly distinguish the zero modes from the non-zero modes. Table 3.2

n	λ_n	$\Delta\lambda_n$	χ_n
0	$1.16 \cdot 10^{-13}$	$1.2 \cdot 10^{-11}$	$+1.000000$
1	$7.55 \cdot 10^{-13}$	$3.0 \cdot 10^{-11}$	$+1.000000$
2	$9.01 \cdot 10^{-13}$	$4.5 \cdot 10^{-11}$	$+1.000000$
3	$5.72 \cdot 10^{-12}$	$1.5 \cdot 10^{-10}$	$+1.000000$
4	$1.55 \cdot 10^{-6}$	$1.2 \cdot 10^{-11}$	$+0.987787$
5	$1.55 \cdot 10^{-6}$	$2.9 \cdot 10^{-12}$	-0.987787
6	$2.56 \cdot 10^{-3}$	$2.1 \cdot 10^{-11}$	-0.971247
7	$2.56 \cdot 10^{-3}$	$1.3 \cdot 10^{-11}$	$+0.971247$
8	$2.84 \cdot 10^{-3}$	$1.2 \cdot 10^{-10}$	-0.112028
9	$2.84 \cdot 10^{-3}$	$9.0 \cdot 10^{-11}$	$+0.112028$

Table 3.2: Example output of Kalkreuter-Simma algorithm at last iteration for configuration no. 129 of the $32^3 \times 8$ ensemble at $1.5\,T_c$. The ten lowest eigenvalues with their error estimates and chiralities are shown.

shows an example output of the algorithm, with four zero modes that are clearly separated not only by having eigenvalues that are several orders of magnitude lower than the following modes but also by showing the pattern that the first four modes have chiralities very close to $+1$, while the following modes have arbitrary chiralities but come in pairs with the same eigenvalue and opposite chiralities.

In this example, the lowest pair of non-zero modes is in fact still well separated in magnitude from the following modes. This is a *near-zero mode pair*, which is the result of two zero modes with opposite chiralities being disturbed away from the real axis as discussed above. These will turn out to play an important role in keeping the axial symmetry broken at high temperatures.

While for many applications the eigenvalues and eigenvectors of $A = D^\dagger D$ are sufficient, sometimes those of D are needed. Once the results are well enough converged such that the topological charge is clearly visible and the higher modes all come in pairs which are clearly separated from other pairs[1], it is possible to compute the necessary coefficients to undo

[1] The following procedure does not work if there are further degeneracies in the non-zero modes. While this does not occur for realistic configurations, it is a problem with, for example, a non-interacting test run where the gauge links are set to unity.

this rotation via $\psi = cx - \bar{z'}sy$. In addition to the chiralities χ_x and χ_y, the combination

$$\chi_{xy} \equiv x^\dagger \gamma_5 y = z'(zc^2 - \bar{z}s^2)$$

can also be easily computed. Its magnitude is in fact related to χ_x because x and y span a subspace that is invariant under the application of γ_5, so

$$|\chi_{xy}|^2 = x^\dagger \gamma_5 y y^\dagger \gamma_5 x = x^\dagger \gamma_5 (1 - xx^\dagger)\gamma_5 x = 1 - \chi_x^2.$$

Therefore, these numbers yield two independent measurements, namely χ_x and the phase of χ_{xy}, which are not enough to determine both missing phases as well as s and c. Even though z is not needed for the reconstruction of ψ, it is not possible to obtain z' from just χ_x and χ_{xy}. Any solution (z, z', s, c) that is compatible with specific values of χ_x and χ_{xy} can be transformed into infinitely many different solutions by changing s, c and z such that the phase of $zc^2 - \bar{z}s^2$ changes while its norm (and therefore also χ_x) does not[2]. This change of phase can be absorbed by an appropriate change of z' such that χ_{xy} also does not change.

Therefore, it is necessary to at least apply D to one of the obtained vectors in order to gain more information. Using $D\psi = \lambda\psi$ and $D\gamma_5\psi = \bar{\lambda}\gamma_5\psi$, it can be assumed without loss of generality that $\operatorname{Im}(\lambda) > 0$—if necessary, this can be achieved by swapping ψ and $\gamma_5\psi$. Applying D on x, the result is

$$\begin{aligned} Dx &= c\lambda\psi + sz\bar{\lambda}\gamma_5\psi = \operatorname{Re}(\lambda)x + i\operatorname{Im}(\lambda)(c\psi - sz\gamma_5\psi) \\ x^\dagger Dx &= \operatorname{Re}(\lambda) + i\operatorname{Im}(\lambda)(c^2 - s^2) \\ y^\dagger Dx &= -2isc\bar{z'}\operatorname{Im}(\lambda). \end{aligned}$$

From these two scalar products, z', s and c can be determined. Namely,

$$\frac{y^\dagger Dx}{|y^\dagger Dx|} = -i\bar{z'}$$

and the complex number

$$\alpha = \operatorname{Im}(x^\dagger Dx) + i|y^\dagger Dx| = \operatorname{Im}(\lambda)(c^2 - s^2 + 2isc)$$

[2] The fact that this is possible can be checked by regarding partial derivatives of the norm and phase with respect to the independent variables c and φ in $z = \mathrm{e}^{i\varphi}$.

gives

$$\sqrt{\frac{\alpha}{|\alpha|}} = \sqrt{c^2 - s^2 + 2isc} = \pm(c + is).$$

This procedure is numerically stable unless the eigenmode pair is actually a pair of accidental zero modes, i.e. $\lambda = 0$. In practice, the near-zero modes were far enough away from zero to give stable results. This was checked by computing $|r - \psi^\dagger D\psi|^2 - r$ and $|D\psi - \psi\psi^\dagger D\psi|^2$. These measure how well the obtained complex eigenvalue lies on the eigenvalue circle and if ψ is indeed a good approximation to an eigenvector of D. If the rotation was not performed correctly, these measures take much larger values than with the correct rotation, and the near-zero modes did not give significantly worse results than higher modes. In fact, the above formulae are chosen such that they are only sensitive to the imaginary part of the eigenvalues and not to the real part. Since the real part is of order ε^2 while the imaginary part is of order ε, it would be much more sensitive to fluctuations because of the closeness to zero.

In order to save disk space, the rotated vectors were not archived together with the eigenvector results. However, the recomputation of the phases takes quite some time because it requires the application of D. As a compromise, only the complex values $x^\dagger Dx$ and $y^\dagger Dx$ were stored and a separate program could be called whenever the rotated vectors were needed which read these values and the eigenvectors of $D^\dagger D$ from disk and stored the eigenvectors of D without needing to apply the overlap operator.

One disadvantage of using $A = D^\dagger D$ is that each application of it requires two applications of the overlap operator, which is the most time critical part of the program. Using the Ginsparg-Wilson equation, it is possible to rewrite

$$D^\dagger D = r(D + D^\dagger),$$

which still requires two applications but it is in principle possible to speed this up if the multishift inverter that is part of the overlap Dirac operator (cf. section 3.4) can be used on two right hand sides at the same time. This will not save any arithmetic operations but might have better memory reusage because the gauge field only needs to be loaded into cache once.

However, the QUDA implementation that was used in this work did not offer this possibility, which would anyhow be difficult to achieve on a graphics card because it would require about twice as much memory on the device. Since two spinors per shift are required for a multishift inverter, a large portion of the device memory was already occupied.

Another problem of using $D^\dagger D$ as the operator in the KS Ritz algorithm is that it will find higher eigenvectors by essentially searching from scratch with the only restriction that the search space is orthogonal to the lower eigenvector candidates that have already been found. It does not take advantage of the fact that some eigenvectors are related to each other, namely that one non-zero mode can be constructed from its partner. It is not straightforward to remedy this because it is not a priori clear how many zero modes a given configuration has and thus which modes are paired. Several attempts were made in this direction, two of which will be discussed now. For the various comparisons, three configurations were chosen from the $32^3 \cdot 8$ ensemble at $1.5\,T_c$ which were subjected to ten steps of HYP smearing. These HYP smeared configurations will later be used in an analysis of the effects of smearing on topological properties, but here they are simply chosen because they are smoother and the application of the overlap operator is therefore faster. The first configuration was chosen such that it had neither zero nor near-zero modes, with only bulk modes starting at $\mu = \frac{\varepsilon^2}{r^2} = \mathcal{O}(10^{-3})$. The second one had no zero modes, but one near-zero mode pair at $\mathcal{O}(10^{-8})$. Finally, the third configuration had two righthanded zero modes and two near-zero mode pairs at $\mathcal{O}(10^{-6})$ and $\mathcal{O}(10^{-4})$. The stopping criteria in the several cases were usually chosen such that each relative error for μ must be below 10^{-6} unless the absolute error is already below 10^{-10}.

3.3.2 Improvement of the Ritz Starting Candidates

Instead of trying to only compute a reduced set of vectors, i.e., only one of each eigenvector pair, a simpler modification is achieved if all modes are still computed but the would-be partners of already computed modes are used to improve candidates for further modes. Specifically, at the start of the Ritz minimization of the mode x_{n+1}, a vector p is constructed from x_n, which is used to improve x_{n+1} by replacing it with $x'_{n+1} = \alpha x_{n+1} + \beta p$ with α and β chosen such that x'_{n+1} is normalized and the eigenvalue

estimate $|Dx'_{n+1}|^2$ takes the smallest possible value. As long as p is in the subspace where the minimization of the eigenvalue estimate of x_{n+1} is allowed, i.e., orthogonal to x_m for any $m \leq n$, this should not give worse results than the original algorithm—if the additional information can not be used to lower the eigenvalue estimate, x_{n+1} will stay unchanged.

The vector p is constructed by computing $\gamma_5 x_n$ and making the result orthogonal to x_m for all $m \leq n+1$. Since the subspace that is spanned by a non-zero mode pair is invariant under the application of γ_5, this will give the partner of x_n if x_n is already well converged but its partner is not yet found. If the norm of p is below some threshold, this means that $\gamma_5 x_n$ does not contain any helpful contribution outside of the subspace that is spanned by the vectors up to x_{n+1}. This can happen in several cases, most of which just mean that the vectors are already converged well enough. First, x_n might be a zero mode, which is also an eigenvector of γ_5. Second, the partner of x_n might be x_{n-1} and both are already determined very well. Third, x_{n+1} might indeed be the partner of x_n, but since they are already determined very well, they already span the correct two-dimensional eigenspace of $D^\dagger D$. Finally, there is also the possibility that x_n is an accidental chiral mode with $x_n^\dagger \gamma_5 x_n \approx \pm 1$. This can happen if it is already mostly converged since the two-dimensional non-zero eigenspace of $D^\dagger D$ also contains a left- and a righthanded mode, but it can also happen before that. The worst case should be that no improvement takes place and the algorithm converges as fast as the unimproved version.

In figs. 3.1 to 3.3, the original algorithm is compared with this improved version in terms of how many applications of the overlap operator are required to get 50 eigenvalues to converge. The runs included two additional dummy modes which were not included in the error estimates. Each mode is plotted as one line, with horizontal sections indicating that the algorithm was working on a different mode at that time or that the values did not change visibly any more. In order to visualize the convergence, at the end of each Kalkreuter-Simma step the average of the error estimates over the 50 modes is shown. The relative errors are also included, but since they do not become small for the zero modes, the arithmetic mean would be dominated by these modes in a simple average. Instead, the geometric mean is shown.

It can be seen that including information from the current estimate of the next lowest mode at the beginning of each Ritz part indeed improves

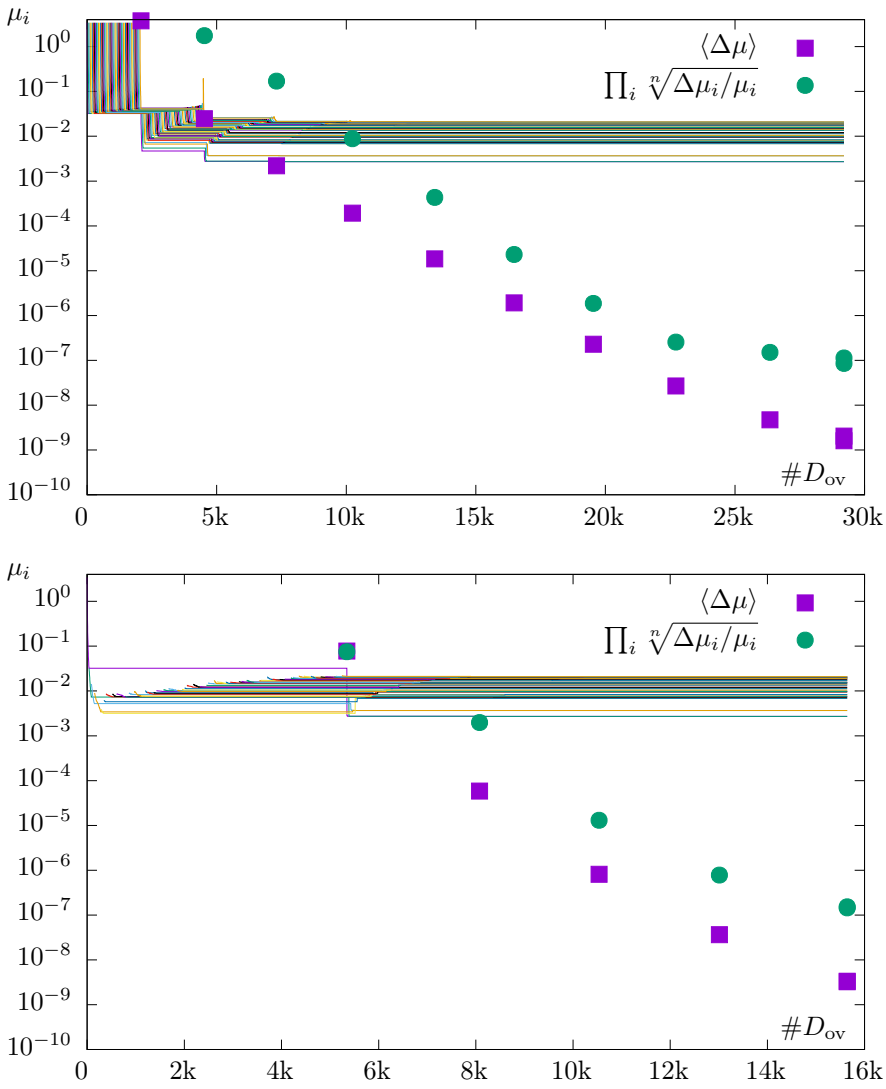

Figure 3.1: Convergence of the 50 lowest eigenvalues of a HYP-smeared configuration at $1.5\,T_c$ that turned out to have neither zero nor near-zero modes. The first plot shows the original Kalkreuter-Simma algorithm with $A = D^\dagger D$ and the second shows the version with improved starting vectors as described in section 3.3.2. On the x-axis, the number of applications of the overlap operator in the Ritz part of the algorithm is denoted and the lines mark the evolution of each eigenvalue estimate. Additionally, the arithmetic mean of the error estimates as well as the geometric mean of the relative errors are plotted. It should be noted that the x-axis has a different range for the two cases.

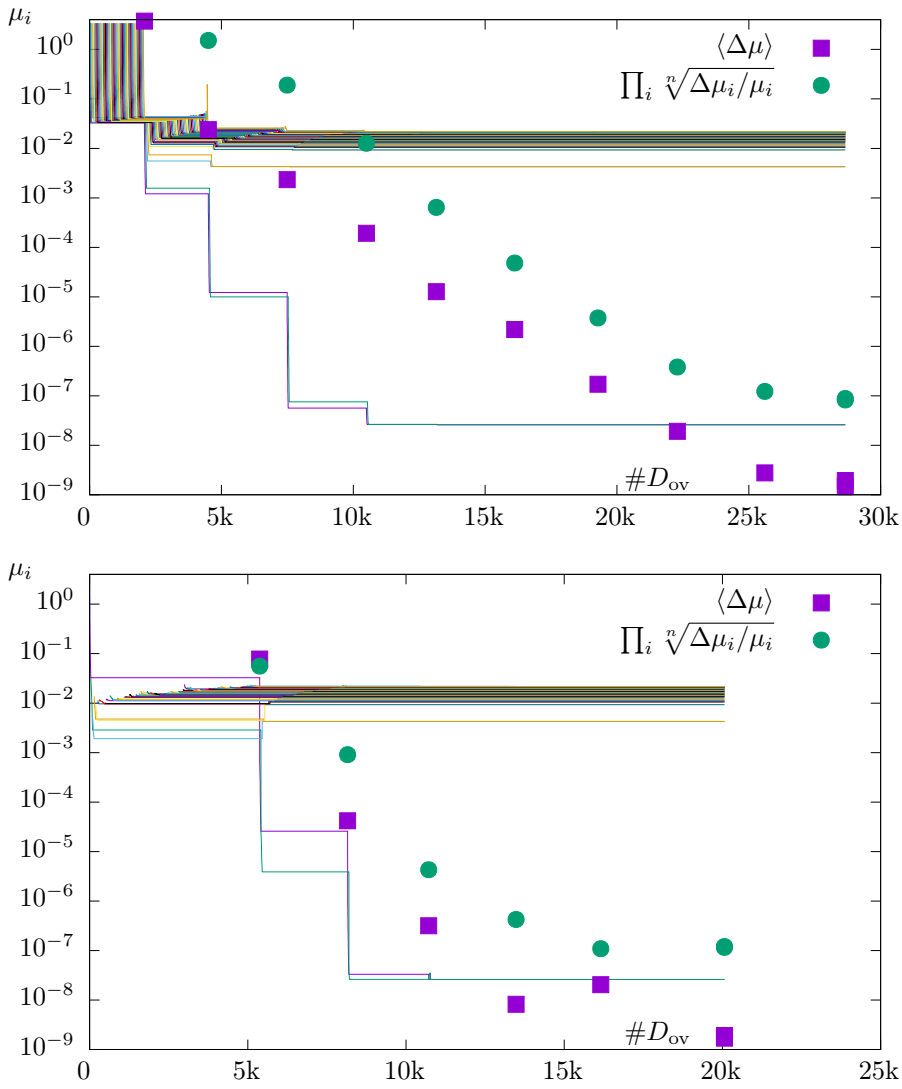

Figure 3.2: Convergence of the 50 lowest eigenvalues of a smeared configuration at $1.5\,T_c$ that turned out to have no zero modes but one near-zero mode pair. See fig. 3.1 for details.

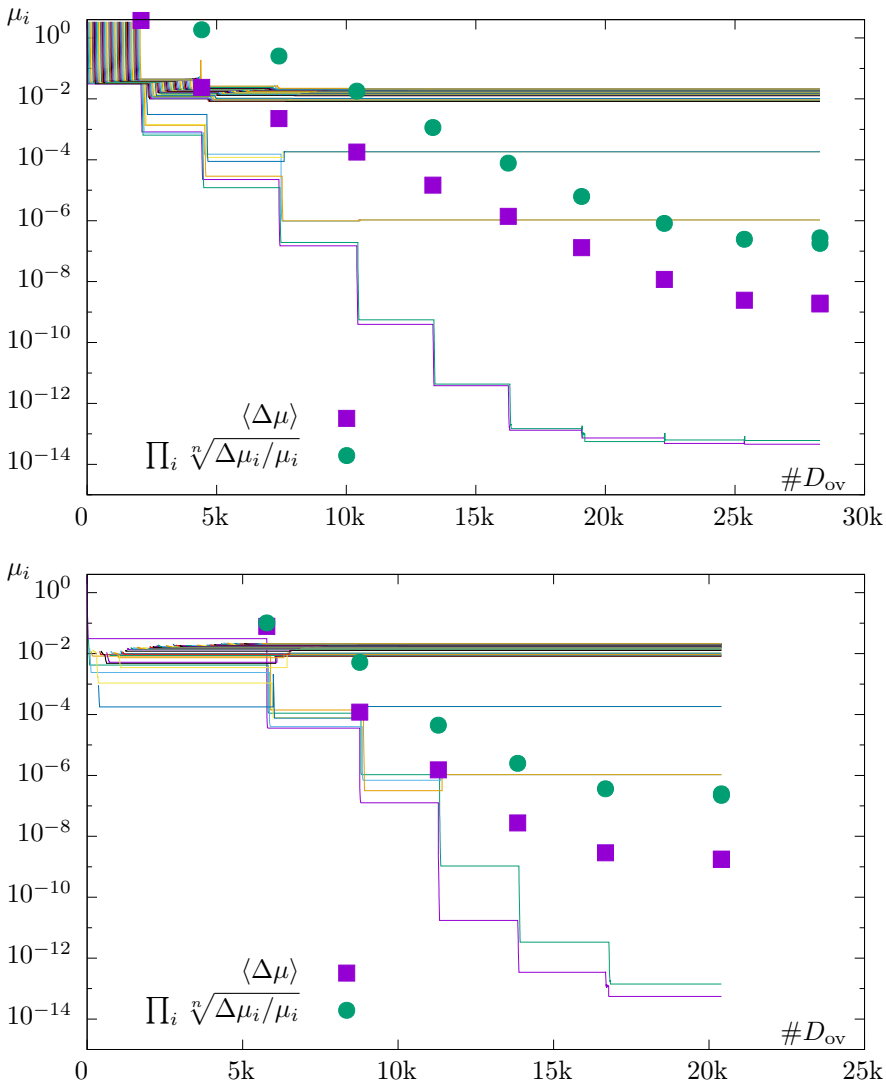

Figure 3.3: Convergence of the 50 lowest eigenvalues of a smeared configuration at $1.5\,T_c$ that turned out to have two zero modes and one near-zero mode pair. See fig. 3.1 for details.

the algorithm such that it takes about 30-50% less applications of the overlap operator. All but the very first mode start the first iteration at values of about 10^{-2} instead of about 1, which gives them a significant head start. The first KS iteration then takes as much time as the first few iterations in the original algorithm together, but the resulting Ritz estimates still drop faster towards their final values. After a few iterations, the algorithms are identical because no further improvement is possible from the previous mode. If this point is reached for multiple modes at the same time, it can happen that the error estimates increase in one iteration instead of decreasing, as can be seen in fig. 3.2.

3.3.3 Inclusion of Partner Modes

Another approach to reduce the number of operations by taking advantage of the pairing of overlap eigenmodes turned out to in fact take longer than the original algorithm more often than not. For the sake of completeness, it will still be described here in the hope that future attempts can take advantage of the experiences.

The idea is to change the algorithm such that only one mode of each pair has to be computed. In order to keep higher modes from picking up contributions that belong to the partners of already computed lower modes, at the end of each Ritz part the best guess for the *partner* of the current *proper* mode is computed and included in all further orthogonalizations.

The number of partner modes does not have to be equal to the number of proper modes because of zero modes, which only span a one-dimensional eigenspace of A. If at the end of the Ritz part for the proper mode x_n the number of partner modes that have already been computed is $m-1$, the next partner mode p_m is computed by normalizing

$$\tilde{p}_m = \gamma_5 x_n - \sum_{i=1}^{n} x_i x_i^\dagger \gamma_5 x_n - \sum_{i=1}^{m-1} p_i p_i^\dagger \gamma_5 x_n.$$

The norm of $\tilde{p}_m$ can be used to distinguish if x_n is a zero mode, since these are also eigenmodes of γ_5 and therefore $\tilde{p}_m$ will be almost vanishing. If this turns out to be the case, the mode is discarded, which is realized by not incrementing the counter for the number of partner modes.

One problem that arises is that higher, non-zero, modes might also accidentally be chiral because it is possible to span the eigenspace of a

non-zero mode pair by two eigenmodes of γ_5 with eigenvalues $+1$ and -1. While this does not usually happen in the original algorithm, where the chiralities of the non-zero modes take arbitrary values between -1 and $+1$, the modification depicted here has the property that in any configuration that has zero modes of a given chirality the proper non-zero modes are driven to the same chirality. The reason seems to be that the partner modes are included in the orthogonalizations for the further modes but not in the intermediate diagonalizations at the end of each KS iteration. While the sum of all chiralities is conserved by such a diagonalization, during the Ritz part the chiralities of the zero mode candidates are driven toward the value ± 1 determined by the topological charge and this seems to be partly distributed onto the non-zero modes in the diagonalization.

If this problem is not fixed, the algorithm fluctuates because once the modes become chiral, their partners will be discarded and higher modes suddenly need to decrease further in order to fill the formed gap. This leads to both modes of each pair being present in the directly computed modes (in contrast to the partner modes), which will again introduce modes with mixed chiralities. If this has the effect that non-zero modes are again driven away from extreme chiralities, the algorithm will show large fluctuations because whether a non-zero mode pair is represented by two separate modes or by a mode and a partner mode is not stable.

One possibility is to include the partners in the diagonalization, but this raises the question of how the resulting modes are again to be separated into proper and partner modes after the diagonalization. Instead, it is possible to give the construction of the partner a second chance if the first candidate yields a vanishing result. The partner mode is then constructed in a similar way as above, but from Dx_n instead of $\gamma_5 x_n$. While this is certainly more time consuming than a simple application of γ_5, it allows to distinguish accidentally chiral non-zero eigenvectors of $D^\dagger D$ from necessarily chiral zero modes. The reason is that while the eigenspace of a non-zero mode pair can either be spanned by eigenvectors of γ_5 or by eigenvectors of D, these bases are not the same and if x_n is a chiral non-zero mode it can not at the same time be an eigenmode of D.

Starting with an almost chiral mode x, the question becomes how to decide if Dx represents the same (zero) mode or if it can be used to construct the partner in a non-zero mode pair. Since the magnitude of Dx is small in the cases of interest regardless of whether it is a zero

mode or not, its norm after orthogonalization with respect to x (and lower modes) is not as helpful as in the case of $\gamma_5 x$, which is automatically normalized. A more stable criterion can be derived from the observation that $y = Dx - xx^\dagger Dx$ is chiral (with chirality opposite to that of x) if x is an accidentally chiral non-zero mode, while no certain prediction can be given if x is a zero mode—since for a zero mode x and Dx are not in any relevant way linearly independent, its components will essentially be determined by numerical fluctuations. The number

$$z = \frac{|y|^2}{|y^\dagger \gamma_5 y|} - 1$$

will therefore become small for chiral non-zero modes and large for zero modes. It has been observed to be $\mathcal{O}(10^{-2})$ or larger for zero modes, while it is $\mathcal{O}(10^{-5})$ or lower for non-zero modes. The algorithm as it was finally implemented checks if it is lower that 10^{-3} and correspondingly decides if the partner mode counter should be increased or not. If the mode is accepted, it is then also orthogonalized with respect to all lower modes and their partners and then normalized.

For this modification, memory for another set of spinors has to be allocated, so if N modes have to be computed, the algorithm needs memory for slightly more than $2N$ spinors. While the algorithm usually anyhow profits from such a second spinor array during the intermediate diagonalizations, the original algorithm can be made to do without it by intelligently swapping spinors to disk during the diagonalization. While this is not the case with the improvement discussed here, this is usually not a problem because it needs to compute less modes in the first place. If the original algorithm is used to compute N modes, n of which are zero modes, an equivalent result can be achieved with an algorithm that computes only one mode of each pair with only $\frac{N+n}{2}$ modes. Since the number of zero modes is not known a priori, the results will usually not be directly comparable. While the computations shown in figs. 3.1 to 3.3 were done with 50 modes and 2 dummies, the corresponding runs with the modification discussed here has been done with 30 modes and 5 dummies.

The results can be seen in figs. 3.4 to 3.6. In one case the algorithm took about the same number of operations as the unaltered version, in another about twice as much and in the third case the errors started to increase and the algorithm stopped because the values were fluctuating. It seems

that this modification is unstable with respect to which modes represent a two-dimensional eigenspace and which only a one-dimensional. While the criteria are chosen such that they become stable once the algorithm is converged well enough, the instabilities at the beginning have an over all negative effect on convergence speed.

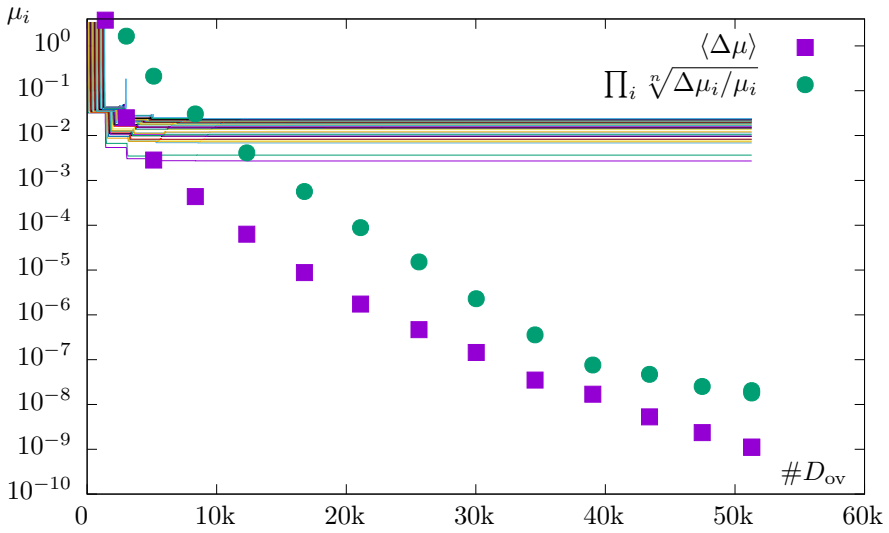

Figure 3.4: Convergence of the modified algorithm described in section 3.3.3 for the configuration with neither zero nor near-zero modes (compare fig. 3.1).

3.3.4 Chirally Projected Operator

The goal of the modifications described in the last section was to somehow compute only one mode of each non-zero mode pair. While the method used there turned out to be quite inefficient, this goal can actually be achieved by a different approach, namely by restricting the search space for eigenmodes to a specific chirality, i.e., to either only lefthanded or only righthanded modes. Since each non-zero mode pair can be rotated to give a lefthanded and a righthanded mode, which are also eigenmodes of $A = D^\dagger D$ with the same eigenvalue ε^2, this will reproduce one of these modes while omitting the other. Since the chiralities of zero modes (if

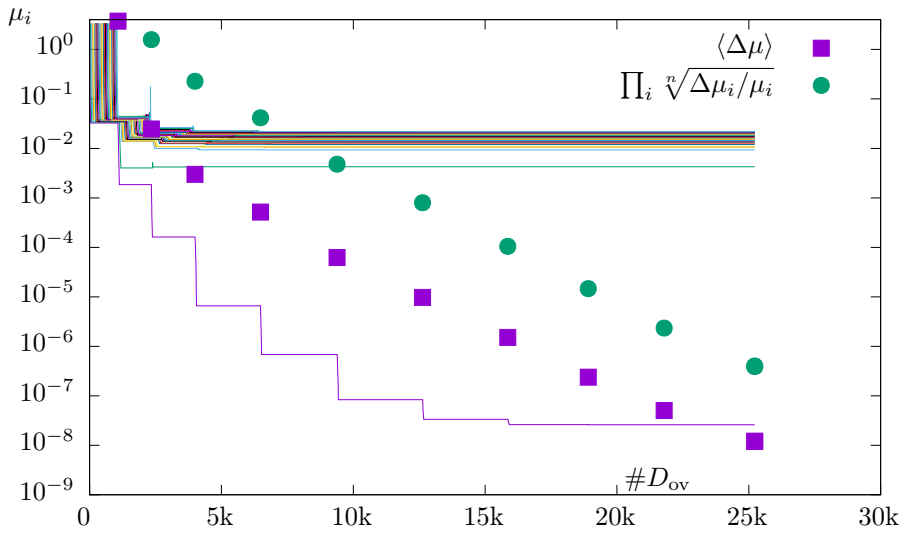

Figure 3.5: Convergence of the modified algorithm described in section 3.3.3 for the configuration with near-zero but no zero modes (compare fig. 3.2).

present) are not known a priori, a clear problem of this approach is that the zero modes might be missed if the wrong chirality is chosen. However, this can be remedied by first calculating all the low modes of a given chirality and then, if there are no zero modes, additionally computing the modes of the opposite chirality. The modes computed in the first run can even be used to create quite good starting candidates for the second run by applying D to them and projecting to the opposite chirality. If Dx does not have any significant contributions from the opposite chirality, this is indicative of a zero mode, which can then be skipped.

The computation of eigenmodes of a chirally projected operator is realized by using a simplified spinor structure for the KS algorithm, which only stores either the first two or the last two Dirac components—this assumes a gamma matrix basis where $\gamma_5 = \mathrm{diag}(1, 1, -1, -1)$. The spinors therefore only take half as much memory, which also makes linear algebra routines quicker. For the application of the chirally projected operator, a chiral spinor is first copied to a full spinor and after the application the correct half of the components is copied to a chiral spinor again.

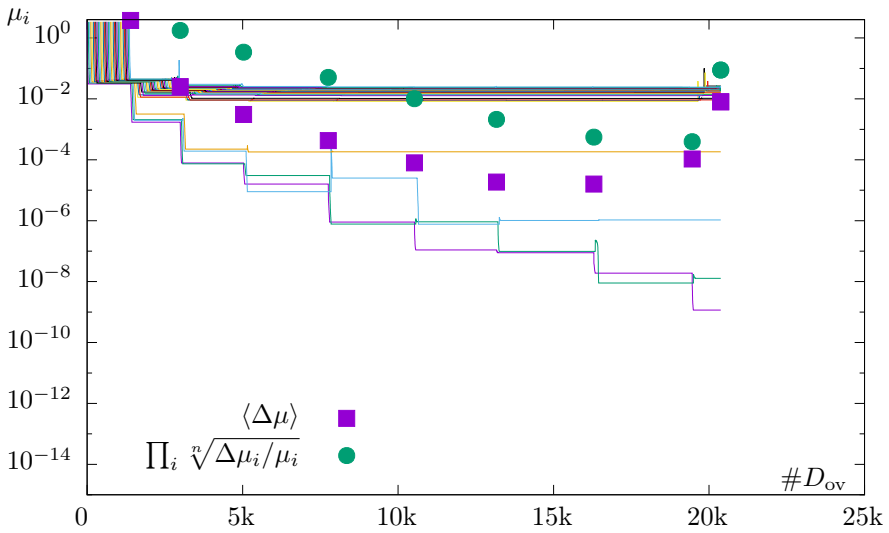

Figure 3.6: Convergence of the modified algorithm described in section 3.3.3 for the configuration with zero and near-zero modes (compare fig. 3.3).

The algorithm can be further accelerated because the chirally projected operator does no longer need to be squared in order to be Hermitian. In fact, if $P_\pm$ is the projection to right- or lefthanded modes, the operator $P_\pm D P_\pm$ is Hermitian because of

$$(P_\pm D P_\pm)^\dagger = P_\pm D^\dagger P_\pm = P_\pm \gamma_5 D \gamma_5 P_\pm = (\pm P_\pm) D (\pm P_\pm) = P_\pm D P_\pm.$$

If this operator is regarded as acting on the whole space, the whole subspace of spinors with opposite chirality is mapped to zero, which makes them eigenvectors with eigenvalue zero. However, since all vectors in the KS algorithm are restricted to the chirality in question, this is not a problem. If

$$\psi_\pm = P_\pm \psi = \frac{1}{2}(\psi \pm \gamma_5 \psi)$$

is the (not normalized) corresponding representative of a non-zero mode

pair $(\psi, \gamma_5\psi)$ with eigenvalues λ and $\bar{\lambda}$,

$$\begin{aligned} P_\pm D P_\pm \psi_\pm &= P_\pm \frac{1}{2}(\lambda\psi \pm \bar{\lambda}\gamma_5\psi) \\ &= \frac{1}{2} P_\pm (\operatorname{Re}(\lambda)(\psi \pm \gamma_5\psi) + i \operatorname{Im}(\lambda)(\psi \mp \gamma_5\psi)) \\ &= \operatorname{Re}(\lambda)\psi_\pm. \end{aligned}$$

Using the representation (2.17), the eigenvalue of this operator is therefore $\frac{\varepsilon^2}{2r}$, in contrast to the eigenvalue ε^2 of $P_\pm D^\dagger D P_\pm$.

In figs. 3.7 to 3.10, the convergence behavior of these runs is plotted in a similar way as before. The eigenvalues are scaled so they can be directly compared to the earlier runs. The number of eigenvalues has been set to 30 plus 5 dummies, but since both chiralities are eventually computed and one of the chiralities does not have zero modes, this corresponds to the computation of 60 non-zero modes in addition to the zero modes. Two important things can be observed here: First, the total number of overlap operator applications that is needed to get more or less correct values is considerably lower than in the original algorithm—even though the number of computed modes is effectively higher—, ranging from about 30% if there are no zero modes to about 50% for the configuration with zero modes. Second, the zero and near-zero modes fluctuate more than before and the zero modes do not reach similarly low values. This also has an effect on the errors, which do not fall much beyond 10^{-8}. If the rescaled values are compared in detail with those obtained from $A = D^\dagger D$, it can be seen that there is a mismatch for a few of the lowest modes, while modes beyond the 10th one or so match very well. Sometimes the lowest modes even took negative values, at which point the algorithm was stopped and resumed with $A = P_\pm D^\dagger D P_\pm$. While this was not the case here, it happend especially for configuations at lower temperatures.

The reason for these instabilities seems to be related to the numerical approximation of the sign function needed in the overlap operator influencing the hermiticity of $P_\pm D P_\pm$. As a check, at the beginning of each Ritz part when Ax is calculated, the complex number $x^\dagger Ax$ is printed out. The algorithm only uses the real part of this number and the imaginary part should anyhow vanish if A is indeed Hermitian. For $A = D^\dagger D$, this number takes values like $\mathcal{O}(1) + \mathcal{O}(10^{-10})i$ if an essentially random vector is plugged in (i.e., in the first KS iteration) and values like $\mathcal{O}(10^{-14}) + \mathcal{O}(10^{-17})i$

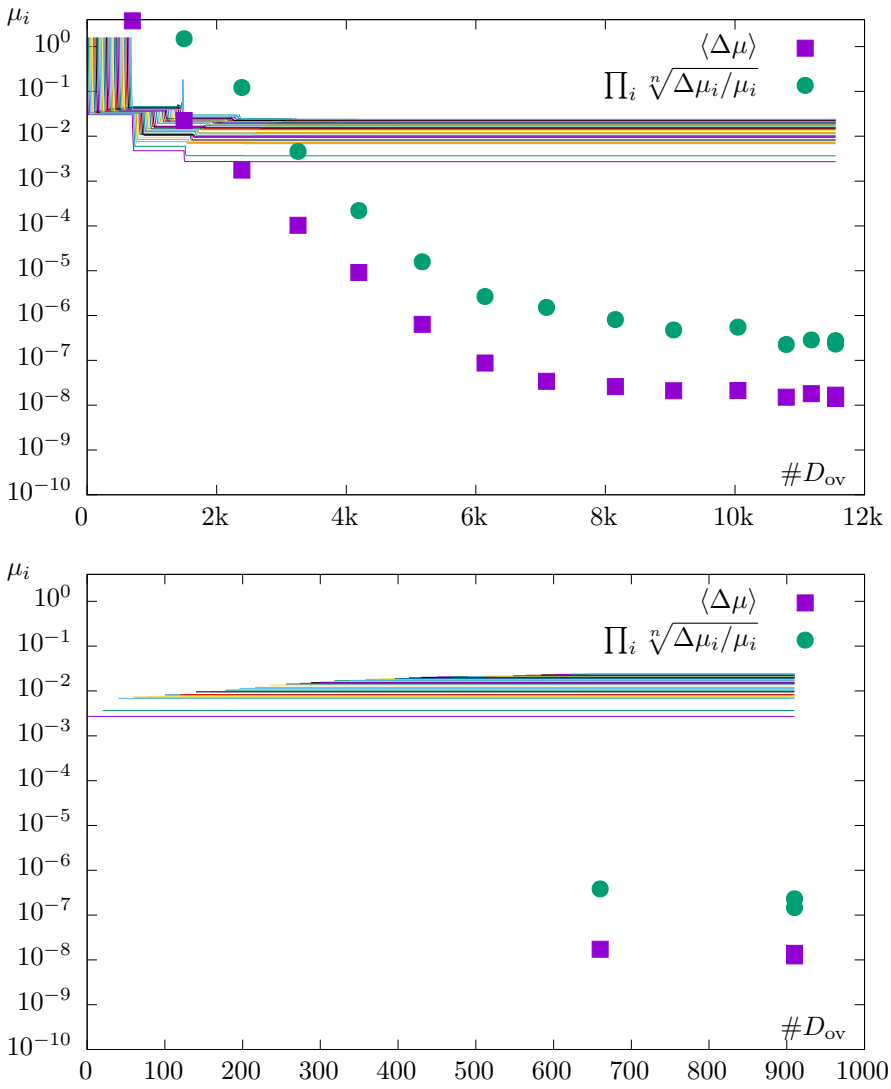

Figure 3.7: Convergence of 30 eigenmodes for the configuration with neither zero nor near-zero modes (cf. fig. 3.1), obtained from first calculating the eigenmodes of $P_{-}DP_{-}$ (top) and then those of $P_{+}DP_{+}$ (bottom figure) starting from righthanded modes created from the first results.

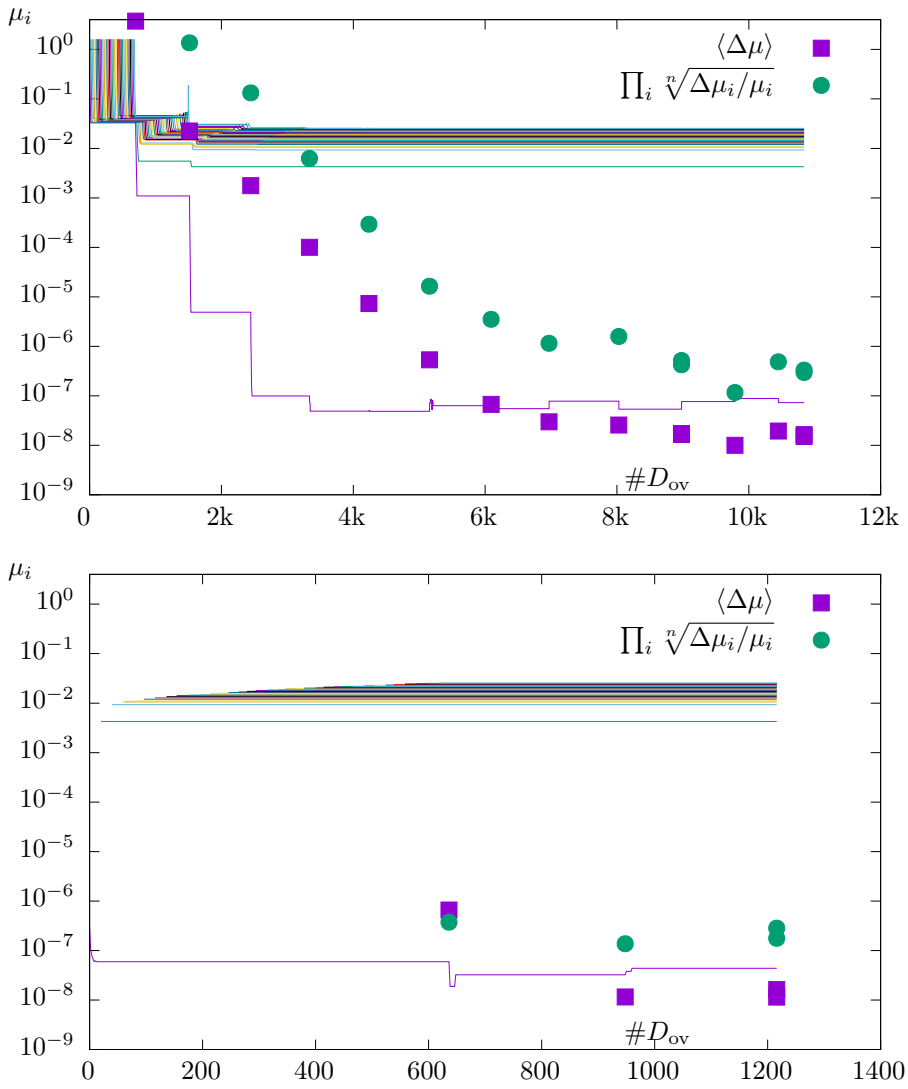

Figure 3.8: Convergence of 30 eigenmodes for the configuration with near-zero modes (compare fig. 3.2), obtained from first calculating the eigenmodes of $P_{-}DP_{-}$ (top) and then those of $P_{+}DP_{+}$ (bottom) starting from righthanded modes created from the first results.

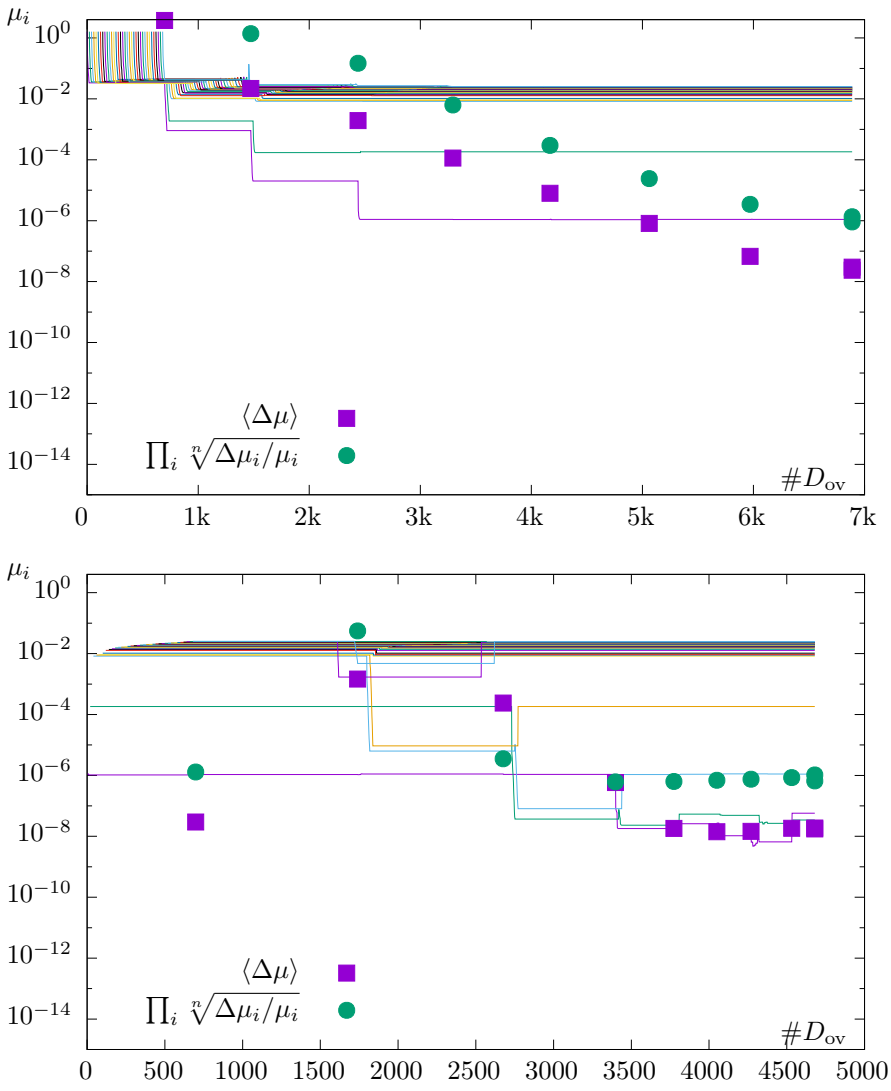

Figure 3.9: Convergence of 30 eigenmodes for the configuration with righthanded zero modes (compare fig. 3.3), obtained from first calculating the eigenmodes of $P_{-}DP_{-}$ (top) and then those of $P_{+}DP_{+}$ (bottom) starting from right-handed modes created from the first results.

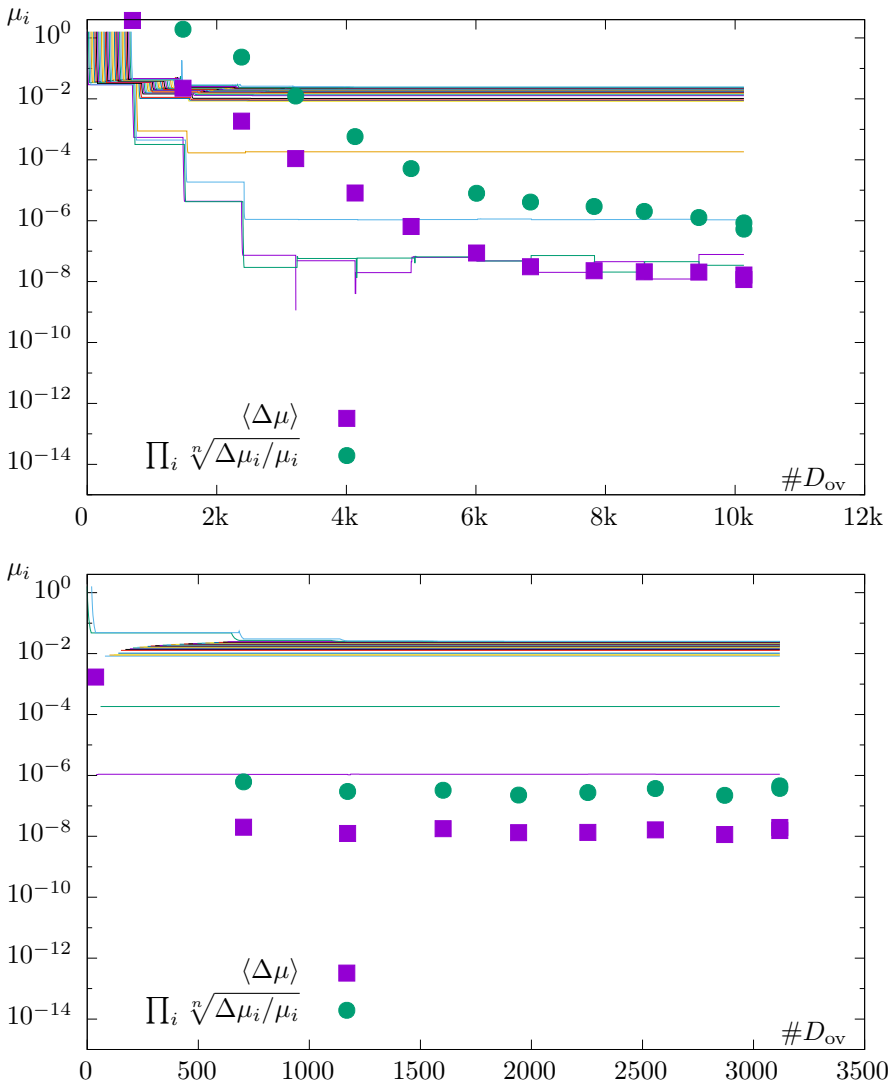

Figure 3.10: Convergence of 30 eigenmodes for the configuration with right-handed zero modes (compare fig. 3.3), obtained from first calculating the eigenmodes of P_+DP_+ (top) and then those of P_-DP_- (bottom) starting from righthanded modes created from the first results.

for the zero modes in later iterations. The imaginary part is always several orders of magnitude smaller than the real part. For $P_{\pm}DP_{\pm}$, on the other hand, the original value is similar but the imaginary part stays at $\mathcal{O}(10^{-10})$ regardless of the real part.

While it seems that the eigenvalues of small modes do not very well obey the exact analytical relations, the eigenvectors seem to be essentially the same. In the case of the configuration with two righthanded zero modes, if the resulting eigenvectors of $P_{+}DP_{+}$ were used as starting vectors for $P_{+}D^{\dagger}DP_{+}$, the KS algorithm was completed very quickly, unable to improve the eigenvectors further. The eigenvalues were then again the same as for $D^{\dagger}D$.

As mentioned earlier, if the eigenmodes of D on a specific chirality are computed and it turns out that there are no zero modes among them, the results can be used to create starting spinors for a computation of the eigenmodes of the opposite chirality by application of D. However, if there are zero modes of the opposite chirality, a problem arises, namely that the KS algorithm starts with relatively well determined eigenvectors which are not the lowest modes of the spectrum. This can result in fluctuations of the values in the first iterations, which have to be ignored in order for the algorithm to continue and find the missing contributions of the zero modes. This effect can be seen in fig. 3.10, where the errors are already low after the first iteration but rise again after the second. After that, they decline and once they are small again the zero modes have been found.

To summarize, it seems that the quickest results are obtained if first the lowest modes of $P_{\pm}DP_{\pm}$ for one of the chiralities are computed, followed by a similar computation on the opposite chirality. If the first run already yields zero modes, the second run may be skipped, depending on whether a fixed number of non-zero modes is wanted. The results of the run with zero modes should be supplemented with an additional iteration with the chirally projected squared operator $P_{\pm}D^{\dagger}DP_{\pm}$ in order to increase the accuracy. It might also be possible to start with the simple operator and switch to the squared one only for the low modes once they are below some threshold, but this would have necessitated a change in much of the algorithm such that different operators are used depending on the magnitude of the eigenvalue; therefore it has not been tested.

Since the idea of using a chirally projected operator only occured after much of the computation was already finished, for compatibility the 50

lowest eigenmodes of $D^\dagger D$ have always been computed using the naive and direct approach. However, in each case the number of eigenmodes has afterwards been increased by computing eigenmodes of $P_\pm D P_\pm$ on the chirality without zero modes. In most of these cases, the computation of an equivalent number of modes using the original algorithm would also have been problematic in terms of memory, in addition to the obvious computing time advantages. For the different analyses, the lowest eigenvalues were then taken from the $D^\dagger D$ runs and the higher ones from the $P_\pm D P_\pm$ runs. It was confirmed that there is an overlapping region where both give the same results.

As in the case of $A = D^\dagger D$, it is possible to obtain eigenvectors of D from those of $P_\pm D P_\pm$ or $P_\pm D^\dagger D P_\pm$. Taking as before the eigenvector of D that has an eigenvalue with positive imaginary part as ψ and its partner with negative imaginary part as $\gamma_5\psi$, the eigenvector of $P_\pm D P_\pm$ is given by

$$\psi_\pm = \frac{1}{\sqrt{2}}(\psi \pm \gamma_5\psi).$$

There might be an additional phase in front of this, but it can be absorbed into ψ. This no longer works if ψ_+ is taken from one run with $P_+ D P_+$ and ψ_- from a different run with $P_- D P_-$, because then they might have different phases. Assuming that only one of the spinors $\psi_\pm$ has been computed, the other one can instead be obtained by an application of D, giving

$$\begin{aligned} D\psi_\pm &= \frac{1}{\sqrt{2}}(\lambda\psi \pm \bar{\lambda}\gamma_5\psi) = \operatorname{Re}(\lambda)\psi_\pm + i\operatorname{Im}(\lambda)\psi_\mp \\ \Rightarrow \quad P_\mp D\psi_\pm &= i\operatorname{Im}(\lambda)\psi_\mp \\ \Rightarrow \quad \psi &= \frac{1}{\sqrt{2}}\left(\psi_\pm - i\frac{P_\mp D\psi_\pm}{|P_\mp D\psi_\pm|}\right). \end{aligned}$$

In this case, it is not sufficient to store a few scalars in order to later quickly create ψ from $\psi_\pm$. Instead, the whole chiral spinor $\psi_\mp$ is needed to be stored additionally. Of course, this still needs less disk space than in the case of $A = D^\dagger D$, where two full spinors are stored for each eigenmode pair.

3.4 Implementation Details

The calculation of the overlap spectrum was split into multiple steps. First, the largest eigenvalue of $K^2 = D_{-M}^{W\dagger} D_{-M}^{W}$, with D_{-M}^{W} being the Wilson Dirac operator, is estimated by ten steps of the Kalkreuter-Simma (KS) algorithm. This is only done to estimate the upper bound of the interval on which the Zolotarev rational function has to be a good approximation, so the eigenvector is not needed and a relatively low precision is sufficient. This value anyhow did not fluctuate much between configurations and since the Wilson eigenvalue density is much larger at its largest eigenvalue than at its lowest, the value can be found quickly. Since the KS algorithm usually computes the lowest rather than the highest eigenvalue, the operator $-K^2$ is used, which is implemented not by actually multiplying the result of K^2 with -1 but by accordingly changing scalar products and linear combinations in the algorithm.

Then, the lowest 20 eigenvectors of K^2 are computed and stored on the disk, together with their eigenvalues. These two steps are done by one program called `wilsonmodes`, which can be compiled to either run scalar on one CPU core, parallelized on multiple CPU cores using MPI [45] or on one CPU core with the aid of one GPU, which performs the computation of K^2. Recently, this mixed version was replaced by a version that keeps the spinors on the GPU memory the whole time and uses QUDA routines for the operator K^2 as well as for all the linear algebra routines in between. This is considerably faster, in particular because the spinor does not have to be transferred between host and device memory for each operator application and also because for the simple K^2 operator a relevant portion of computing time is spent on linear algebra, namely during the Gram-Schmidt orthogonalizations needed for higher eigenvectors in order to only search the subspace orthogonal to already found lower eigenvectors.

The results of this program were then read in for any program that needs to apply the overlap operator, foremost by `overlap`, which computes its spectrum. The borders of the interval for the Zolotarev approximation are given by the largest eigenvalue in the subspace which is treated explicitly by means of the eigenmodes (so, for example, the 20th lowest eigenvalue) and the largest of the total spectrum of K^2, multiplied by 0.9 and 1.1, respectively. Therefore, all eigenvalues of K^2 that are not explicitly treated should be inside this interval. The computation of the Zolotarev coef-

ficients is done during the initialization of the overlap operator and not stored on the disk, because it does not take any significant amount of time.

Since the KS algorithm is used with different operators, an abstraction layer was introduced that allows to use the same code for different operators. The code is written in C++, so this is achieved in an object-oriented way by using virtual classes. An abstract base class for all different kinds of operators is called `LinearOperator` and essentially consists of one virtual method called `apply`. The `LinearOperator` takes as a template argument the spinor class that it acts on since it is used with, for example, full spinors, spinors that only store a left- or righthanded part, and spinors that are kept in GPU memory. `LinearOperator::apply` takes references to two spinors and a boolean which controls if the operator itself or its Hermitian conjugate is to be applied to the first spinor, storing the result in the second. The base class does not have a default implementation for this operator, making it abstract. Classes that derive from this, like `OverlapDirac` and `DslashOp` (which applies the Wilson Dirac operator), have to implement the `apply` method before it is possible to create instances of these classes.

Building on this, the class `HermiteanOperator` is defined, which implements everything that the KS algorithm needs to see of an operator. The method `KSRitz::compute_eigenvalues` therefore takes a reference to a `HermiteanOperator` and just uses this interface, without knowledge of the details about which Hermitian operator is actually used. In addition to an `apply` method similar to that of a `LinearOperator`, but without the third argument, a Hermitian operator has a method called `products`, which takes an array of spinors $\{x_i\}$ and returns the matrix with components $A_{ij} = x_i^\dagger A x_j$, where A is the Hermitian operator represented by the class. If the operator can be written as $A = B^\dagger B$ with some other linear operator B which takes less time to apply, it is possible to compute $y_i = Bx_i$ and create the matrix from the scalar products $A_{ij} = y_i^\dagger y_j$. A `HermiteanOperator` also offers an interface to query whether such a representation is possible for this specific Hermitian operator and to apply the operator B instead of A.

There are several possibilities to create a `HermiteanOperator` from a `LinearOperator`. The simplest one is to square it, which is implemented by the class `SquaredLinearOperator`. Another possibility is to act on spinors of a specific chirality with an operator and project the result back to that chi-

rality, which at least in the case of the overlap operator gives a Hermitian operator. `ChiralLinOp` therefore takes the reference to a `LinearOperator` that acts on full spinors and implements a `HermiteanOperator` that acts on chiral spinors. The code to call the KS algorithm with the correct operator depending on parameters therefore can be written similar to

```
OverlapDirac ov(...);   //create overlap operator
//create squared overlap operator
SquaredLinearOperator<SpinorT,OverlapDirac> ov2(lat,ov);
if (param.chirality.isSet()) {
  //Pointer to either ov or ov2
  LinearOperator<SpinorT> *op = &ov;
  if (param.squared())
    op = &ov2;
  //Create projected operator
  ChiralLinOp<SpinorT, HalfSpinorT>
    chiop(*op,param.chirality());
  //chiral spinors and projected operator
  KSRitz<HalfSpinorT> ks(...);
  ks.compute_eigenvalues(chiop);
} else {
  //full spinors and squared overlap operator
  KSRitz<SpinorT> ks(...);
  ks.compute_eigenvalues(ov2);
}
```

Here, `SpinorT` is an alias for a spinor class that represents a full spinor—which differed depending on if the code was compiled for CPU or GPU—and `HalfSpinorT` an alias for a spinor class representing only the left- or righthanded part of a spinor.

4 The Microscopic Picture of Axial Symmetry Breaking

4.1 The Overlap Spectrum and the Axial Anomaly

4.1.1 Topological Charge Distribution

The discussion of different topological sectors for SU(3) gauge fields that was given in section 1.4 can not easily be translated to a lattice discretized version of SU(3) gauge theory that is restricted to a finite volume. In fact, any lattice gauge configuration on a finite volume can be continuously deformed into any other (with the same number of lattice points) by accordingly deforming the finite number of link variables. Since the gauge action is finite for any choice of the gauge field, the set of all lattice gauge configurations is simply connected. It still has multiple local minima of the action, which are separated by finite barriers that only become infinite in the thermodynamic (i.e., infinite volume) limit, which reproduces the topological sectors of the continuum theory. To put it differently, in an infinite volume the action of a gauge configuration is determined by its topological content, which determines the topological sector the configuration is found in, and quantum fluctuations, which disturb the gauge configuration away from the minimum of the action but can not change the topological sector it is in [46]. In a finite volume, the sectors are not as clearly separated and quantum fluctuations can mix them, giving gauge configurations with ambiguous topological content.

The continuum definition of the topological charge (see (1.13)) is a continuous function of the gauge fields and can therefore not be expected to have a lattice counterpart that also gives integer values. Different techniques have been used to create a lattice observable that in the continuum and thermodynamic limits reproduces the topological charge. The obvious solution is to *cool* the configuration, such that it is successively replaced by

similar configurations that have a lower action, resulting in a configuration at a local minimum [47]. If a gauge configuration is a local minimum, it should not be influenced significantly by the finiteness of the barriers and a discretized version of the topological charge operator $\tilde{F}F$ on the cooled configuration can give a good estimate of the topological charge.

Another possibility that has been used extensively is to *smear* the configuration. A smearing step consists of replacing each link by another one using information from links in the neighborhood, with the goal of removing ultraviolet fluctuations. For example, HYP smearing [48] replaces each link using information from links on hyper-cubes around that link. It is assumed that the critical behavior and therefore the universality class of the theory is not affected by this substitution since only links in a finite neighborhood are included, which is certainly the case for an infinite volume. The argument is somewhat weakened on a finite lattice since repeated application of smearing will eventually induce an influence over the whole lattice. It has however been successfully used to reduce taste symmetry breaking in staggered fermion formulations and improve chiral symmetry of Wilson fermions. Most notably in this context, if a configuration is sufficiently smeared the non-topological fluctuations are removed and the topological charge can be measured even on a finite and discrete lattice.

However, both procedures are ambiguous if multiple minima are close and structures that increase the gauge action but might anyhow have an influence on the infrared fermionic modes might be lost. For example, it will turn out that a gauge configuration that consists of a superposition of an instanton and anti-instanton, which are separated by some distance, gives rise to near-zero modes, but along a path of steepest descend of the action these structures come closer and annihilate [23].

Since the spectrum of the overlap operator has been computed for this work, it opens a different possibility to measure the topological charge, which does not suffer from such ambiguities and even works comparatively far from the continuum. As discussed in section 3.3, the overlap operator allows to clearly distinguish zero modes from non-zero modes by their chirality as well as by their eigenvalues, so by simply counting the number of zero modes of each chirality the topological charge can be obtained

using the overlap index theorem

$$Q_{\text{top}} = n_- - n_+.$$

At first it has to be checked that the configurations are sufficiently uncorrelated. Since they are the result of a Markov chain, it is possible that successive configurations show an autocorrelation with an autocorrelation time that depends on the observable that is measured on them. The topological charge has a particularly large autocorrelation time since the update algorithm can in principle become trapped in a specific topological sector, giving only configurations of this sector for a long time. When the configurations that were available for this work had been created, only every tenth of them was stored to disk, so they are separated by ten *Rational Hybrid Monte Carlo* steps. While this is a sufficient separation for many observables, that might not be the case for topological properties. However, since it is very expensive to calculate overlap eigenmodes, not every configuration of a given stream has been used. Instead, only $\mathcal{O}(100)$ configurations have been used from each ensemble (cf. table 3.1), which were chosen such that the distance between them was as large as possible. As can be seen in fig. 4.1, this seems to have been enough to ensure that there is no noticeable autocorrelation of the topological charge.

Having the expensive but less ambiguous tool of the overlap index theorem at one's disposal, it is possible to compare to the results of the smearing technique. For the ensemble at $1.5\,T_c$, it was found that after a few steps of HYP smearing the topological charge as measured by the gluonic $\tilde{F}F$ operator on the lattice gave an integer result that did not change with further steps. A subset of 50 configurations was subjected to ten steps of HYP smearing and the spectrum of the overlap operator was recomputed on them. It was found that the topological charge of these smeared configurations is identical whether it is computed using the overlap index or the gluonic operator $\tilde{F}F$. It is, however, not always the same as before smearing (fig. 4.2). Smeared configurations tend to have fewer zero modes, although there are also configurations that have more zero modes after smearing (fig. 4.3). The topological charges before and after smearing are correlated with a correlation coefficient of 0.60(11).

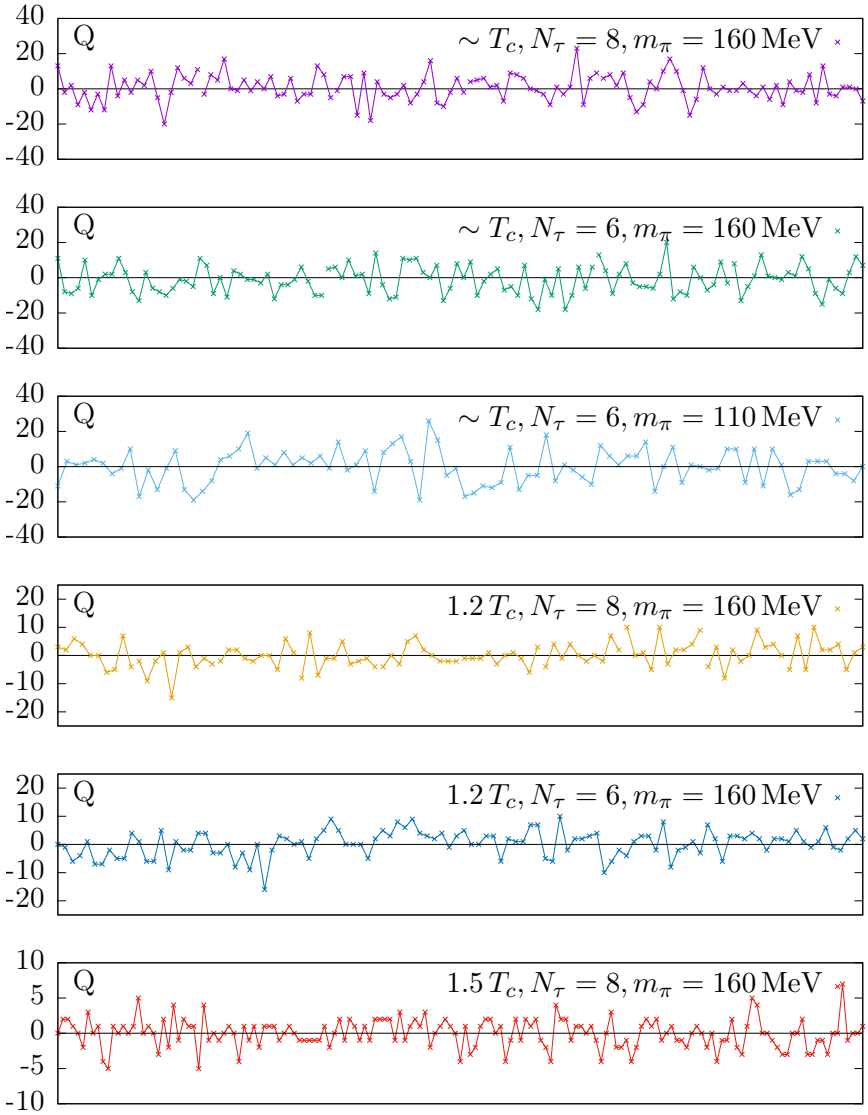

Figure 4.1: Time history of topological charge as measured by the number and chirality of zero modes according to the index theorem. Configurations belonging to the same independent stream are connected by lines.

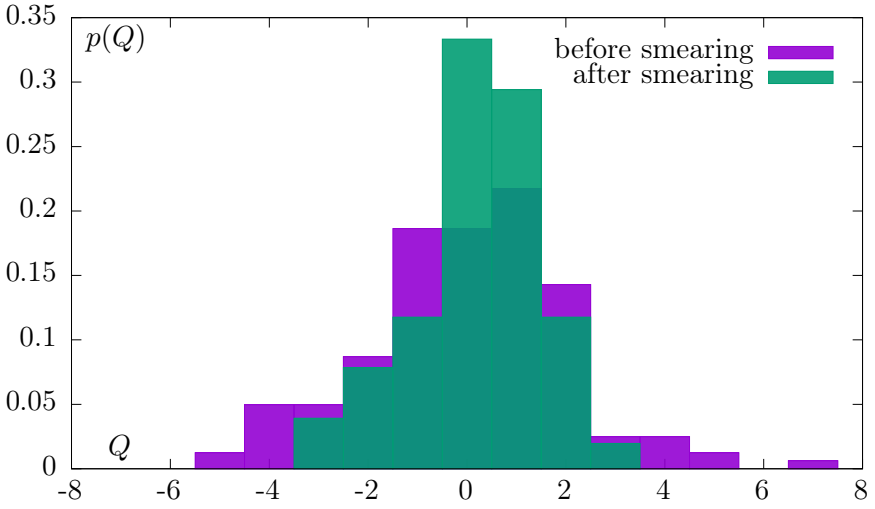

Figure 4.2: Topological charge distribution before and after ten steps of HYP smearing.

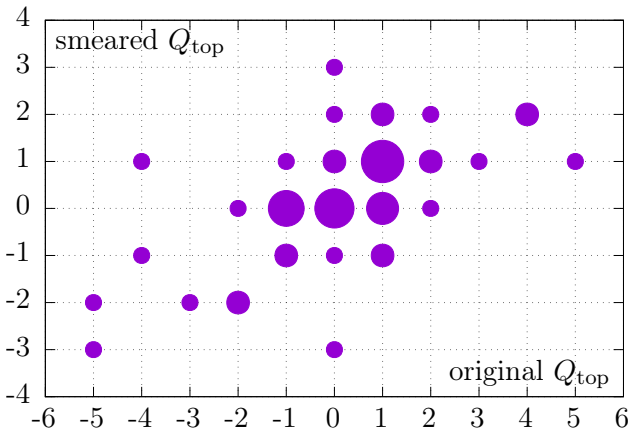

Figure 4.3: Correlation between topological charge before and after ten steps of HYP smearing on a given configuration. The area of each point is proportional to the number of configurations with the given values.

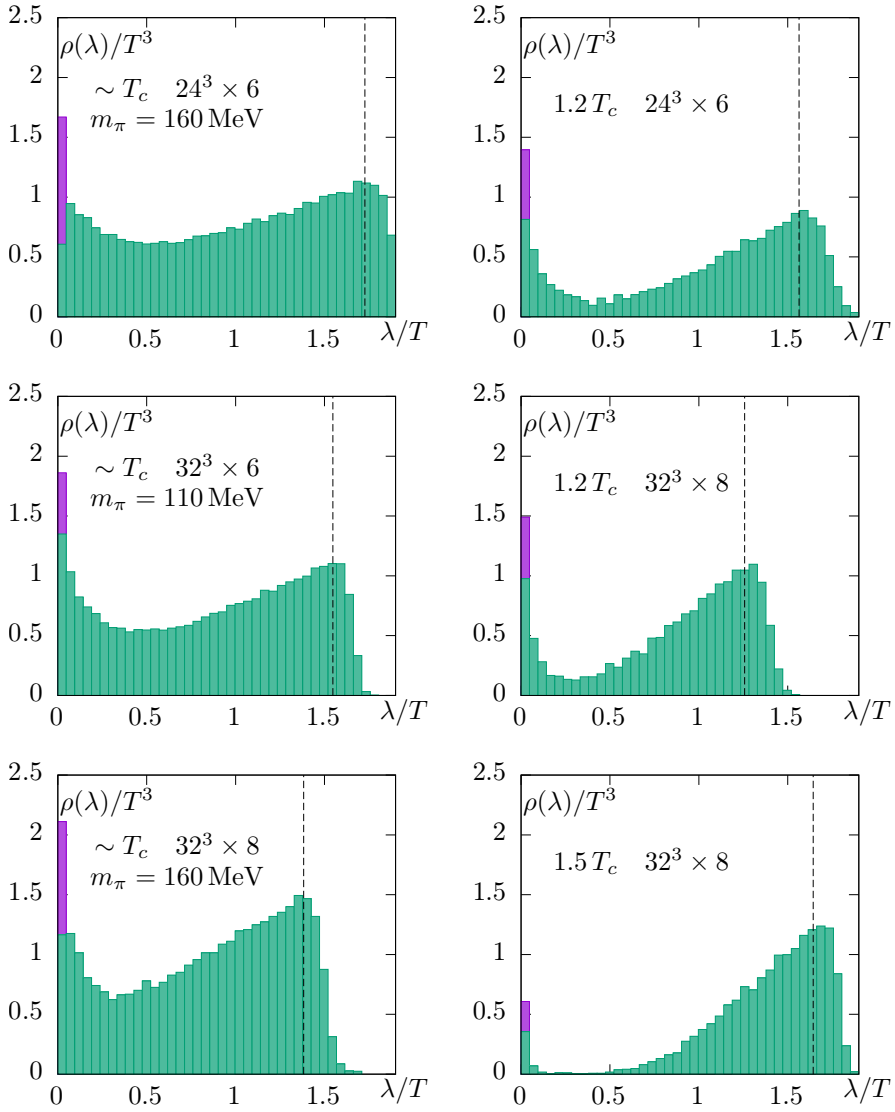

Figure 4.4: Spectrum of the overlap operator on HISQ configurations at different temperatures, lattice spacings and light quark masses. The dashed line indicates $\min(\lambda_{\max})$, the lowest of the values if from each configuration the highest computed eigenvalue is taken. The purple box shows the contribution of exact zero modes to the first bin.

4.1.2 Near-Zero and Bulk Spectrum

In fig. 4.4, the eigenvalue density

$$\rho(\lambda) = \left\langle \frac{T}{V} \sum_i \delta(\lambda - r\phi_i) \right\rangle \tag{4.1}$$

is plotted, with the real ϕ_i being related to a complex eigenvalue λ_i of the massless overlap Dirac operator by $\lambda_i = r(1 - \mathrm{e}^{-i\phi_i})$, as mentioned in section 2.3.1. For eigenvalues near zero, $r\phi_i \approx \mathrm{Im}(\lambda_i)$ and $\rho(\lambda)$ is essentially the density of the imaginary parts of the eigenvalues. The eigenvalues as well as the densities are rescaled by powers of the temperature T in order to obtain dimensionless quantities and the δ-function is plotted using a histogram such that the area in each box corresponds to the integral of (4.1) over the corresponding range of λ values. Since only the range of positive λ is shown, only one mode of each non-zero mode pair is included in the histograms. The contribution of zero modes is accordingly divided by 2, so if the spectrum were to be extended to negative values, the same amount of zero modes would be found in the bin that has 0 as its upper bound. Since only a fraction of the total number of eigenvalues has been computed for each configuration, the eigenvalue density is only valid up to a certain point which is denoted by a dashed line. It is determined by taking the highest computed eigenvalue of each configuration and taking the minimum of these values over the set of configurations.

In addition to the zero modes, which can be distinguished clearly because of their chiralities, the spectrum shows two very articulated features, namely a near-zero mode peak and a bulk part. While these overlap for the lower temperatures, with increasing temperature they get more separated. It is important to quantify these features and, in particular, gain some understanding how they change in the thermodynamic, chiral and continuum limits. In general, it is expected that an increase in the volume does not significantly change the spectral density as long as the volume is already large enough to suppress finite volume effects. Instead, additional eigenvalues are sampled according to the same distribution, which does not change the spectrum since it is normalized by the volume. Roughly, this can be understood by considering the simple case of doubling the volume. Gauge configurations of the total system can approximately be

constructed by choosing gauge configurations for each half independently and according to the action of the smaller system. Any fermionic mode of the smaller system then gives rise to two modes of the larger system, each localized on a different half. The effect of an increased volume is therefore similar to that of increased statistics in the computation of the average over gauge configurations. The density $\rho(\lambda)$ that is obtained by such an average can therefore—if appropriately binned—be used as an estimate of the density in the thermodynamic limit.

The zero mode peak forms an exception to this in that it is expected to vanish in the thermodynamic limit. This can be seen by assuming that the number of instantons and that of anti-instantons are independent and have an expectation value that is proportional to the volume. This results in a corresponding number of left- and righthanded zero modes, but if there are $n_{\mp}$ of these modes, they will form $\min(n_-, n_+)$ pairs and $|n_- - n_+|$ remaining zero modes. The pairs will then be shifted away from zero by any small perturbation, resulting in near-zero modes. Drawing n_- and n_+ from, for example, a Poisson distribution with expectation value κ, the value $|n_- - n_+|$ turns out to have an expectation value roughly proportional to $\sqrt{\kappa}$. The number of remaining zero modes of a single chirality therefore only scales with the square root of the volume, such that the zero mode part of the first bin will vanish as $1/\sqrt{V}$ in the thermodynamic limit. However, this does not influence the total first bin, since the total amount of near-zero and zero modes is equal to $n_+ + n_-$, which has an expectation value proportional to the volume. According to this model, at higher volumes an increasing portion of zero modes becomes paired up to form near-zero modes.

4.1.3 Quantifying the Spectral Density

In order to capture the features of the spectra for different ensembles, the ansatz

$$\rho(\lambda) = \frac{\alpha\sigma}{\pi(\sigma^2 + \lambda^2)} + a|\lambda|^b \tag{4.2}$$

presents a reasonable choice. The first term describes a Breit-Wigner peak with width σ and area α, while the rest is the leading part of the power series expansion of the bulk spectrum. The impact of such a spectrum on

the axial anomaly for different values of the parameters and its dependence on how these parameters change in the appropriate limits will be discussed below. Before that, several possibilities to obtain values for the parameters will be discussed and compared.

The most obvious way to match the ansatz (4.2) to the obtained eigenvalues is to fit the function to the histogram. However, this method has some problems. For example, the result may differ depending on the bin width that is used in creating the histogram. Also, most bin widths that give a relatively smooth histogram will only give two or three bins for the near-zero mode peak, at least for the highest temperature. This means that the parameters that describe the near-zero mode peak can not be very well determined from this. There is also the question of how to get error estimates for each bin, which are necessary for a meaningful fit. One possibility is to just take the square root of the number of eigenvalues found in a bin, which results from the assumption that this number will follow a Poisson distribution, where the average is equal to the variance. This however is especially problematic for the gap at $1.5\,T_c$, where some bins have zero eigenvalues in them, giving an error of zero which breaks the fit. Another possibility with the same problem is to use some resampling method based on the gauge configurations. Again, a bin with zero eigenvalues will not give any variation if the set of contributing configurations is varied, so the error estimate will again be zero.

One method that works somewhat better is to take some equidistant λ values like in the formation of a histogram and then estimate the density at these points by varying the width of an interval with λ at the center and dividing the number of eigenvalues contained in this interval by its width. The interval widths are drawn from an exponential distribution with expectation value equal to the distance between two adjacent values of λ. The average and variance over the different intervals then provide a good guess including an error estimate that can be used for a fit and it was checked that these results are relatively stable with respect to a change in the number of λ values. The results are compiled in table 4.1.

For the configurations close to T_c, the chiral condensate will not necessarily vanish in the chiral limit. It is not a priori clear if a non-vanishing chiral condensate should be the result of the near-zero mode peak or of an additional constant offset c that is added to the ansatz (4.2)—or a combination of both. Therefore, a cross-check was performed for the ensembles

#	$N_\sigma^3 \cdot N_\tau$	m_l/m_s	α/T^4	σ/T	a/T^3	b
1	$24^3 \cdot 6$	1/20	0.75(5)	0.25(3)	0.685(14)	0.77(5)
2	$32^3 \cdot 6$	1/40	0.65(3)	0.188(11)	0.717(9)	0.91(4)
3	$32^3 \cdot 8$	1/20	0.61(3)	0.150(10)	1.108(11)	0.85(4)
4	$24^3 \cdot 6$	1/20	0.275(10)	0.103(7)	0.368(6)	1.95(6)
5	$32^3 \cdot 8$	1/20	0.213(10)	0.059(5)	0.746(11)	1.87(5)
6	$32^3 \cdot 8$	1/20	0.1(5)	0.003(16)	0.250(10)	3.55(10)

Table 4.1: Fit results for the ansatz (4.2). The ensemble index is the same as in table 3.1, so #1–3 are at $\sim T_c$, #4 and #5 at $1.2\,T_c$ and #6 at $1.5\,T_c$.

#	α/T^4	σ/T	a/T^3	b	c/T^3
1	0.39(10)	0.19(4)	0.28(9)	1.5(4)	0.43(9)
2	0.32(3)	0.111(11)	0.31(4)	1.88(18)	0.41(3)
3	0.45(9)	0.132(16)	0.82(15)	1.2(3)	0.29(15)

Table 4.2: Fit results for the ansatz (4.2) with an additional offset c for the ensembles near T_c.

at T_c with a fit that includes such an offset. The results are compiled in table 4.2.

Before the results and their implications for the axial anomaly are discussed, a complementary method that seems to work especially well at high temperatures shall be introduced. The motivation for that is that the near-zero mode peak at least at the highest temperature can not be well determined by a fit because it needs some binning and the peak is usually only represented by a few bins. Therefore, a method that does not rely on binning is desirable, even if it only serves as a cross-check. Since many or most statistical analysis tools can be derived in some way from Bayes' theorem, going back to using it more directly should remove any additional assumptions and ambiguities of specific methods.

Bayes' theorem connects the probability that a specific hypothesis is true given some data, $P(p|x)$, to the *a priori* probability of that hypothesis, $P(p)$, and the probabilities of obtaining the data under the given

hypothesis, $P(x|p)$, as well as under all competing hypotheses. As such, it is well suited for this problem. After all, working under the assumption that the spectrum follows a given functional form like (4.2), it is easy to compute the probability of getting a specific set of eigenvalues if the parameters α, σ, a and b are given, and the goal is to obtain the probability that these parameters take specific values given the eigenvalues that were actually obtained. In the notation above, the parameters are collectively denoted as p and the measured data as x and Bayes' theorem says

$$P(p|x) = \frac{P(x|p) \cdot P(p)}{\sum_{p'} P(x|p')P(p')}. \tag{4.3}$$

If N values are drawn independently according to some probability distribution $f_p(x)$, the probability that the lowest n of them take the values $x_1, \ldots, x_n$ is given by

$$P(x|p) = \frac{N!}{(N-n)!} \prod_{i=1}^{n} f_p(x_i) \cdot \left(\int_{x_n}^{\infty} \mathrm{d}x f_p(x) \right)^{N-n}. \tag{4.4}$$

This is a multinomial probability distribution with n of the samples taking specific values and the rest taking values that are larger than x_n. Since it is not feasible to compute the denominator in Bayes' formula, a Metropolis algorithm was used to obtain a sample of parameter sets p_i that are distributed according to (4.3), which only needs the ratio $P(p_1|x)/P(p_2|x)$. The *a priori* distribution is chosen such that each of the parameters is simply equally distributed in some reasonable range, so $P(p_1)/P(p_2)$ cancels. $f_p(x)$ is assumed to take the form (4.2) in the range where eigenvalues were computed and some arbitrary form beyond that—the integral in (4.4) can be determined by the normalization of $f_p(x)$.

In table 4.3, the results are shown for the ensembles at $1.2\,T_c$ and $1.5\,T_c$. The error estimates given there are obtained from the variance of (4.3), without the factor $1/N$ often found in error estimates from Monte Carlo samples. As such, it describes the width of the *a posteriori* distribution of parameter values and not the confidence that the given average is indeed the average of the distribution. In particular, the error will not decrease with increasing Metropolis samples.

For the ensembles that were close to the critical temperature, this method did not give satisfactory results. With the original ansatz as

#	α/T^4	σ/T	a/T^3	b
4	0.304(8)	0.055(3)	0.401(6)	1.69(4)
5	0.243(6)	0.029(2)	0.751(7)	1.63(4)
6	0.066(3)	0.0029(3)	0.306(6)	2.91(5)

Table 4.3: Average and standard deviation of the parameters in (4.2) from Bayes' formula at $1.2\,T_c$ and $1.5\,T_c$.

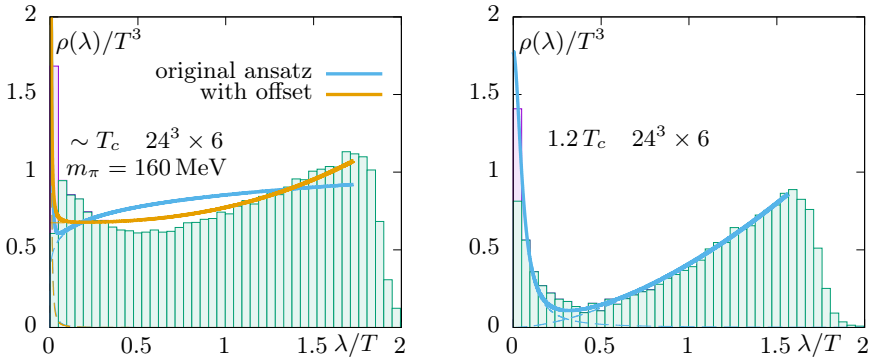

Figure 4.5: Examples of the Bayesian best guess of the spectrum parametrization near T_c and at $1.2\,T_c$.

well as with an offset, the resulting graph did not match the histogram nearly as well as at higher temperatures (cf. fig. 4.5). In both cases the estimate for the width of the near-zero mode peak was too low, which was compensated by either a small exponent or a large offset. One possible source for this was investigated, namely insufficient floating point precision in the evaluation of $P(x|p_1)/P(x|p_2)$. This term can be difficult to evaluate numerically since it contains products with as many terms as the number of eigenvalues that were computed for all configurations. Also, the probability of an eigenvalue falling in the range $[x_n, \infty]$ is taken to the power $N - n$, which is quite large. In the Metropolis implementation, the terms were always first divided by the corresponding terms in the denominator before they were multiplied or raised to the power $N - n$. This way, no floating point overflow should occur, but the transition probability is given

by a product of many numbers which are each close to 1. However, even using 4096 bit floating point numbers did not change the result. It might be necessary to change the assumption that the eigenvalues of a given configuration are simply drawn independently from each other according to the distribution $\rho(\lambda)$ to get reasonable results even close to T_c.

Bulk Contribution to the Axial Anomaly

Taking first a look at the behavior of the bulk spectrum as seen in table 4.1, there is a clear tendency of the exponent to grow with the temperature, from a value slightly below 1 at the chiral transition temperature T_c to a value close to 2 at $1.2\,T_c$ and finally a value above 3 at $1.5\,T_c$. If an offset is allowed for the low temperature fits, the exponent rises to values above 1 and in the Bayesian analysis the exponents are all slightly lower than from the fits, with the exponent at $1.5\,T_c$ being close to but still below 3. A cubic behavior of the bulk spectrum is somewhat expected at high temperatures since such an exponent is the result of calculating the spectrum of the free continuum Dirac operator and QCD is expected to become asymptotically free at high temperatures. However, strictly speaking the cubic result only holds for a free fermionic theory at zero temperature and is replaced by

$$\rho(\lambda) \propto \sum_{n\in\mathbb{N}} \lambda\sqrt{\lambda^2-\omega_n^2}\,\theta(\lambda-\omega_n) \qquad \text{with} \qquad \omega_n = (2n+1)\pi T$$

at finite temperatures. This has a gap on $[0, \pi T]$, which originates from the fact that fermionic modes have to be antiperiodic in the fourth coordinate. The bulk spectrum at $1.5\,T_c$ indeed seems to develop a gap, but its width is at most somewhere around $0.4\,T$.

The question whether $U_A(1)$ is effectively restored is determined by the spectrum in the chiral limit. If the bulk spectrum in this limit takes the form $a\lambda^b$, the $U_A(1)$ breaking ω (cf. (2.26)) is given by

$$\omega \propto \int_0^{\lambda_c} \mathrm{d}\lambda \frac{m^2\lambda^b}{(\lambda^2+m^2)^2} \underset{\lambda=mx}{=} m^{b-1}\int_0^{\lambda_c/m} \mathrm{d}x \frac{x^b}{(1+x^2)^2},$$

where the continuum formula has been used for simplicity and the integral is cut off at some point where the rest of the integral can be neglected

because the denominator becomes too large—which should happen even for large exponents b because corrections to the simple leading exponent behavior come into play, suppressing the spectrum at high eigenvalues. For $b > 1$, the remaining integral can be split into a constant part that vanishes after multiplication with m^{b-1} and a part where the constant in the denominator can be neglected, giving

$$\omega \propto m^{b-1} \left[\int^{\lambda_c/m} \mathrm{d}x x^{b-4} + \mathrm{const} \right] = \mathcal{O}(m^2) + \mathcal{O}(m^{b-1}).$$

Any exponent larger than 1 will therefore not contribute to ω in the chiral limit.

Having determined the spectrum at two different light quark masses, namely at $m_s/20$ for ensemble #1 and $m_s/40$ for ensemble #2, some hints about the change of the different features of the spectrum in the chiral limit can be obtained. A priori, it is expected that higher eigenvalues are not as sensitive to a change in the light quark mass because they are determined by the dynamics of the strange quark, which has a mass that was kept fixed. The bulk exponent still shows some increase when the quark mass is reduced, which can happen especially for low exponents since they imply many small eigenvalues belonging to the bulk spectrum, which can still be sensitive to the light quark mass. The question whether the exponent will rise above the critical value of 1 when approaching the chiral limit can not be answered from just these two data points. In the fits that include an offset c, the exponent takes a value larger than one, so the bulk does not contribute to ω. Instead, there is a strong indication that the offset gives a contribution, since it is practically unchanged under a change of the light quark mass. It can not necessarily be concluded that this contribution takes the form of a bulk exponent smaller than one in the original ansatz, since the near-zero mode peak also changes if the offset is included and it might be that switching on the offset in the fit simply redistributes the near-zero mode contribution between the near-zero mode peak and the offset. It is, however, plausible that some of it also comes from the bulk exponent.

From the gathered data it is also possible to obtain an impression of how the different parts of the spectra change in the continuum limit, since the pairs (#1, #3) and (#4, #5) contain ensembles of the same meson masses

at the same temperature and the same physical volume, but with different lattice spacings. For most parameters, it is first necessary to renormalize the eigenvalues, since they are bare quantities comparable to the bare quark masses and not physical. The exponent b, however, is dimensionless and not affected by this—at least at leading order, where the eigenvalues and their density simply have to be multiplied by some renormalization factors. In both cases, the exponents at the different lattice spacings are compatible with each other within error bounds and while the exponent near T_c shows a slight rise when going to smaller lattice spacings, at $1.2\,T_c$ the trend is in the other direction. It can therefore be assumed that the bulk spectrum does not contain any relevant lattice artifacts.

The near-zero mode peak

Taking now a look at the near-zero mode peak, it seems that a decrease of the light quark mass by a factor of 2 (#1 to #2) slightly sharpens the near-zero mode peak (i.e., it decreases the peak width σ) and also slightly decreases the area under the peak (i.e., α). For two light flavors, a zero mode of the massless Dirac operator is an eigenmode with eigenvalue m of the massive Dirac operator and will therefore give a contributing factor of m^2 to the fermion determinant. The typical magnitude of the zero and near-zero eigenvalues seems to decrease in the chiral limit, as seen by the behavior of the peak width. If their magnitude turned out to be negligible in comparison to the light quark mass, remaining so even in the chiral limit, their contribution to the fermion determinant would also essentially be quadratic in m. Under this assumption, the zero and near-zero modes are therefore expected to have a contribution to the spectrum proportional to $m^2\delta(\lambda)$, with $\delta(\lambda)$ being smeared at finite m and becoming sharper in the chiral limit. Such a near-zero mode peak is particularly interesting because its contribution to the chiral condensate is vanishing,

$$\Sigma \propto \lim_{m\to 0} \int \mathrm{d}\lambda \frac{m^3\delta(\lambda)}{m^2+\lambda^2} = \lim_{m\to 0} m = 0,$$

while the $U_A(1)$ symmetry is still effectively broken,

$$\omega \propto \lim_{m\to 0} \int \mathrm{d}\lambda \frac{2m^4\delta(\lambda)}{(m^2+\lambda^2)^2} = \text{const.}$$

While the behavior of the peak supports this general picture, the prefactor α does not seem to be proportional to m^2. The reason is probably that the width of the peak is not negligible with respect to the light quark mass. If the prefactor is assumed to be proportional to m^γ instead, γ turns out to be even smaller than one. This implies that the chiral condensate will not vanish in the chiral limit, but since these configurations represent a system at a finite volume near T_c, this is not to be expected anyway since the chiral transition is only sharp in the thermodynamic limit. An exponent of 2 might be visible in a comparison of different light quark masses for systems at higher temperatures, but this was not part of the investigation done for this work. In any case it seems that near T_c the axial anomaly is not effectively restored and a large contribution to its breaking is due to the near-zero mode peak, which becomes sharper in the chiral limit. This ensures that its contribution does not vanish once the light quark mass drops below the typical magnitude of the eigenvalues in this peak. The total area of the peak also decreases, but even a decrease quadratic in the light quark mass would still give a contribution to the breaking of $U_A(1)$, and the observed decrease is much slower.

In order to establish that the near-zero mode peak is not a lattice artifact, a comparison at different lattice spacings is necessary. However, this is more involved since a change in the lattice spacing changes the renormalization point of the simulation. It is in general necessary to change the values of *bare* quantities, which do not correspond to any directly observable physical quantity and are to be regarded as input parameters of the theory, in order to regain the same values of actually observable quantities. In particular, the values of bare quantities can not be simply taken over from one discretization scheme to another. Among the bare quantities of QCD are the coupling, the quark masses and the eigenvalues, so if the renormalization point is changed, the eigenvalue spectrum can no longer be directly compared. In the next section, an attempt to renormalize the eigenvalues by tuning the quark masses will be described. It can however be argued that the prefactor α in fact *can* be compared directly, since to leading order it remains unchanged under renormalization.

While the quark mass is not directly observable, close to the chiral limit the product of the chiral condensate and the light quark mass can be

expressed as [49]

$$2m\Sigma = -f_\pi^2 M_{\pi^+}^2$$

where M_{π^+} is the mass of the π^+ pion and f_π is the pion decay constant. Since these are physical quantities that can be measured, renormalization factors of m and Σ have to cancel each other.

The simplest way to accomplish this is to scale the eigenvalues by the same renormalization factor as the quark masses. If a quark mass changes from m to $\tilde{m} = Zm$ and each eigenvalue with $|\lambda|^2 = \varepsilon^2$ from ε to $\tilde{\varepsilon} = Z\varepsilon$, this has the effect

$$\tilde{m}\tilde{\Sigma} = \left\langle \frac{T}{V} \sum_i \frac{Z^2 m^2}{Z^2 m^2 + Z^2 \varepsilon_i^2} \right\rangle = m\Sigma,$$

where the continuum equation has been used instead of the proper equation (2.24) because otherwise the necessary adjustment of the eigenvalues becomes quite involved. For eigenvalues that are much smaller than the radius r of the eigenvalue circle, the difference is negligible. The eigenvalue density at $\tilde{\lambda} = Z\lambda$ becomes

$$\tilde{\rho}(\tilde{\lambda}) = \left\langle \frac{T}{V} \sum_i \delta(\tilde{\lambda} - \tilde{\varepsilon}_i) \right\rangle = Z^{-1} \left\langle \frac{T}{V} \sum_i \delta(\lambda - \varepsilon_i) \right\rangle = Z^{-1} \rho(\lambda).$$

From this, a density that absorbs these renormalization factors to leading order and is roughly invariant under renormalization can be constructed, namely

$$f(x) = \left\langle \frac{T}{V} \sum_i \delta\left(x - {}^{\varepsilon_i}/_{m}\right) \right\rangle = m\rho(mx).$$

If the eigenvalue density is given by the near-zero mode peak

$$\rho(\lambda) = \frac{\alpha\sigma}{\pi(\sigma^2 + \lambda^2)},$$

this results in

$$f(x) = \frac{m\alpha\sigma}{\pi(\sigma^2 + m^2x^2)} = \frac{m^2 \alpha\, {}^{\sigma}/_{m}}{\pi m^2 (({}^{\sigma}/_{m})^2 + x^2)} = \frac{\alpha\, {}^{\sigma}/_{m}}{\pi(({}^{\sigma}/_{m})^2 + x^2)},$$

which is a peak that is characterized by a width that scales with the quark mass and an area that is independent of the mass. The prefactor α can therefore be compared even if the bare quark masses at the different lattice spacings are not known.

A comparison between different lattice spacings can be done at T_c as well as at $1.2\,T_c$. In the first case, fit results with and without an offset are available, while in the second, there are results from the fit as well as from the Bayesian best guess. Of these, all but the fit with offset at T_c show a decrease of the infrared peak area α with decreasing lattice spacing. It is possible that the total infrared contribution consisting of the infrared peak and the offset in fact decreases also in this case, but the offset can not be compared without first renormalizing the quark masses and even then a comparison will be difficult. Unless ω is to diverge in the continuum limit, the renormalized offset has to become zero in the chiral limit and whether it has a finite contribution to ω will depend on how fast it vanishes. The offset is also one of the features of the spectrum that might be sensitive to finite volume effects since these systems are close to T_c.

It is not clear from these results how much of the infrared peak will survive the continuum limit. While there is a tendency for the area under the infrared peak to decrease with decreasing lattice spacing, a simple linear extrapolation, which is hardly justified with two data points each, still gives a non-vanishing value at zero lattice spacing. If it turns out that part of the infrared peak is a finite lattice spacing effect, it probably originates in the underlying HISQ discretization since the staggered Dirac operator only exhibits full chiral symmetry in the continuum limit.

4.2 Quark Mass Dependence of the Axial Anomaly

In order to calculate the potential restoration of the axial anomaly, the observable ω defined in section 1.3 and for overlap fermions in section 2.3.3 technically has to be evaluated at the quark mass that was also used for the generation of the gauge configurations. However, the quark mass is a bare quantity that can differ between different regularizations. The configurations used for this work were created with the HISQ discretization scheme at some specific values of the light and the strange quark mass, but in order to compute observables with overlap eigenvalues, the cor-

responding overlap mass first has to be tuned. Conceptually, the quark mass plays two roles, namely that of the sea quark mass that is used in the generation of gauge configurations and that of the valence quark mass that is used in the computation of observables. More specifically, if the expectation value of an observable is expressed by a path integral and the fermionic part of the integral is carried out, this takes the general form

$$\int \mathcal{D}[U] \int \mathcal{D}[\psi, \bar{\psi}] A(\psi, \bar{\psi}, U) \mathrm{e}^{-S_G[U] - \bar{\psi} D_m \psi} = \int \mathcal{D}[U] \det [D_m] \, \tilde{A}(D_m, U) \mathrm{e}^{-S_G[U]}$$

with $\tilde{A}$ depending on the form of the observable A and usually containing traces of operators built from D_m. The quark mass enters this expression in the fermion determinant $\det [D_m]$ as well as in the observable $\tilde{A}$, and conceptually it is possible to use different quark masses for these terms, which are then called the sea and valence quark mass. Of course, if these take different values it is in general no longer possible to again write the expectation value as a path integral with a local action. The quenched approximation is equivalent to setting the sea quark mass to infinity, which makes the determinant constant and therefore irrelevant. More generally, a computation is called *partially quenched* if the Dirac operator in the determinant and that in the observable differ, be it only in the value of the mass or by using a completely different discretization scheme.

As long as two discretization schemes are equivalent in their continuum limits and therefore belong to the same universality class, the values of measured quantities should be the same if extrapolated to the continuum. It should therefore be possible to find values for the bare quark masses in a simulation using overlap fermions such that the simulation describes the same physics as the HISQ scheme at given quark masses, at least if these are extrapolated to the continuum. The trick is to use an observable that can reasonably well be determined in the HISQ scheme and is not expected to be very sensitive to effects from not being close enough to the continuum, and match the overlap quark mass such that the observable gives the same values if computed with the overlap operator. These parameters can then be used to compute something where the continuum extrapolation is easier for overlap fermions than for HISQ fermions. In particular, for HISQ fermions, full chiral symmetry is only restored in the

continuum, while overlap fermions implement full chiral symmetry even at finite lattice spacing. For observables that are sensitive to the light quark mass, the HISQ scheme will therefore not be as reliable as the overlap formulation. This unfortunately also means that it is difficult to tune the light quark mass since no observable that is sensitive to it can reliably be compared between the two schemes.

These problems are not as pronounced if the strange quark mass is tuned. Once a value is obtained for it, a range of light quark masses can be sampled such that the ratio between the light and strange quark mass is of the same order of magnitude as in the HISQ formulation. The tuning of the strange quark mass is done using an observable similar to the $U_A(1)$ breaking term ω, with the difference that m_l is replaced by m_s, i.e. (cf. (2.26))

$$\omega_s = \frac{T}{V}\left\langle \frac{1}{m_s}\operatorname{tr}\left[\tilde{D}_s^{-1}\right] + \operatorname{tr}\left[\tilde{D}_s^{-2}\right]\right\rangle = \frac{T}{V}\left\langle \sum_{\varepsilon} \frac{2m_s^2}{\left(m_s^2 + \frac{4r^2}{4r^2-\varepsilon^2}\varepsilon^2\right)^2}\right\rangle.$$

For HISQ fermions, where the massive Dirac operator is simply given by $D_m = D + m$ with an antihermitian massless Dirac operator D, this simplifies to

$$\omega_s = \frac{T}{V}\left\langle \frac{1}{m_s}\operatorname{tr}\left[D_{m_s}^{-1}\right] + \operatorname{tr}\left[D_{m_s}^{-2}\right]\right\rangle = \frac{T}{V}\left\langle \sum_{\lambda} \frac{2m_s^2}{\left(m_s^2 + |\lambda|^2\right)^2}\right\rangle.$$

In order to compute the expectation value of the trace of some inverse operator, the usually used strategy consists of taking random vectors, inverting the operator on them and taking the scalar product of the result with the original random vector, i.e.

$$\left\langle \operatorname{tr}\left[A^{-1}\right]\right\rangle \approx \frac{N}{n}\sum_{i=1}^{n} x_i^\dagger A^{-1} x_i$$

with n being the number of normalized random vectors x_i and N being the dimensionality of these vectors. Taking a single random vector and writing it as linear combination of the eigenvectors v_i of A with eigenvalues λ_i, $x = \sum_i \xi_i v_i$, results in

$$x^\dagger A^{-1} x = \sum_i |\xi_i|^2 \lambda_i^{-1}.$$

Each $|\xi_i|^2$ is randomly distributed with expectation value $1/N$ and variance $\sim 2/N^2$ since for large dimensionality it can be approximated as a quotient between independent random variables distributed with $\chi^2(1)$ and $\chi^2(N)$ distributions. The standard deviation is therefore of the same order of magnitude as the value which usually means that a lot of random vectors are needed to get a reliable result. However, if a lot of eigenvalues of A^{-1} lie close together, the fluctuations of their contributions tend to cancel each other. Another source of error lies in the fact that the evaluation of $A^{-1}x$ can usually only be done approximately and stops once the candidate y for $A^{-1}x$ gives a small residual $r = x - Ay$. If the candidate y and the correct solution $\tilde{y}$ differ along the direction of an eigenvector of A with a particularly small eigenvalue, this does not affect the residual as much as with larger eigenvalues. However, the small eigenvalues of A have the largest contributions to the trace of A^{-1}.

Fortunately, since the lowest eigenvectors and eigenvalues of the overlap operator have anyhow been computed for this work and the eigenvectors of D and $\tilde{D}^{-1}$ are the same, they can be used to deflate the inversion needed for the computation of $\tilde{D}^{-1}x$. In this case, an incomplete deflation has been implemented (cf. [50]) which does not require that the vectors used in the deflation are exact eigenvectors. The disadvantage with respect to a complete deflation is that it requires some linear algebra in each step of the inversion and not only at the beginning and the end, but since each step consists of a time-consuming application of the overlap operator, this does not matter much. For the inversion, a simple conjugate gradient was used to solve the normal equation $D_m^\dagger D_m y = D_m^\dagger x$. In principle, it should be possible to use a direct solver like BiCGstab [51], but this often gave non-converging results so the stabler CG algorithm was used. The operator $D_m^\dagger D_m$ can be written in the form $\alpha(D^\dagger D + f(m))$, but since the right-hand side of the equation also differs for the different masses, it was not possible to use a multi-shift inverter. Also, while it may be possible to adjust the incomplete deflation for a multi-shift solver, it is not obvious how this could be achieved.

The deflation also has the advantage that the condition number of the remaining operator is much smaller, so fluctuations in the contributions of specific eigenvalues will tend to cancel each other and less random vectors are needed. In fact, it turned out that only one random vector per configuration and mass was sufficient and computing more of them did not

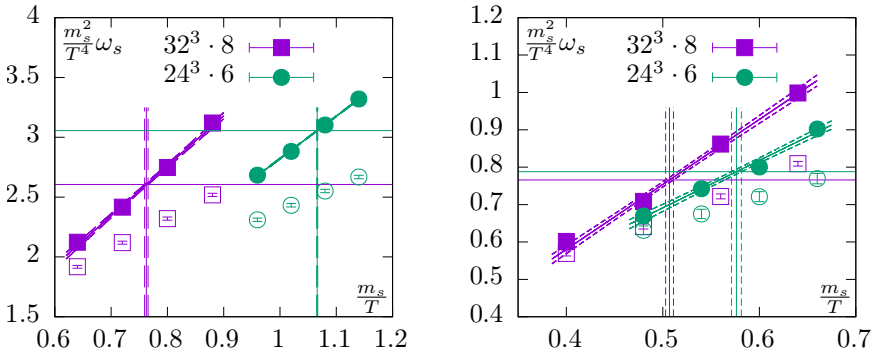

Figure 4.6: Tuning of the bare overlap strange quark mass at T_c (left) and $1.2\,T_c$ (right) for different lattice spacings. The horizontal lines indicate the corresponding HISQ results where the valence quark mass is equal to the HISQ sea quark mass. The full results from incomplete deflation are marked by filled symbols, results computed from just the eigenvalues by empty ones.

change the result noticeably.

In fig. 4.6, the observable $\frac{m_s}{T^4}\omega_s$ at different strange quark masses and their intercept with the HISQ value are visualized. Although the observable had to be computed for several more masses in order to pinpoint the location of the intercept, only a few points around each result are shown. When comparing these results to the ones reported in [5], it should be noted that here and later in fig. 4.7 the zero mode contribution is included unless mentioned otherwise. While the relative number of zero modes should vanish in the thermodynamic limit, arguments laid out in section 4.1.2 suggest that the corresponding contributions will instead be given by near-zero modes, so they should not simply be ignored.

It stands out that especially near T_c the bare quark masses at different lattice spacings are very different, with m_s at $N_\tau = 6$ coming out to be 1.4 times as large as at $N_\tau = 8$. The corresponding bare HISQ quark masses only have a ratio of 1.08, which is more expected since the renormalization constants should be similar. A possible reason could be that while taking the same renormalization constant for the eigenvalues and for the quark masses is sufficient to provide the correct renormalization for the chiral condensate Σ, especially for the larger eigenvalues, which do not contribute

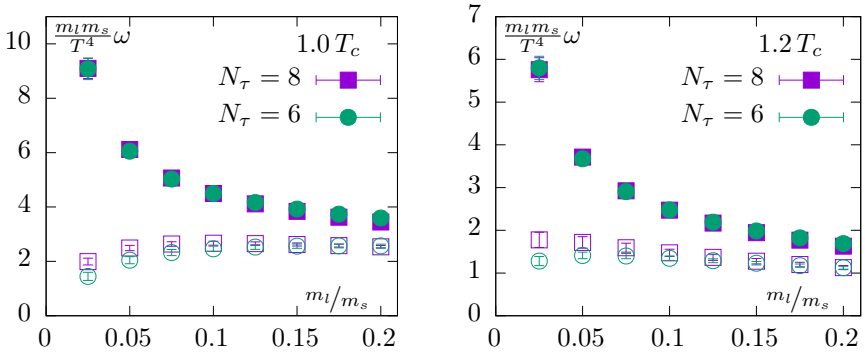

Figure 4.7: Renormalized measure of $U_A(1)$ breaking for different valence light quark masses. The strange quark mass is taken from the tuning done before (cf. fig. 4.6). The empty points are results after subtraction of the zero mode contribution.

to Σ in the chiral limit, it is not necessary. The obtained quark masses should therefore only be taken as a rough guide for the correct values.

Any observable that might be used to similarly tune the light quark mass will at the same time be sensitive to the fact that for HISQ fermions the chiral symmetry group is reduced, so at finite lattice spacing it might be argued that the light quark mass plays a different role than for overlap fermions. For example, the staggered formulation gives rise to more would-be Goldstone bosons than there are physical pions because even if during the generation of the gauge configurations a rooting procedure is used, the observable sees four staggered tastes. These bosons are not exactly degenerate, so there is some ambiguity about whether this actually describes a system with two dynamical light quarks that have the mass that was used in the staggered formulation. Even if there are no conceptual problems, the observable as computed with HISQ fermions might have large discretization errors. In any case it would defeat the purpose of being able to compute ω with a discretization scheme that, in contrast to HISQ fermions, has full chiral symmetry if the same quantity were to be used to tune the light quark mass, which would make the obtained values equal by construction.

It is however possible to compute the $U_A(1)$ breaking measure ω for

different light quark masses and look at its lattice spacing dependence and also at the partial chiral limit, where only the valence light quark mass is sent to zero. Since for small quark masses ω is dominated by the contributions from small modes and in fig. 4.6 it is visible that even for masses that are only slightly lower than the strange quark mass the contributions from higher modes that are provided by the inversion already can be neglected, fig. 4.7 has been computed only from the eigenvalues. Here, the combination (cf. (2.26))

$$\frac{m_l m_s}{T^4}\omega$$

has been plotted, which is dimensionless and renormalization invariant under the assumption that the eigenvalues and the light and strange quark masses need the same renormalization constants. For a spectrum that is given by a Breit-Wigner peak with area α and width σ, it results in

$$\frac{m_l m_s}{T^4}\omega \propto \alpha \frac{\sigma + 2m_l}{(\sigma + m_l)^2}.$$

This has the advantage that the partial chiral limit $m_l \to 0$ at fixed eigenvalue distribution gives a finite value, so it is not that important to insert the correct light quark mass since it is not very sensitive to it. In fig. 4.7, it can be seen that this combination gives very similar values independent of the lattice spacing. Moreover, the considered combination seems to diverge if the valence quark mass is reduced, with an increasing contribution from the zero modes. The remaining contribution essentially comes only from the near-zero modes, which can be seen if only modes below some threshold are included in the sum. However, since the near-zero mode peak and the bulk spectrum overlap at T_c and $1.2\,T_c$, such a threshold is somewhat ambiguous.

While this might no longer be the case in a full chiral limit, this result gives a strong indication that $U_A(1)$ is not effectively restored at the same temperature as chiral symmetry and that its breaking is caused by zero as well as near-zero modes. Even at $1.5\,T_c$, fig. 4.8 suggests that the axial anomaly is still in effect.

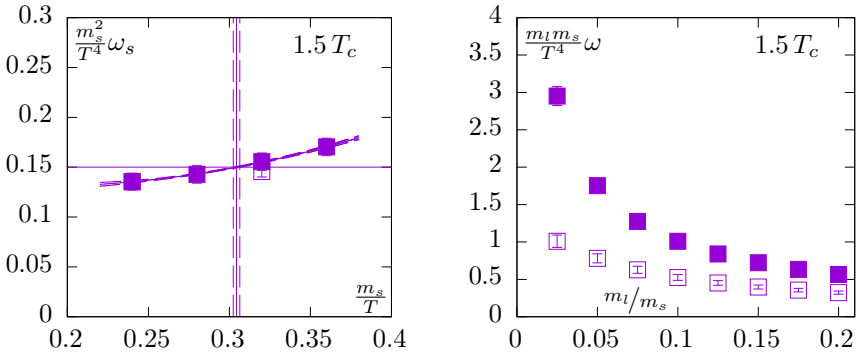

Figure 4.8: Tuning of the strange quark mass and computation of the $U_A(1)$ breaking for different light quark masses at $1.5\,T_c$. Compare figs. 4.6 and 4.7.

4.3 The Space-Time Structure of Infrared Dirac Modes

Having determined the infrared spectrum of the overlap Dirac operator on HISQ gauge configurations, it is not only possible to gather information from the eigenvalues but also from the eigenvectors. In the last sections, some indications have been gathered that the axial anomaly is not effectively restored at the chiral transition temperature. The zero modes of the Dirac operator as well as the near-zero mode peak were identified as mainly contributing to its breaking and even at temperatures as high as $1.5\,T_c$ such an infrared peak is still present.

In this section, a closer look at these infrared modes and in particular their lattice coordinate (i.e., space-"time") profiles will be taken. These profiles in essence embody a change of basis for the vector space spanned by the fermionic degrees of freedom, between the basis given by the eigenvectors of the Dirac operator and the basis given by the lattice coordinates. Since both representations can be linked to different aspects of the dynamics of QCD, their interplay is of great interest.

For these analyses, it is important to use the proper eigenvectors of the Dirac operator and not simply the eigenvectors of $D^\dagger D$. In section 3.3, it was discussed how these can be obtained from a non-zero mode pair of $D^\dagger D$ by an appropriate rotation or from a non-zero chiral eigenvector of

$P_\pm D P_\pm$ by combination with its partner with opposite chirality. There is unfortunately no similarly distinguished basis of the subspace spanned by the zero modes if a configuration has multiple of them, which will also be visible in the profiles.

4.3.1 Localization

A simple measurement for the localization of a normalized continuum vector $\psi(x)$, where the space-time coordinate x is written out explicitly and vector notation is used for internal degrees of freedom, is given by the *participation ratio*

$$\mathrm{PR}(\psi) = \frac{1}{V_4}\left[\int \mathrm{d}^4x |\psi(x)|^4\right]^{-1} \qquad \text{with} \qquad |\psi(x)|^2 = \psi^\dagger(x)\psi(x)$$

or similarly for a spinor $\psi(x)$ on a lattice with discrete x,

$$\mathrm{PR}(\psi) = \frac{1}{N_\sigma^3 N_\tau}\left[\sum_x |\psi(x)|^4\right]^{-1}. \tag{4.5}$$

Here, $V_4 = {}^V\!/_T$ is the volume of the space-"time" that determines the number of path integration variables. If a (continuum) spinor is localized on some four-volume V_4' such that $|\psi(x)|^2$ is constant inside this volume with a value of ${}^1\!/_{V_4'}$ due to normalization and $|\psi(x)|^2 = 0$ outside of it, the participation ratio takes the value

$$\mathrm{PR}(\psi) = \frac{1}{V_4}\left[\int_{V_4'} \mathrm{d}^4x \frac{1}{V_4'^2}\right]^{-1} = \frac{V_4'}{V_4},$$

which explains the name.

In fig. 4.9, the participation ratios of the lowest eigenmodes of each configuration are plotted against their eigenvalues. While there is much fluctuation, there is also a clear tendency for low modes to be much more localized than higher modes. Moreover, at T_c many low modes have a nonvanishing participation ratio and the average relationship between the PR value and the eigenvalue is given by a concave function, while at higher temperatures it is convex and low modes are highly localized. At $1.5\,T_c$, the near-zero modes and bulk modes show a clear separation such that

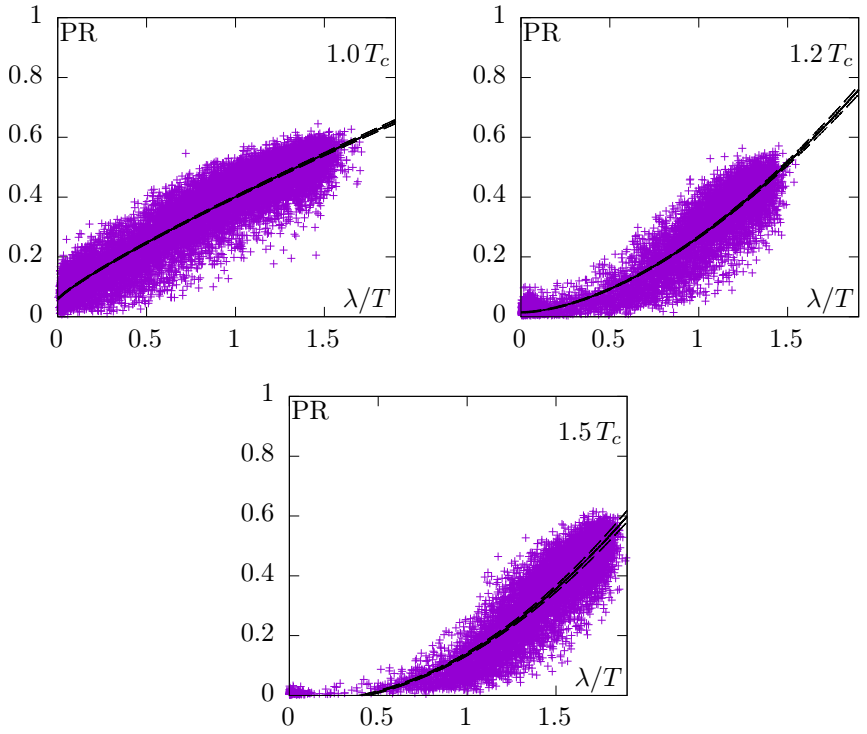

Figure 4.9: Participation ratio of non-zero eigenmodes of the overlap operator for the ensembles at lattice size $32^3 \cdot 8$ at different temperatures. The black line shows the result of a fit to the function $\mathrm{PR} = a\lambda^b + c$.

the fit to the function $\mathrm{PR} = a\lambda^b + c$ gives an intercept at $\lambda \sim 0.42\,T$, indicating that the bulk modes are shifted away from $\lambda = 0$.

In section 1.4, it has been discussed that a gauge configuration that contains an instanton gives rise to a similarly localized zero mode of the Dirac operator, which matches the trend seen here that low modes are more localized that high modes. If a configuration contains several instantons which are far enough apart such that they do not influence each other much, they will accordingly give rise to multiple zero modes, each localized at one of the instantons. However, it is not guaranteed that the zero modes that are computed as, for example, eigenvectors of $D^\dagger D$ are

exactly these localized modes instead of some linear combinations of them. Since the eigenvalue is degenerate, a computation of the eigenvectors will give some relatively arbitrary orthonormal set of vectors that spans the appropriate eigenspace, with any splittings coming from numerical fluctuations that will in general not be aligned to the localized structures. The participation ratio as defined in (4.5) is not invariant under a unitary transformation, so if two highly localized modes are rotated to form, for example, the combinations $\frac{1}{\sqrt{2}}(\psi_1 + \psi_2)$ and $\frac{1}{\sqrt{2}}(\psi_1 - \psi_2)$, these will have a much larger participation ratio—in this case, about twice as large. A more appropriate definition of the participation ratio that can be applied to a set of n orthonormal vectors is therefore given by

$$\mathrm{PR}(\psi_1, \ldots, \psi_n) = \frac{n}{V_4} \left[\int \mathrm{d}x \left(\sum_{i=1}^{n} |\psi_i(x)|^2 \right)^2 \right]^{-1} . \tag{4.6}$$

It is invariant under a change of basis within the subspace spanned by the vectors. If n modes are each localized on some four-volume and these four-volumes have no overlap with each other, this results in an inverse participation ratio $\mathrm{IPR} = {}^1\!/\!_{\mathrm{PR}}$ that is the average of the individual IPRs.

If a configuration contains instantons as well as anti-instantons, the two-dimensional subspace spanned by the corresponding righthanded and lefthanded zero modes can also be spanned by some other basis. A specific basis is distinguished from other possibilities in that it is equivalent to a non-zero mode pair—where one mode is obtained from the other by application of γ_5 and both have zero chirality—except that the eigenvalue happens to be zero. It can therefore be disturbed away from zero by fluctuations in the gauge field (cf. section 2.3.1). If this is the origin of the near-zero modes, which can most clearly be separated from the bulk modes at $1.5\,T_c$, the participation ratio of a near-zero mode should be about twice as large as the participation ratio of a zero mode. In fig. 4.10, the inverse of the participation ratios (IPR) of zero as well as near-zero modes at $1.5\,T_c$ are shown. The magnitude of the zero mode eigenvalues is mostly due to the fact that the algorithm was stopped once the separation between zero and near-zero modes was clear enough, so by computing a few extra iterations it is possible to reduce the numerical eigenvalues of the zero modes. While there are some outliers, the average values have a ratio of 2.18(9) between the IPR of zero modes and that of near-zero

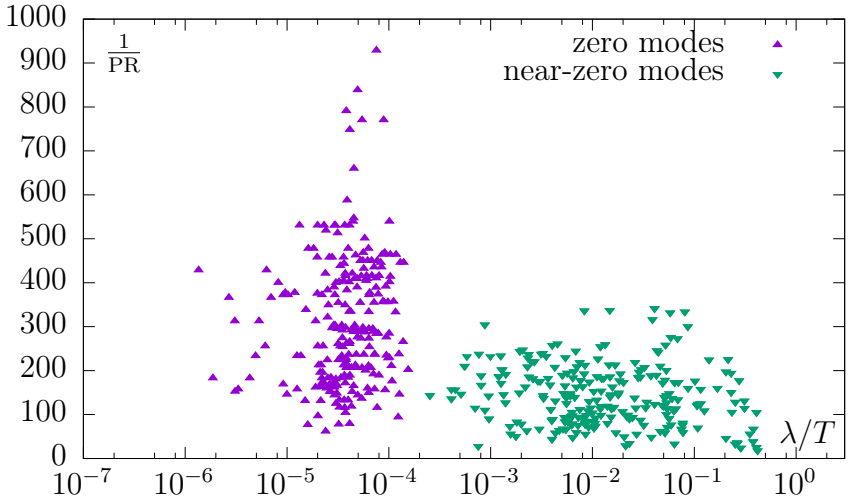

Figure 4.10: Inverse participation ratios of zero modes (using (4.6)) and near-zero modes ($\lambda < 0.4\,T$) at $1.5\,T_c$.

modes, which supports the picture that many near-zero modes are formed by a superposition of zero modes localized on an instanton and an anti-instanton, which is then disturbed away from zero.

4.3.2 Density Profiles of Zero and Near-Zero Modes

In the last section, several explanations for the obtained trends in the participation ratios were given that can be checked by looking at the profiles of specific eigenvectors. These can not replace a collective picture since only a few of them can be looked at at the same time, which carries the danger of a selection bias. But they can be useful for a graphic visualization. All profiles shown in this section are taken from the ensembles with $32^3 \cdot 8$ lattices.

In fig. 4.11, the zero mode of a configuration that only has one of them is shown. It is clearly visible how the mode is practically vanishing everywhere except in some small region where there is a peak of density. This corroborates the analytic result that zero modes are induced by instantons and localized at the same position.

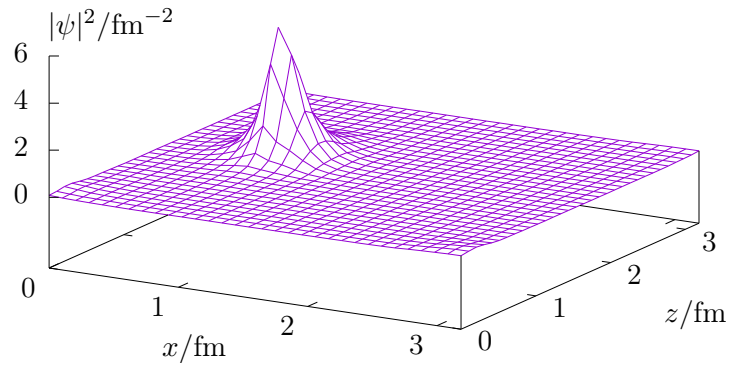

Figure 4.11: Density profile of the zero mode of a configuration with $|Q| = 1$ at $1.5\,T_c$. The internal degrees of freedom and the other coordinates are integrated out.

If a configuration has multiple zero modes of the same chirality due to multiple instantons, the zero modes are not necessarily each localized at one position each. In fig. 4.12 it can be seen how the zero modes as computed by the algorithm are linear combinations of the localized modes. Each mode shows two peaks, both of which are at the same position for the two modes. In this case, one peak is dominant for one mode while the other is dominant for the other, which simply means that the rotation matrix that transforms the computed modes to modes that are localized on one peak each can be chosen such that the diagonal elements will be larger than the off-diagonal ones.

As discussed before, near-zero modes can arise if a configuration has instantons as well as anti-instantons, such that the actual overlap eigenvectors are linear combinations of the would-be zero modes. The profile in fig. 4.13 fully supports this picture, since a near-zero mode seems to consist of two peaks that have the same height. In the chirality profile $\psi^\dagger(x)\gamma_5\psi(x)$, it is even visible that one of the peaks gives a positive contribution to the chirality while the other gives a negative one. The near-zero mode therefore is given by a linear combination of a righthanded and a lefthanded mode that are each highly localized. The prefactors in the linear combination also have the same norm, which is required for a vanishing

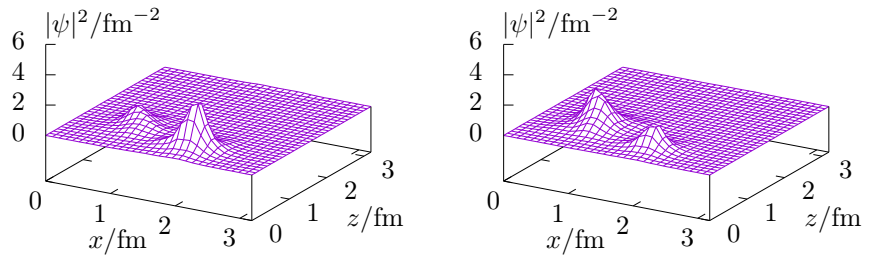

Figure 4.12: Density profiles of the zero modes of a configuration with $|Q| = 2$ at $1.5\,T_c$. The internal degrees of freedom and the other coordinates are integrated out.

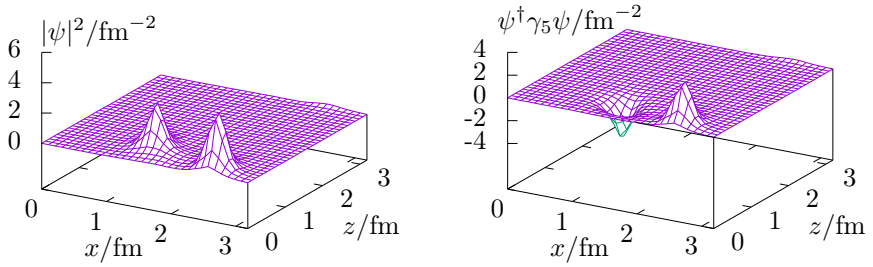

Figure 4.13: Density and chirality profile of a near-zero mode at $1.5\,T_c$. The internal degrees of freedom and the other coordinates are integrated out.

chirality and results in the two peaks having the same height. As a side remark, the two modes of the near-zero mode pair have indistinguishable profiles.

The profiles shown so far have all been extracted from configurations at the highest temperature, since the correspondence between instantons and infrared modes seems to be the clearest there. At lower temperatures and especially close to T_c, there is often much fluctuation in the profiles with some peaks still visible for low modes. An example that is relatively clean is shown in fig. 4.14. Even though the configuration only has one zero mode, the chirality profile of the zero mode has two peaks and some further fluctuations. Taking a look at the lowest near-zero mode of the

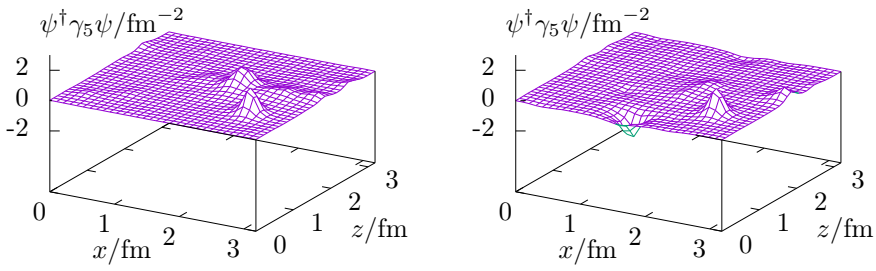

Figure 4.14: Chirality profile of a zero mode and the lowest near-zero mode of a configuration with $|Q| = 1$ at T_c.

same configuration for comparison, it seems that one of the peaks is also present in the near-zero mode. In fact, even the other peak is slightly visible in the near-zero mode. In addition, it has a peak of opposite chirality. So it seems that there are multiple localized structures in the underlying gauge field, but the lowest modes are not aligned completely along these structures. Instead, the overlap eigenvectors seem to be linear combinations of several localized modes.

4.3.3 Size and Distribution of Localized Structures

The analytic result for the zero mode associated with the instanton solution has the density ([23], see also section 1.4)

$$|\psi(x)|^2 = \frac{2\rho^2}{\pi^2 \left(x^2 + \rho^2\right)^3}.$$

The derivation of this result assumes an infinite volume in all directions including the time direction, i.e., a system at temperature zero. The zero mode is normalized such that $\int \mathrm{d}^4x |\psi(x)|^2 = 1$. In fig. 4.15, it can be seen that sometimes the extent of the localized structures is not negligible compared to the inverse temperature of the system. Gauge field solutions with minimal action similar to instantons but on the compactified manifold $\mathbb{R}^3 \times S^1$ are called *calorons* and known in the literature [52, 53]. In the simplest case these are simply periodically repeated instantons, but there are also solutions with non-trivial holonomy, i.e., where the gauge field

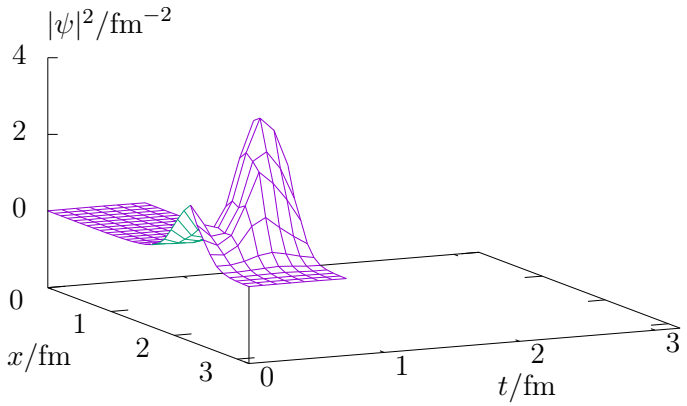

Figure 4.15: Density profile of a zero mode along the temporal and one spatial direction. Taken from a configuration with $|Q| = 1$ at $1.5\,T_c$.

is not repeated exactly. Since the field strength tensor must be periodic, the gauge field at $x + \beta\hat{x}_\tau$ with $\beta = 1/T$ is still gauge-equivalent to the gauge field at x. For this analysis however, the analytic expression for the density is simply replaced by

$$|\psi(\vec{x},\tau)|^2 = \sum_{n\in\mathbb{Z}} f\left(\vec{x},\tau+n\beta\right) \tag{4.7}$$

$$\text{with} \qquad f(\vec{x},\tau) = \frac{\alpha}{\left(1+\left(\vec{x}/\rho_\sigma\right)^2+\left(\tau/\rho_\tau\right)^2\right)^3}$$

In order to accommodate the possibility that the spatial and temporal extents are different, the instanton size ρ was split into ρ_σ and ρ_τ. The normalization α can be obtained by observing that

$$\int_0^\beta \mathrm{d}\tau \sum_{n\in\mathbb{Z}} g(\tau+n\beta) = \sum_{n\in\mathbb{Z}} \int_{n\beta}^{(n+1)\beta} \mathrm{d}\tau g(\tau) = \int_{-\infty}^{\infty} \mathrm{d}\tau g(\tau),$$

giving

$$1 = \int \mathrm{d}^3x \int_0^\beta \mathrm{d}\tau |\psi(\vec{x},\tau)|^2 = \int \mathrm{d}^4x f(x) = \frac{\alpha\pi^2}{2}\rho_\sigma^3\rho_\tau$$

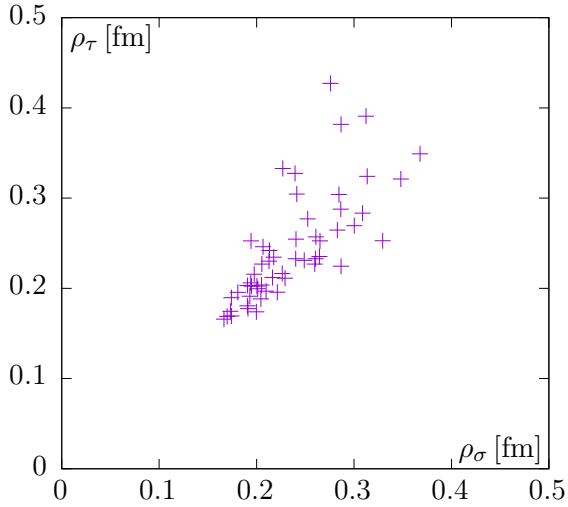

Figure 4.16: Spatial and temporal instanton size from fit to (4.7) of $|Q| = 1$ zero modes at $1.5\,T_c$.

and therefore

$$f(\vec{x},\tau) = \frac{2}{\pi^2 \rho_\sigma^3 \rho_\tau \left(1 + (\vec{x}/\rho_\sigma)^2 + (\tau/\rho_\tau)^2\right)^3}.$$

Equation (4.7) can be fitted to the numerical data obtained from integrating out the internal degrees of freedom of zero modes of configurations with $|Q| = 1$ at $1.5\,T_c$. It is necessary to truncate the sum over the periodic copies, so it was only running from -2 to 2, which is enough such that the omitted copies would have fallen off sufficiently anyway. In the spatial directions, the peaks always fall off fast enough such that the periodic boundary conditions can be ignored and no periodic copies are needed. It is however necessary to shift the coordinates of the spinor such that the peak is positioned somewhat centered on the lattice. The exact position of the peak was also determined by the fit and the lattice point that has the highest density was used as the initial guess. The results can be seen in fig. 4.16 and give an average of $\rho_\sigma = 0.236(7)\,\mathrm{fm}$ and $\rho_\tau = 0.243(8)\,\mathrm{fm}$. The sizes in spatial and temporal directions are compatible within error

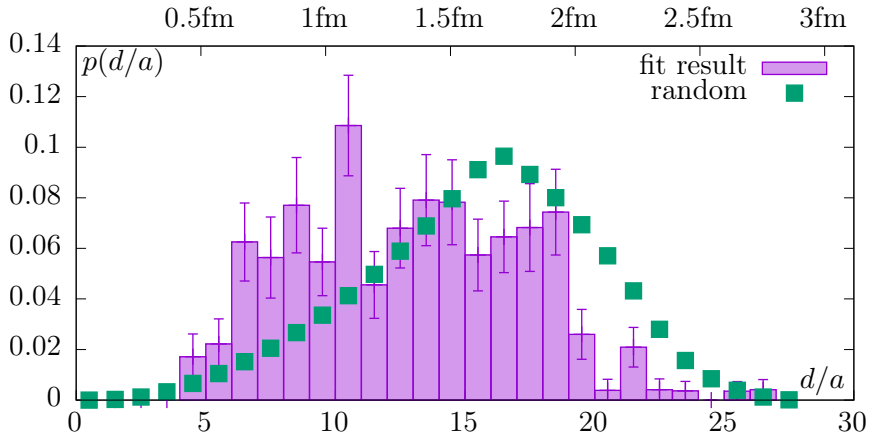

Figure 4.17: Distribution of distances between the two peaks in the chirality profile of a near-zero mode on $32^3 \cdot 8$ lattices at $1.5\,T_c$. The green points show the distance between the origin and a random lattice point for comparison.

bars, with the temporal extent being slightly larger. The temporal extent of the lattice is roughly 0.83 fm, so for a typical instanton localized at the center of the lattice the density at the border will be about 3.3 % of its maximal value. There are some modes where the extent is larger with values of 0.3–0.4 fm and for these modes the finite size of the lattice in the temporal direction is important. It can further be seen that the spatial and temporal extent of a given instanton are highly correlated, with a correlation coefficient of 0.75(6).

If a near-zero mode is created by a linear combination of a right- and a lefthanded zero mode which are localized at different positions, their sizes and the distance between them can similarly be obtained from such a fit. Instead of fitting a function with two peaks and therefore twice as many parameters, it is easier to first rotate the near-zero mode pair by diagonalizing γ_5 on the subspace spanned by it. This creates two modes that each have only one peak, so the same fit as with zero modes can be used. Again, the coordinates can be shifted such that the peaks are not at the spatial borders of the lattice, but the different shifts for the two modes of one pair have to be compensated when calculating the distance between the instanton and the anti-instanton. For simplicity, only one

extent $\rho = \rho_\sigma = \rho_\tau$ was used since for the zero modes it was seen that the spatial and temporal extents are highly correlated anyway.

In fig. 4.17, the distribution of the distances $d = |x^+ - x^-|$ with x^+ and x^- being the position of the peaks with positive and negative chirality, respectively, is shown and compared to the distribution of the distance from a fixed point to some random point on the lattice. It seems that the instanton-anti-instanton (I-AI) pair is almost randomly distributed with a slight correction towards being closer together, corroborating the picture of a gas of weakly interacting topological structures that sometimes form weakly bound molecules consisting of an I-AI pair. The action of an I-AI pair in pure gauge theory decreases with the distance between them [23], so unless the presence of dynamical fermions changes this behavior, there is a weak attracting force between instantons and anti-instantons such that configurations with a close I-AI pair will be sampled more often than ones where the pair is far apart. Also, it seems plausible that if there are multiple instantons and anti-instantons, the pairings will be chosen in such a way that the distances between partners is somehow minimized.

While the positions of the instanton and anti-instanton that are paired to create near-zero modes are somewhat anticorrelated, it seems that there is no significant correlation between their sizes. This can be seen in fig. 4.18, where the sizes of the two peaks are compared for each near-zero mode pair. The lack of correlation is also reflected in the correlation coefficient, which has a value of 0.09(8).

At least at $1.5\,T_c$, it seems that most zero modes correspond to one instanton or anti-instanton and most near-zero mode pairs correspond to an I-AI pair. Under the assumption that the occurrence of each of these localized structures is independent from the others, the total number n of zero and near-zero modes should follow a Poisson distribution,

$$P(n) = \mathrm{e}^{-\kappa}\frac{\kappa^n}{n!}.$$

In fig. 4.19, it has been counted how many configurations have a specific total number of zero and near-zero modes at $1.5\,T_c$. A mode has been regarded as near-zero mode if its eigenvalue was below some threshold, in this case $0.44\,T$. Several thresholds in the range $[0.1\,T, 0.5\,T]$, which covers the gap in the spectrum at $1.5\,T_c$, have been tried and for this value a Poisson fit to the data gave the χ^2 per degree of freedom that

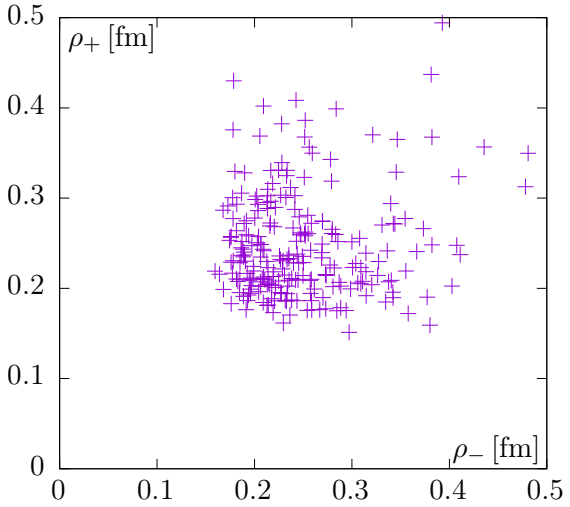

Figure 4.18: Correlation between the sizes of the peaks that form a near-zero mode pair at $1.5\,T_c$. ρ_- is the size of the peak that contributes negative values to the chirality of the mode and ρ_+ the one that contributes positive values.

was closest to 1, namely 0.99. The fit gives a value of $\kappa = 4.50(13)$, which for a Poisson distribution is equal to the mean value as well as the variance. The measured average is $\langle n \rangle = 4.53(17)$ and the measured variance $\sigma^2 = 4.1(4)$, so the assumption of independent occurence seems to be justified. Setting $\kappa = 4.50(13)$ in relation to the total four-volume of the lattice, QCD at this temperature shows the behavior of a weakly interacting dilute gas of instantons and anti-instantons that have sizes of $0.239(4)\,\mathrm{fm}$, with $0.154(5)$ topological objects per fm^4.

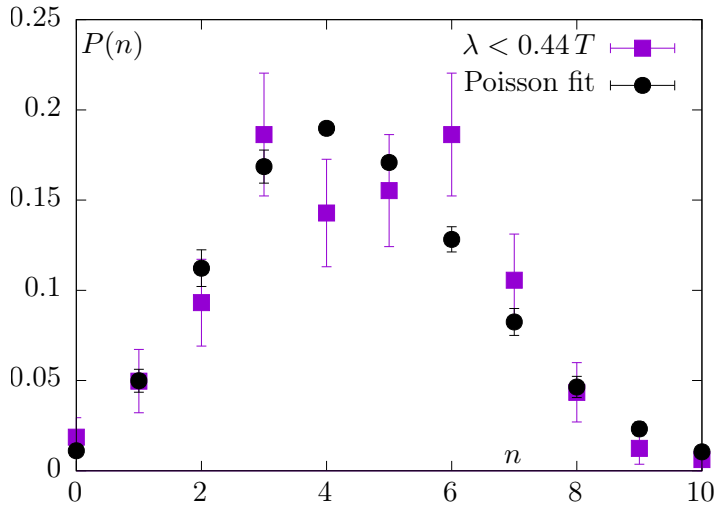

Figure 4.19: Relative number of zero and near-zero modes per configuration and Poisson fit to the data.

5 Conclusion

In this work, the spectrum of the overlap Dirac operator has been computed and analyzed on configurations that had been created using highly improved staggered quarks. Although the overlap operator is expensive to compute, it has the advantage that it fully implements chiral symmetry in the same way as the continuum QCD Dirac operator even at finite lattice spacings. This opened the possibility to investigate chiral aspects of QCD and, in particular, the question if the axial anomaly is suppressed at the chiral transition temperature T_c.

The obtained results indicate that the axial anomaly is still present at T_c and even at $1.5\,T_c$ as evidenced by a splitting in the integrated pion and delta susceptibilites. The spectrum shows a peak in the near-zero region consisting of zero modes and pairs of near-zero modes. The breaking of the axial symmetry was identified as being caused by these infrared modes. It was discussed how this infrared contribution might change in the thermodynamic, continuum, and chiral limits. The obtained data supports the expectation that the peak becomes narrower with decreasing quark masses, resulting in a Dirac-delta peak in the chiral limit. The area under the peak was found to decrease with decreasing lattice spacing, so in order to resolve how much of it survives the continuum limit further investigations are needed, in particular ones where already for the generation of gauge configurations chiral fermions are used.

The infrared modes were investigated and found to be highly localized, supporting the picture of QCD at high temperatures as a dilute instanton gas. The instantons were found to have an average size of $0.239(4)\,\mathrm{fm}$ and a density of $0.154(5)\,\mathrm{fm}^{-4}$ at $1.5\,T_c$. Near-zero modes were found to be induced by instanton-anti-instanton molecules, which are weakly bound. At temperatures closer to T_c, this picture becomes more complicated but these features sometimes still can be recognized.

In conclusion, in QCD at temperatures above but close to T_c the chiral anomaly does not seem to be effectively suppressed yet. Topological ob-

jects like instantons and anti-instantons induce an accumulation of highly localized infrared Dirac modes and thereby cause the anomalous chiral symmetry to be broken.

Bibliography

[1] **Particle Data Group** Collaboration, K. A. Olive et al., *Review of Particle Physics*, *Chin. Phys.* **C38** (2014) 090001, [DOI: 10.1088/1674-1137/38/9/090001].

[2] M. Gell-Mann, *Symmetries of Baryons and Mesons*, *Phys. Rev.* **125** (1962) 1067, [DOI: 10.1103/PhysRev.125.1067].

[3] K. G. Wilson, *Confinement of Quarks*, *Phys. Rev.* **D10** (1974) 2445, [DOI: 10.1103/PhysRevD.10.2445].

[4] P. Petreczky, *Lattice QCD at Non-Zero Temperature*, *J. Phys.* **G39** (2012) 093002, [arXiv:1203.5320].

[5] V. Dick, F. Karsch, E. Laermann, S. Mukherjee, and S. Sharma, *Microscopic Origin of $U_A(1)$ Symmetry Violation in the High Temperature Phase of QCD*, *Phys. Rev.* **D91** (2015), no. 9 094504, [arXiv:1502.06190].

[6] S. Sharma, V. Dick, F. Karsch, E. Laermann, and S. Mukherjee, *Investigation of the $U_A(1)$ in High Temperature QCD on the Lattice*, in *Proceedings, 31st International Symposium on Lattice Field Theory (Lattice 2013)*, vol. LATTICE2013, p. 164, 2014. arXiv:1311.3943.

[7] S. Sharma, V. Dick, F. Karsch, E. Laermann, and S. Mukherjee, *The $U_A(1)$ Anomaly in High Temperature QCD with Chiral Fermions on the Lattice*, in *Proceedings, 33rd International Symposium on Lattice Field Theory (Lattice 2015)*, 2015. arXiv:1510.03930.

[8] S. Sharma, V. Dick, F. Karsch, E. Laermann, and S. Mukherjee, *The Topological Structures in Strongly Coupled QGP with Chiral Fermions on the Lattice*, in *25th International Conference on*

Ultra-Relativistic Nucleus-Nucleus Collisions (Quark Matter 2015) Kobe, Japan, September 27-October 3, 2015, 2016. arXiv:1602.02197.

[9] S. Weinberg, *The Quantum Theory of Fields. Vol. 1: Foundations.* University Press, Cambridge, 2005.

[10] M. Le Bellac, *Thermal Field Theory.* Cambridge monographs on mathematical physics. University Press, Cambridge, 1996.

[11] J. I. Kapusta, *Finite-Temperature Field Theory.* University Press, Cambridge, 1989.

[12] D. J. Gross, R. D. Pisarski, and L. G. Yaffe, *QCD and Instantons at Finite Temperature*, *Rev. Mod. Phys.* **53** (1981) 43, [DOI: 10.1103/RevModPhys.53.43].

[13] A. Zee, *Quantum Field Theory in a Nutshell.* Princeton Univ. Press, 2003.

[14] S. Weinberg, *The Quantum Theory of Fields. Vol. 2: Modern Applications.* University Press, Cambridge, 2013.

[15] C. Gattringer and C. B. Lang, *Quantum Chromodynamics on the Lattice: An Introductory Presentation.* Lecture Notes in Physics 788. Springer-Verlag Berlin Heidelberg, 2010, [DOI: 10.1007/978-3-642-01850-3].

[16] A. Bazavov et al., *The Chiral and Deconfinement Aspects of the QCD Transition*, *Phys. Rev.* **D85** (2012) 054503, [arXiv:1111.1710].

[17] R. D. Pisarski and F. Wilczek, *Remarks on the Chiral Phase Transition in Chromodynamics*, *Phys. Rev. D* **29** (Jan, 1984) 338, [DOI: 10.1103/PhysRevD.29.338].

[18] A. Butti, A. Pelissetto, and E. Vicari, *On the Nature of the Finite Temperature Transition in QCD*, *JHEP* **08** (2003) 029, [hep-ph/0307036].

[19] M. Grahl and D. H. Rischke, *Functional Renormalization Group Study of the Two-Flavor Linear Sigma Model in the Presence of the Axial Anomaly*, *Phys. Rev.* **D88** (2013), no. 5 056014, [arXiv:1307.2184].

[20] A. Pelissetto and E. Vicari, *Relevance of the Axial Anomaly at the Finite-Temperature Chiral Transition in QCD*, *Phys. Rev.* **D88** (2013), no. 10 105018, [arXiv:1309.5446].

[21] R. Rajaraman, *Solitons and Instantons: an Introduction to Solitons and Instantons in Quantum Field Theory*. North-Holland Publ. Co., Amsterdam, 1982.

[22] A. A. Belavin, A. M. Polyakov, A. S. Schwartz, and Yu. S. Tyupkin, *Pseudoparticle Solutions of the Yang-Mills Equations*, *Phys. Lett.* **B59** (1975) 85, [DOI: 10.1016/0370-2693(75)90163-X].

[23] T. Schäfer and E. V. Shuryak, *Instantons in QCD*, *Rev. Mod. Phys.* **70** (1998) 323, [hep-ph/9610451].

[24] G. 't Hooft, *Computation of the Quantum Effects due to a Four-dimensional Pseudoparticle*, *Phys. Rev.* **D14** (1976) 3432, [DOI: 10.1103/PhysRevD.14.3432].

[25] G. 't Hooft, *Symmetry Breaking through Bell-Jackiw Anomalies*, *Phys. Rev. Lett.* **37** (1976) 8, [DOI: 10.1103/PhysRevLett.37.8].

[26] H. J. Rothe, *Lattice Gauge Theories: An Introduction*, vol. 43 of *World Scientific lecture notes in physics*. World Scientific, Singapore, 1992.

[27] T. DeGrand and C. DeTar, *Lattice Methods for Quantum Chromodynamics*. World Scientific, Singapore, 2006.

[28] N. Sadooghi and H. J. Rothe, *Continuum Behavior of Lattice QED, Discretized with One-Sided Lattice Differences, in One-Loop Order*, *Phys. Rev.* **D55** (1997) 6749, [hep-lat/9610001].

[29] R. V. Gavai and S. Sharma, *Divergences in the Quark Number Susceptibility: The Origin and a Cure*, *Phys. Lett.* **B749** (2015) 8, [arXiv:1406.0474].

[30] H. B. Nielsen and M. Ninomiya, *A No-Go Theorem for Regularizing Chiral Fermions*, *Phys. Lett.* **B105** (1981) 219, [DOI: 10.1016/0370-2693(81)91026-1].

[31] J. Kogut and L. Susskind, *Hamiltonian Formulation of Wilson's Lattice Gauge Theories*, *Phys. Rev.* **D11** (1975) 395, [DOI: 10.1103/PhysRevD.11.395].

[32] A. Zichichi, ed., *New Phenomena in Subnuclear Physics. Proceedings of the 14th International School of Subnuclear Physics (NATO MPI MRST Advanced Study Institute) held in Erice, Sicily, July 11 – August 1, 1975*. Plenum Press, New York.

[33] P. H. Ginsparg and K. G. Wilson, *A Remnant of Chiral Symmetry on the Lattice*, *Phys. Rev.* **D25** (May, 1982) 2649, [DOI: 10.1103/PhysRevD.25.2649].

[34] P. Hernández, K. Jansen, and M. Lüscher, *Locality Properties of Neuberger's Lattice Dirac Operator*, *Nucl. Phys.* **B552** (1999) 363, [DOI: 10.1016/S0550-3213(99)00213-8].

[35] **HPQCD, UKQCD** Collaboration, E. Follana, Q. Mason, C. Davies, K. Hornbostel, G. P. Lepage, J. Shigemitsu, H. Trottier, and K. Wong, *Highly Improved Staggered Quarks on the Lattice, with Applications to Charm Physics*, *Phys. Rev.* **D75** (2007) 054502, [hep-lat/0610092].

[36] H. T. Ding, A. Bazavov, F. Karsch, Y. Maezawa, S. Mukherjee, and P. Petreczky, *Chiral Phase Transition of N_f=2+1 QCD with the HISQ Action*, *PoS* **LATTICE2013** (2014) 157, [arXiv:1312.0119].

[37] M. Müller, *Meson Correlations and Spectral Functions in the Deconfined Phase: a Systematic Analysis in Quenched Lattice QCD*. PhD thesis, Universität Bielefeld, 2013.

[38] J. van den Eshof, A. Frommer, T. Lippert, K. Schilling, and H. A. van der Vorst, *Numerical Methods for the QCD Overlap Operator: I. Sign Function and Error Bounds*, *Comput. Phys. Commun.* **146** (2002) 203, [hep-lat/0202025].

[39] P. P. Petrušev and V. A. Popov, *Rational Approximation of Real Functions*, vol. 28 of *Encyclopedia of Mathematics and its Applications*. University Press, Cambridge, 1987.

[40] B. Jegerlehner, *Krylov Space Solvers for Shifted Linear Systems*, hep-lat/9612014.

[41] M. A. Clark, R. Babich, K. Barros, R. C. Brower, and C. Rebbi, *Solving Lattice QCD systems of equations using mixed precision solvers on GPUs*, *Comput. Phys. Commun.* **181** (2010) 1517, [arXiv:0911.3191].

[42] T. Kalkreuter and H. Simma, *An Accelerated Conjugate Gradient Algorithm to Compute Low Lying Eigenvalues: A Study for the Dirac Operator in SU(2) Lattice QCD*, *Comput. Phys. Commun.* **93** (1996) 33, [hep-lat/9507023].

[43] V. Dick, *Lattice Investigation of the Dirac-Spectrum in the Vicinity of the Chiral Transition*, 2012.

[44] J. R. Shewchuk, *An Introduction to the Conjugate Gradient Method Without the Agonizing Pain*, tech. rep., Pittsburgh, PA, USA, 1994.

[45] MPI Forum, *MPI: A Message-Passing Interface Standard, Version 3.1*. HLRS, 2015.

[46] A. Hasenfratz and C. Nieter, *Instanton Content of the SU(3) Vacuum*, *Phys. Lett.* **B439** (1998) 366, [hep-lat/9806026].

[47] P. de Forcrand, M. Garcia Perez, and I.-O. Stamatescu, *Topology by Improved Cooling: Susceptibility and Size Distributions*, *Nucl. Phys. Proc. Suppl.* **53** (1997) 557, [hep-lat/9608032].

[48] A. Hasenfratz and F. Knechtli, *Flavor Symmetry and the Static Potential with Hypercubic Blocking*, *Phys. Rev.* **D64** (2001) 034504, [hep-lat/0103029].

[49] J. Gasser and H. Leutwyler, *Quark Masses*, *Phys. Rep.* **87** (1982), no. 3 [DOI: 10.1016/0370-1573(82)90035-7].

[50] M. Lüscher, *Local Coherence and Deflation of the Low Quark Modes in Lattice QCD*, *JHEP* **07** (2007) 081, [arXiv:0706.2298].

[51] A. Meister, *Numerik linearer Gleichungssysteme: Eine Einführung in moderne Verfahren*. Springer Fachmedien Wiesbaden, 2015.

[52] B. J. Harrington and H. K. Shepard, *Periodic Euclidean Solutions and the Finite-Temperature Yang-Mills Gas*, *Phys. Rev.* **D17** (Apr, 1978) 2122, [DOI: 10.1103/PhysRevD.17.2122].

[53] T. C. Kraan and P. van Baal, *Periodic Instantons with Nontrivial Holonomy*, *Nucl. Phys.* **B533** (1998) 627, [hep-th/9805168].

Acknowledgments

My first thanks go to Professor Laermann for the great supervision, many fruitful discussions and the opportunity to research such an interesting topic.

Further thanks go to Sayantan for frequent and fruitful discussions and for help with all of the more advanced topics.

I want to thank Florian, Olaf, Professor Karsch and the other members of the Lattice QCD group in Bielefeld as well as Swagato and Hiroshi in Brookhaven for valuable input and helpful explanations of the big picture.

Marcel, Markus and Hauke were often a great help with software and programming issues, which I would like to thank them for.

Through all these years, I have had constant support from Kira as well as from my parents and siblings, which I am deeply grateful for.

I also thank the GSI for financial support during the last years as well as the DAAD for the opportunity to visit the BNL to discuss several topics.